Control and Fault Accommodation for Attitude Control Subsystem of Formation Flying Satellites Subject to Constraints

Narges Roofigari Esfahani

A Thesis

in

The Department

of

Electrical and Computer Engineering

Presented in Partial Fulfillment of the Requirements
for the Degree of Master of Science at
Concordia University,
Montreal, Quebec, Canada

December, 2013

CONCORDIA UNIVERSITY
SCHOOL OF GRADUATE STUDIES

This is to certify that the thesis prepared

By: Narges Roofigari Esfahani

Entitled: "Control and Fault Accommodation for Attitude Control Subsystem of Formation Flying Satellites Subject to Constraints"

and submitted in partial fulfillment of the requirements for the degree of

Master of Applied Science

Complies with the regulations of this University and meets the accepted standards with respect to originality and quality.

Signed by the final examining committee:

_____ Chair
Dr. M. Z. Kabir

_____ Examiner, External
Dr. W. F. Xie, MIE To the Program

_____ Examiner
Dr. L. A. Lopes

_____ Supervisor
Dr. K. Khorasani

Approved by: _____
Dr. W. E. Lynch, Chair
Department of Electrical and Computer Engineering

_____20_____ _____
Dr. C. W. Trueman
Interim Dean, Faculty of Engineering
and Computer Science

ABSTRACT

Control and Fault Accommodation for Attitude Control Subsystem of Formation Flying Satellites Subject to Constraints

Stringent precision requirements, communication limitations and automated fault accommodation are three important considerations that need to be taken into account in design of formation control of satellites. In this work a more accurate relative state modeling for the attitude dynamics is developed and a semi-decentralized control strategy is proposed that is accomplished by the model predictive control (MPC) scheme. The proposed MPC incorporates the effects of the actuator constraints in design of the control laws. Furthermore, a semi-decentralized active system recovery scheme is proposed that uses on-line fault information to compensate for the identified characteristics losses under actuator fault conditions.

Simulation results for a team of four satellites in formation are presented and the formation precision is compared with the centralized scheme. The results verify that the proposed semi-decentralized strategy yields a quite satisfactory formation performance in a sense that the team behaves similar to a centralized MPC control scheme, however without imposing significant computational complexity that is associated with solving the problem of high dimension with stringent communication requirement as in the centralized scheme.

Moreover, the performance of our proposed semi-decentralized recovery scheme is compared with the centralized recovery scheme subject to the reaction wheel (RW) faults in the attitude control subsystem (ACS) of the formation flying satellites. The proposed semi-decentralized recovery scheme satisfies the formation recovery specifications and also imposes lower fault compensation control effort cost as compared with the centralized recovery scheme. It has been validated through multiple fault severity scenarios.

Acknowledgements

I would like to express my deep gratitude to my supervisor Prof. Khorasani for his patient guidance, support and useful critiques of this research work. His expertise contributed considerably to my research experience. I gratefully acknowledge the support of this research by Concordia University through bursaries and teaching assistantship. I would like to express my appreciation to my committee members Prof. Lopes, Dr. Kabir and Dr. Xie for their time, support and guidance through the review of this thesis. Finally I want to thank my parents and my sisters for their love and persistent support and I am thankful to my friends for helping me overcome the obstacles. I greatly value their friendship.

Contents

List of Figures

List of Tables

List of Acronyms

Γ	Control effectiveness loss matrix
$\hat{\mathbf{I}}$	Principle line
$\mathbf{q}$	Quaternion vector component
ω	Angular velocity
ω_w	Wheel angular velocity
$\overline{\mathbf{q}}$	Quaternion vector
$\overline{Q}$	Terminal cost
Φ	Quaternion principle angle
Π	Viscous friction loss matrix
τ_v	Wheel viscous friction
G_d	Driver gain
h	Satellite angular momentum
h_w	Wheel angular momentum
I_s	Satellite inertia matrix
I_w	Wheel inertia matrix
K_t	Motor torque constant
N	Prediction horizon
N_m	Motor torque

N_r	Reaction torque
Q	State penalty matrix
q_4	Quaternion scalar component
R	Input penalty matrix
T	Temperature
T_c	External control moment
T_d	Disturbance torque
T_e	External torque
u	Controller torque command
ACS	Attitude Control Subsystem
ART	Adaptive Resonance Theroy
CFTOC	Constrained Finite-Time Optimal Control
CSP	Constraint Satisfcaiton Problem
DRE	Differentail Riccati Equation
DSM	Dynamic Safety Margin
EKF	Extended Kalman Filter
FDI	Fault Detection and Identification
FDIR	Fault Detection, Identification and Recovery
LQR	Linear Quadratic Regulator
MPC	Model Predictive Control
PI	Performance Index
RW	Reaction Wheel
SPC	Subspace Predictive Control

UAV Unmanned Aerial Vehicle

VSRC Variable Structure Reliable Control

Chapter 1

Introduction

1.1 Statement of the Problem

The attitude control subsystems (ACS) of the formation flying satellites coordinate the orientation of satellites. Stringent precision requirements, communication limitations, physical limitations of the process and fault tolerance are of major importance in the design of formation control. Firstly, the closed-loop control structure including the system modeling and the corresponding measurements provide different levels of precision in the formation control. Secondly, developing a semi-decentralized scheme reduces the computational complexity and the communication requirements. Thirdly, considering physical constraints of the components, e.g., actuator saturation constraints, in determining the control law increases reliability of the control design, and finally, utilizing the system with a fault accommodation scheme, yields a graceful recovery performance of individual agents and an acceptable level of formation precision under the fault conditions. In the following section we review the available approaches for addressing the aforementioned issues.

1.2 Previous Work

In this section we review the available works with emphasize on the formation control and fault accommodation schemes.

1.2.1 The Coordination Methods and Information Distribution for Multi-Agents Formation Control

Multi-agent systems are becoming more popular in a wide range of applications. Formation flying satellites exhibit numerous advantages in many space missions. For data collection applications it allows integration of data from several satellites and inferring an accurate measurement instead of employing multiple instruments on a single satellite. According to NASA's Goddard Space Flight Center (GSFC), satellites formation flying is defined as: [1]

"The tracking or maintenance of a desired relative separation, orientation or position between or among spacecraft."

Performing a team task in a multi-agent system requires coordination among agents. This coordination can be accomplished through different control distribution schemes namely centralized and decentralized methods. Smith and Hadaegh in [2] described decentralization as a trade-off between formation performance and complexity of the controller and communication requirements. They considered decentralization for both design and implementation. In the decentralized design the actuation of each individual agent is calculated based on a subset of formation variables as opposed to all. This subset of information requires certain exchanges among agents. In the decentralized implementation the individual controllers determine their local actuation in contrast to a central controller which determines all the required actuation and communicate that to all agents. The design for these local controllers can be either a centralized or a decentralized design. The semi-decentralized control is the term

used by Semsar and Khorasani in [3] to convey the interactions through the control design and the independent operation of the regulators through a decentralized control implementation scheme. In contrast to this scheme, in a distributed control scheme, as defined by Scattolini in [4], some information is transmitted among the regulators and the regulators do not operate in a completely independent fashion. In this framework, some information is transmitted among agents such that each of them has knowledge on future behavior of the others. The main idea of decentralized, semi-decentralized and distributed frameworks is to break a centralized problem into problems of smaller size. This approach is profitable in terms of computational complexity, communication requirements and not being affected by the problem of one point of failure for the entire team, but at the same time the solution will be suboptimal in terms of cost and task coordination. Another challenge for this approach is to ensure that the distributed decision making causes consistent actions among the agents.

Another specification for the multi-agent formation control is their formation coordination method. Three important methods are leader-follower, virtual structure and behavior-based.

In a leader-follower structure, one or more agents are designated as leader and the rest of the agents follow their path such that their relative state is kept as desired [5–8]. This architecture is employed in the missions where the group trajectory is strict and becomes executed by the leader. In this architecture the objective for the followers is formation keeping which is translated to a regulation or tracking problem. In this structure there is no feedback from the followers to the leader and the leader determines the overall behavior of the team in an open-loop fashion. It has the disadvantage of an inherent single point of failure feature.

In the virtual structure method, the idea is that all agents follow a virtual leader [9, 10]. Once the virtual leader trajectory is determined, similar arguments applied to the leader-follower structure can be applied to this architecture and the implementation

Table 1.1: Comparison of Coordination Methods

		Method	
		Leader-Follower / Virtual Structure (non consensus-based case)	behavior-based
characteristic	Mission Application	Leader trajectory : strict and open-loop with respect to followers	Assignment of desirable behavior to each agent
	Formation Keeping Complexity	Simple and straightforward	More complex because of interactions
	Individual Goals	Regulating relative state with respect to the leader	Pairwise relative states tracking and possibility of including individual states tracking
	Behavior in The Presence of Fault	Fault in the leader: problem of a single point of failure, Fault in the followers: open-loop operation of leader and thus incapable of team compensation	Capable of incorporating compensation strategies because of the close interactions among agents

is similar. However the strategy for the virtual leader trajectory determination specifies the formation characteristics. This trajectory can be either a fixed information communicated to all the agents, it can be obtained through implementing a consensus strategy among agents, or it can be a combination of these. By specifying a consensus reaching strategy, the structure becomes more flexible as each agent's movements can be influenced by others and all the agents actively influence the formation performance as opposed to the case where the virtual leader acts independently. Communication topology is a key factor that influences accomplishing the consensus among agents and consequently the stability of the entire system. The consensus also creates synchronization among agents. In this structure finally the whole structure behaves as one rigid body. The simple form of the virtual structure architecture, where the virtual leader information is communicated to all agents, shares all the disadvantages corresponding to the leader-follower structure. In the more complex scheme the

problem of consensus exists. In this case there is not a leader for the followers to follow so they must reach to an agreement through some strategy.

The third structure is the behavior-based structure [11, 12]. This structure fits certain types of formation mission where rather than an strict formation keeping objective, the goal is to achieve multiple desired behaviors including goal seeking and formation keeping. The final control move is determined based on a performance index that consists of a weighted average for achieving each behavior. Therefore this structure is more flexible and also, has the potential to exhibit a desirable performance in the case of fault. In Table 1.1 we highlight some important characteristics of this structure by comparing it with other two architectures. In the formation missions, a proper cooperative control between the pairs of agents through the behavior-based structure ensures connectivity and successful team performance rather than relying on a leader in leader-follower based architectures. Depending on the priority executed on the control strategy in this architecture, the set of agents would be stricter in individual or team performance criteria.

Followed by the coordination task imposed on the multi-agent systems, the overall dynamics of the system is more complicated when compared with the single agent system. This is due to the coupled nature of multi-agent systems as each agent relies on the behavior of the adjacent neighboring agents. In other words, controlling each agent is a function of its states and its adjacent neighbor's states. Adjacent neighbors are the agents that have a direct communication. Thus the overall system can be considered as a system with multiple inputs and outputs.

1.2.2 Decentralized Formation Control

An optimal control method relies on an internal model of the system. In the formation control, if a cooperative design based on relative states is desirable, then the internal model will generally include the neighboring agent's input signal as variables in

an optimal control strategy. Therefore, due to the explicit presence of neighboring agent's input signal as variables in the local control design, a decentralized control implementation does not seem to be achievable unless one imposes the assumption of fixed dynamics for the neighboring agents when performs the design of each local controller [3, 13]. Due to this feature of the optimal control method most of the available research focusing on decentralized formation control implementation utilize other types of control laws such as PD or output feedback [10,11,14–16]. The drawback of these methods is that the input constraints cannot be incorporated into the design solution.

Wang and Davison in [15] analyzed the stability of a decentralized scheme which relies on local control stations with output-feedback based control law (dynamic output feedback). The stability is related to the input-output relations in each local controllers that can be inferred through the controllability and observability features. The notion of fixed-modes is introduced to provide the necessary conditions for the stability of the system. The actuator saturation constraints can not be taken into account through their proposed control law.

In the work published by Chang *et al.* in [13] the decentralized formation keeping control is based on relative dynamics. In this work a decentralized control implementation is achieved by making the relative dynamic equations employed in each individual controller input-decoupled by analyzing the relative dynamical behavior within the proximity of a certain operating condition. The linearized input-decoupled relative dynamics equation is valid for the specified operating point and is not generic. This is the main drawback of this scheme. The final control input is considered to be the weighted sum of control moves corresponding to the relative states for each pair of agents.

Lawton *et al.* in [14] introduced a decentralized scheme for formation maneuvers. They developed a behavior-based approach and proposed the control law for achieving

the desired behaviors. In their approach which they labeled, coupled dynamics approach, two competing behaviors of goal seeking and formation keeping are considered and the objective is that vehicles stays in formation while reaching the final goal. The local feedback is from both relative and absolute measurements. The proposed control law has the advantage of not relying on internal model of the system. Lawton and Beard in [11] developed a leader-follower and behavior-based control law for attitude formation maneuver. However, the actuator saturation constraints can not be incorporated in this design scheme. Ren and Beard in [10] modified the control law which was proposed by Lawton to develop a decentralized virtual structure scheme for the same application.

Semsar and Khorasani in [3] designed a semi-decentralized optimal controller. In this optimal control design, the objective function includes an individual term and an interaction term. Solving the optimization problem is performed by making the assumption that other agents dynamics are fixed and the effect of other agents are incorporated in the design through the interaction terms. Finite and infinite horizon cases for the optimal controller are both analyzed where in the former case a differential riccati equation (DRE) must be solved and in the latter case an agreement protocol is given as the solution to the problem.

1.2.3 Model Predictive Control (MPC)-Based Formation Control

The model predictive control (MPC) method has been widely used in various control applications. In the survey by Garcia *et al.* [17] the constraint handling capability of MPC is highlighted. Morari and Lee in [18] provide an overview of this method and describe the evolution of the formulation since its origins. Reader is referred to [19] and [20] for a detailed formulation of linear MPC problem. On-line computational efforts involved in the MPC design is relatively high which is one of limitations of this

method [21–24].

Finite horizon numerical-based methods such as MPC provide a more flexible formulation of an objective function which allows incorporating the neighboring agent's dynamics in each local control design as opposed to imposing the assumption of fixed dynamics for the neighboring agents. This method requires prediction of the states during future horizons while no explicit requirement exists to include neighboring agent dynamics into the design as long as the predicted values are provided in the optimization problem. However, providing these information imposes significant communication requirements on the system. The methods proposed by [25–30] rely on exchange of optimal solutions in the form of the predicted values or the planned data that are transmitted from the neighboring agents and this imposes stringent communication requirements for every control update.

Longhi *et al.* in [27] worked based on a leader-follower structure and utilized a decentralized MPC control as a supervisory module which plans the movements in a way that the relative states track the desired values. In this work every leader communicates the resulting control move to its followers. They need the information as an interaction vector, that is, a reference for future behavior of their neighbor to be able to perform a proper prediction for their own behavior since their relative states depend on future moves of their neighbor as well. Then the next follower which is the leader for a couple of other agents performs the same task. The key point here is considering each relative state a function of control moves corresponding to each of the involved agents and thus, a coupled dynamics for the relative states. However the formation is achieved by a leader-follower structure which inherits the problem of single point of failure. Also the communications load is very high because of communicating the control moves to the followers. The movements are implemented in a vehicle level by allocating proper inflation and drive to the bladders.

In the paper published by Hadaegh *et al.* [26] MPC is aiming at tracking the

desired absolute state values rather than relative. The coordination among agents is achieved by transmitting optimal predicted states by the leader and online calculation of desired follower states at each instant of prediction horizon accordingly.

Dunbar and Muray in [25] discussed both centralized and distributed control of multi-vehicle formations. The control strategy that they used was receding horizon. They compared stability issues in these two cases. In the centralized control the only information about agents required by the central controller is their current states while in distributed control future control trajectory for neighboring agents is also required for each agent. This data will be communicated prior to the next receding horizon update for each agent. This is because in distributed control, considering each individual agent, the variables to be determined by the controller are only control moves for the same agent as opposed to the centralized case where all control moves were determined by a central controller. However, the communication imposes a large communication load on the system.

Keviczky *et al.* in [31] discussed a degree of conservatism introduced by a decentralized approach. Authors in [32], which is based on the receding horizon control scheme, proposed an approach in which a decentralized formulation does not rely on the exchange of optimal solutions among the neighbors and they provided the necessary conditions for ensuring the stability of their approach. Their strategy involves solving the optimization problem as a function of the input of each agent itself and its neighbors. At the implementation level, the inputs for the neighbors are discarded and only the first sample of the control trajectory for the corresponding agent was implemented. They also presented their methodology on the application of coordination of autonomous vehicle formation in their work published in 2008 [33].

The reference [28] implemented robust decentralized MPC for a a team of unmanned aerial vehicles (UAVs) and compared the decentralized and centralized schemes in terms of computation time and target arrival time.

In a cooperative MPC-based framework, the predictions of the neighbors states must be provided in a local control design. Thus either the predicted values must be transmitted from agents or determined in the same agent. The next two sections discuss the significance of providing a system recovery scheme in formation flying satellites.

1.2.4 Formation Flying Satellites Fault Accommodation

Utilizing multi-agent systems with fault detection, identification and recovery (FDIR) is a new area of research which has been extensively studied in different applications. Consider formation flying satellites for instance, they offer many advantages in space missions including space interferometry and defense but at the same time are considered as safety critical systems and depending on the coordination policy and the required performance specifications, one ill-managed fault might cause the whole mission to fail or impose large costs to the system. Therefore, incorporating an automated active fault accommodation in satellites will save costs and increase the reliability in terms of mission success by obtaining an acceptable degraded performance.

Adaptive control-based methods are widely used for developing fault accommodation schemes. Reader is referred to [34] as a comprehensive study of adaptive control schemes and their stability analysis. From the point of view of controller design in the fault condition, one can perform the design based on an explicit plant model or based on an implicit plant model. The former results in a control scheme in which the controller parameters are adapted indirectly according to the fault estimates without relying on an estimation update law [35, 36]. The control design must be parametrized with respect to the fault estimates and the controller parameters be selected such that the desirable specifications are satisfied. The latter relies on the controller parameters adapted directly through updating their estimates and the fault accommodation scheme relies on this fault compensating update law such that the

stability of the system is guaranteed [37, 38].

Semsar and Khorasani in [37] developed an adaptive control for the position of UAV leader-follower formation, based on the estimates of uncertainty. In their adaptive Lyapanov-based control framework, ensuring the magnitude limits of control signal is not guaranteed. The reference [35] also assumed a formation flying with a leader-follower structure and developed a fault-tolerant scheme for the follower vehicle. They assumed that vector of control inputs is a redundant control. The reconfiguration is performed by updating the corresponding control allocation matrix in adaptive way to deal with possible fault detection and identification (FDI) inaccuracies during the course of time. Their assumption is not practical and cost efficient for many applications because it requires presence of multiple actuators producing same effect on the plant dynamics.

A direct adaptive control scheme provides a certain level of robustness with respect to the fault uncertainties. However, the imposed extra design constraints in these schemes results in a trade-off between the performance and robustness which might be undesirable in some applications. Furthermore, an indirect adaptive scheme or an active reconfiguration mechanism can be adjusted to address a wider range of abnormalities. This is achieved at the expense of utilizing a fault detection and identification (FDI) module and also providing an active fault accommodation strategy rather than an adaptively compensating scheme.

Azizi and Khorasani in [39] used relative-state measurements in their framework and proposed a two-level accommodation approach which decomposed the control law into two parts. One part addressed the closed-loop system stability and the other, the tracking-error performance. The closed-loop system stability was shown to be guaranteed even in the presence of inaccurate fault estimation. The tracking-error performance was guaranteed to be zero in fault-free condition or when the fault was accurately estimated. This is not a realistic assumption because in practice there is

always a limited error in estimating the magnitude of fault. The authors addressed this problem by adjusting the controller parameters according to an achievable tracking-error specification which was suggested to be determined by solving an optimization problem. They did not address accommodating the absolute states of satellites in fault condition. In addition, control signal limits are not guaranteed to fit within the allowable limits by their method of control.

Authors in [40] provided passive and active variable structure reliable control (VSRC) control design laws subject to actuator faults and analyzed the performance of two schemes. In an adaptive Lyapanov-based control framework [37], and conventional linear dynamic output feedback [39] control signal limits were not guaranteed to fit within the allowable limits.

FDI is one important part of any active fault tolerant system. This module performs detection, isolation and identification (diagnosis) of the faults in a system. Comparing the actual output of the system with an index from a redundant component yields a monitoring for the status of the system and further analysis on the residual signal yields isolation and identification. The concept of FDI is based on utilizing the system with the analytical redundancy. In general, redundancy can be hardware or software redundancy. Hardware redundancy has many limitations and for many applications utilizing a redundant component is either impossible or expensive. Software redundancy or analytical redundancy requires *a priori* knowledge about the system.

Considering the required *a priori* knowledge, FDI methods can be grouped into two important diagnostic algorithms, namely, model-based methods and historical-data based methods. The first category requires a fundamental understanding of the system which can be described by a mathematical model of the system. There has been extensive research in this area. Hwang *et al.* in [41] discussed various FDI model-based techniques. Venkatasubramanina *et al.* presented a review paper [42] which includes important remarks about model-based FDI with their focus on process control.

Quantitative model-based FDI approaches consists of observer-based method [43–45], parity space method [46] and extended kalman filter (EKF). Moreover, the concepts of system identification can be utilized for the purpose of fault detection. For instance parameter estimation methods such as least square parameter estimation can be adapted for this goal as proposed by Isermann in [47]. Gertler in [48] presented the residual generation methods of model-based FDI and compared the procedure required for residual enhancement for each of these method. Residual enhancement can be accomplished by two main approaches, namely, structured residuals and fixed-direction residuals.

Frank and Ding in [49] focused on fault detection using observer-based approaches in a robust fashion. Fault detection is the first step for a FDI. The detection will be carried out by residual generation and residual evaluation using a decision function. Patton and Chen in [50] discussed observer-based fault detection and isolation with its robustness issues. Utilizing parity relations for the purpose of fault detection and isolation is another important method of residual generation. Gertler in [48] showed that any model-based residual generator can also be expressed in the form of parity relations. The same author in his other work [51] presented the methodology for developing parity equations for the purpose of FDI for additive and parametric faults. The derivations from both transfer function and state space representation were outlined.

Hostiorical-based methods are the second group of algorithms that provide a tool for FDI [52–56]. These methods require large amounts of historical data. Srinivasan *et al.* in [53] employed neural networks for the purpose of fault detection and isolation. They solved the least square problem of parameter estimation by using a Hopfield network. This way they took advantage of parallel processing capability of the Hopfield networks. The process of fault detection is carried out based on identifying some transition zones for the estimation errors (residuals). These zones are identified

by performing statistical tests during certain intervals (moving window). It was established in this work that when the system is in transition period, due to a fault occurrence, some statistical quantities such as auto-correlation, mean and sum of squares will change from zero (corresponding to white noise) to a non-zero value. The next contribution of the work was to perform fault isolation by classifying different fault situations. They used adaptive resonance theory (ART) neural network to introduce an unsupervised learning environment and clustering algorithm capable of identifying new unencountered faults.

Integration of FDI and recovery module is an important issue in FDIR. Patton in [57] discussed the interactions of FDI and the control system. Three approaches are possible for this integration. (i) An open-loop approach is defined as the case where the FDI module has no effect on the control function. In this case, the control system influences the FDI operation and can influence the residual signals and violate the capability of the FDI to detect or isolate a fault. Therefore, FDI robustness with respect to the control signal must be provided. (ii) As suggested by [57], another approach for integrating FDI and the controller is establishing a relation between the FDI information and the controller. Once the fault is diagnosed by the FDI, the recovery module starts the fault accommodation. This procedure can be carried out through controller reconfiguration or controller re-structuring. The former performs the recovery without changing the control philosophy while in the latter, a new control structure is employed. Reader is referred to [58] for a more detailed discussion of reconfigurable control. (iii) Another strategy is developing a robust FDI approach and mixing the control design and fault estimation. Imposing the extra design constraints, results in a trade-off between the performance and robustness which is not desirable for the precision control applications.

1.2.5 Satellite's Reaction Wheel (RW) Fault Accommodation

Satellite instrumentation including sensors and actuators are prone to develop a malfunction. Actuators are important components of a satellite. Basically, they provide translational and angular accelerations. Actuators are heavier compared with the sensors, and it is impossible for certain applications to provide the system with redundant actuators. Thus studying its fault and analytic redundancy is of importance.

According to Sidi [59] and [60] there are four general classes of control actuators as sources of force and torque, namely, propulsion systems, solar radiation pressure, momentum exchange devices and magnetic torqrods. Momentum exchange devices allow distribution of momentum inside the satellite without changing the total inertial momentum of the entire system. Due to this intrinsic property, they do not involve fuel expending. They are electrically powered and thus, are well suited for long duration missions. We consider the attitude control subsystem (ACS) actuator to be a momentum exchange device. There are two basic momentum exchange devices, namely, momentum wheels and reaction wheels (RWs). The former kind is primarily used for inertial attitude stability and the latter for attitude tracking control and maneuvering. We focus on reaction wheel devices as the source of actuation.

Drawbacks of RW are relatively small effective torque produced and possible RW saturation [61]. The latter drawback is related to physical limitations of this device. In other words, it can not exert more than a certain amount of torque. An accumulated influence of disturbance torques will impose excessive torque on wheels through the control law and causes it to saturate [62].

When a defect due to a partial malfunction of the RW occurs in a satellite, its maneuverability deteriorates. As an example, Dawn, NASA's spacecraft dedicated to collecting data in space, experienced a RW fault in August 2012 [63] . The nature

of the RW fault was increased friction. The system software responded by turning the wheels off. The accommodation action to resume the mission was made from the ground station by switching to thrusters for attitude control. NASA's Mars Odyssey, the longest-working spacecraft ever sent to Mars, experienced a RW fault in June 2012 [64]. One of the three primaries RW was temporarily immobilized. In response, the system software placed the satellite in a reduced-activity mode. In order to recover, engineers from the ground station switched from the immobilized wheel to a spare.

1.2.6 Model Predictive Control (MPC)-Based Fault Accommodation

Due to the online control design in model predictive control (MPC), this method is more robust than static feedback control mechanisms and has the capability to deal with certain faults even without reconfiguration. Moreover, it is possible to incorporate robustness with respect to model uncertainties in the MPC design [65–68]. For the applications where there are no redundant actuators, an active system recovery strategy can be executed and the MPC controller can be reconfigured according to the data received form the FDI module. This property is attributed to the control signal being computed at each sample time making changes to the problem formulation possible. It also has the capability to find solutions near the constraints which is the case when a fault occurs. Moreover, in some cases the nature of fault is nonlinear, for instance, the fault of actuator stuck. In those cases, the input constraints which are nonlinear components of the MPC strategy can handle it. In addition, depending on the type of fault, fault occurrence is likely to result in increased torque demand by the controller and yielding actuator saturation which can be avoided by using the MPC method [69].

One important issue in developing an MPC controller with set-point regulation objective is the problem of feasibility of the equilibrium point. In the set-point

regulation problem for nonlinear systems using linear control methods, it is necessary to have knowledge about the steady-state value of the input that maintains the desired set-point, which according to [70], can be sensitive to parameter perturbations. In order to maintain the MPC problem a feasible optimization problem, the input set-point values must be reconfigured such that its value become an equilibrium-point for the faulty system. Once the input set point is reconfigured, the input constraints also need to be reconfigured. There are different approaches suggested in literature for recovering the system model from infeasibility. Extensive research has been dedicated to the stability of this methodology of control and provided relevant sufficient conditions in this regard.

The mismatch between internal model of the MPC and real process on the other hand, does not cause infeasibility of the problem but will create an offset between the desired set point and the final values, thus, it must be reconfigured such that an accepted performance will be achieved. In developing a robust MPC the mismatch can be captured by a disturbance model and further analysis is required to tackle the resulting offset [71].

An active fault tolerant MPC scheme accommodates faults by re-designing the control design using direct fault information from the FDI module [72–78]. Authors in [72] discussed the integration of FDI and recovery module in detail. They proposed a recovery strategy based on a modification made on the MPC formulation, particularly, for soft faults such as bias in the actuator or sensor. The modification they made is adding extra innovation terms in the MPC internal model. For producing robustness with respect to FDI information, they introduced an integral action in the added term and therefore, the error in the estimated faults will be corrected in the course of time. They compared it with the conventional method. In the conventional approach MPC state space model is integrated with state observers with new states representing faults or model mismatches in the system. Consequently conventional

approaches can guaranty fault tolerance for limited number of faults that does not deteriorate observability condition. Although their proposed method is not efficient in terms of determined control signal but it can handle actuator and sensor fault simultaneously. Kerrigan *et al.* in [73] demonstrated the relative robustness of MPC in the presence of internal faults in a ship propulsion system and active fault tolerance is practiced for sensor fault by utilizing FDI information for making correction to faulty sensor measurements. Miksch *et al.* in [74] presented an online accommodation of actuator faults using the MPC. Different issues involved in this practice has been investigated including feasibility evaluation of control problem after occurrence of fault and its corresponding solutions yielding a feasible solution but a degraded performance. Authors in [79] developed an MPC scheme that is capable of compensating for faults of communication loss/delay in cooperative multiple vehicles. Joosten *et al.* [80] proposed incorporating a control allocation strategy in the MPC framework towards providing fault tolerance.

The MPC method can be joint with other techniques through modifying its formulation for developing a fault tolerant scheme. Examples include subspace predictive control (SPC), dynamic safety margin (DSM) and admissibility evaluation using constraint satisfaction problem (CSP) techniques [81–83].

1.3 Thesis Contributions

The contributions of the thesis are listed below.

1. A more realistic linear dynamical modeling of satellites is used in the control design instead of a simplified model that is used in most of the available literature. The objective is to improve the formation precision and also to handle component faults by developing an online recovery scheme. The linear dynamical model of a satellite that is used for the control design is improved in terms of satellite

absolute dynamics as well as the relative dynamics. In particular, (i) the actuator dynamics is included in a single satellite dynamical model that enhances the representation precision due to the use of a more realistic model that also results in fault handling capability , and (ii) a more precise approximation of the relative attitude dynamical model is obtained by using similarity transformations that contributes to an improved formation precision.

2. A behavior-based formation control strategy is proposed in which the objectives of the behavior-based control are specified as (a) goal seeking where a desirable orientation is assigned to each individual agent to track, and (b) formation keeping where the relative orientation of the agents is maintained to a desirable value. Associated with the second objective, the relative state measurements and the coupled dynamics model are used for achieving the desirable formation behavior. In other words, we propose to incorporate the interactions among the agents in the control design by using coupled dynamics model. The coupled dynamics model contributes to achieving a precise formation by (i) providing a precise knowledge through a relative attitude determination system [84] and (ii) development of a novel behavior-based control scheme based on coupled dynamic modeling.

3. A semi-decentralized MPC-based scheme is proposed that satisfies the formation control objectives and mitigates the computational complexity and communication requirements as demonstrated quantitatively through simulation studies.

4. The centralized approach to solving the problem is presented and the proposed semi-decentralized approach is compared with this centralized approach in the simulation studies and the improvements and limitations are identified.

5. The decentralized approach to solving the problem is presented and the proposed semi-decentralized approach is compared with this non-cooperative decentralized

approach in the simulation studies and the improvements and limitations are highlighted.

6. The centralized LQR-based approach is provided and its performance is compared with the centralized MPC-based approach in the simulation studies and the improvements and limitations are highlighted.

7. A two-level active system recovery strategy is proposed that incorporates the fault information into the semi-decentralized MPC-based control to compensate for the identified characteristics losses. The local-level recovery accommodates the faulty agent's performance by using local fault information and the formation-level recovery enhances the recovery performance by reducing the oscillatory behavior.

8. A centralized recovery scheme is provided and the formation system recovery performance by using this centralized recovery approach is compared with our proposed semi-decentralized recovery scheme subject to the RW faults in the ACS of formation flying satellites.

9. A decentralized recovery scheme is provided and its limitations subject to the RW faults in the ACS of formation flying satellites are analyzed in the stimulation studies.

1.4 Conclusions

In the most of the current works in the domain of attitude motion control of satellites, actuator dynamics and constraints are not taken into account and this component is characterized as an ideal component. In this thesis, the actuator dynamics is incorporated in the satellite modeling to obtain a more realistic model for the satellite, in fault free and actuator fault conditions. A more realistic modeling contributes to

achieving more precision in the formation control. Moreover, by taking the actuator dynamics into account in the control design, the recovery of the system under certain fault conditions that are related to the higher order dynamics will also be realized.

The relative-state based control of attitude motion is specifically of interest due to high-precision capabilities of relative attitude determination systems. The nonlinearity of the relative-state dynamics with respect to absolute states, which has not been included in the available linearized relative dynamical modeling in the literature, is taken into account in this work by combining relative and absolute states through utilizing suitable coordinate system transformation, and results in introducing a more accurate relative dynamical modeling and development of a novel behavior-based control formulation based on coupled dynamic modeling.

The stringent communication requirements problem involved in the cooperative formation control inspired us to develop a semi-decentralized MPC-based scheme because the reliance of communicating the input information among agents within a dynamically coupled MPC approach, yields excessive communication requirements. Therefore, individual subsystems are characterized such that the predictions are performed based on the input information of each individual agent. Using this strategy each agent undergoes a lower level of computational load and communications with neighbors. The proposed semi-decentralized scheme takes into account actuator dynamics and the actuator constraints.

Fault in actuators, a control component of the system, can lead to loss of convergence or an offset from the desirable steady-state values. An ill-managed fault can cause the whole mission to fail or impose large costs to the formation system. To avoid the aforementioned problems, an active system recovery scheme is developed that incorporates the fault information into the semi-decentralized MPC-based control to compensate for the identified characteristics losses. The recovery strategy accommodates the faults in two levels. The first level recovers the faulty agent performance by

using a local recovery scheme, and the second level enhances the recovery performance by using a formation recovery scheme. This study focuses on two common faults on the satellites RWs, namely loss of effectiveness and friction faults. These faults were identified as sources of RW malfunction in two of the recent reports corresponding to Mars Odyssey and Dawn, NASA's spacecraft and as mentioned previously, were handled by switching to redundant components. Providing an automatic fault recovery scheme, as addressed in this work, reduces the mission cost significantly by not relying on the need for component redundancy. The FDI channel accuracy and time delay considerations are taken into account in the simulation studies.

The organization of this thesis is as follows. Chapter 2 covers a single satellite attitude dynamics modeling and also formation flying satellite relative dynamics modeling and the information flow structure. Two common RW faults are described and their mathematical modeling is presented and two optimal control-based methods of MPC and LQR are explained. Chapter 3 discusses the proposed semi-decentralized MPC-based approach for fault-free condition. In this chapter the proposed semi-decentralized control design is compared with centralized and decentralized control schemes. A centralized LQR-based approach is also provided and compared with the centralized MPC-based scheme. Chapter 4 focuses on faulty case and investigates the performance of the proposed semi-decentralized system recovery strategy by comparing it with other schemes, namely, centralized and decentralized recovery schemes. Finally in Chapter 5 concluding remarks of this study are summarized and the potential future works are suggested.

1.5 Publication of the Author

- [Submitted] N. R. Esfahani and K. Khorasani, "Model predictive control (MPC)-based attitude control of formation flying satellites: A semi-decentralized ap-

proach," in *European Control Conference*, 2014.

Chapter 2

Background Information

In this chapter the kinematic and dynamic equations describing the attitude motion of a single satellite are provided. The reaction wheel (RW) which is a very common actuator in satellites and its dynamics are included in this modeling. The formation flying satellites information flow, and the relative motion dynamics are presented, and the mathematical modeling of fault in this component of the attitude control subsystem (ACS) is provided. Finally, the model predictive control (MPC) and the linear quadratic regulator (LQR) frameworks are briefly explained.

2.1 Single Satellite Attitude Dynamics and Its Linear Model

2.1.1 Attitude Representation

Attitude dynamics describe the rotational motion of an object about its center of mass [59, 85]. There exist alternative representations for parametrization of the attitude of an object in three dimensional space such as direction cosine matrix, Euler axes/angle, Euler symmetric parameters (quaternion), Gibbs vector and Euler angles. Reader is referred to [85] where a comparison between these methods is presented.

Diebal in [86] provided a detailed theory, for conversion among direction cosine, Euler angles and quaternion representations, and their key properties. In this study, the quaternion representation is selected for the control design. The reason behind this selection is that they are free from the problem of singularity that exists in the Euler angles representation. Also number of redundant parameters is less than direction cosine matrix representation (four versus six). Furthermore, Quaternion parameters follow a convenient product rule that is efficient for successive rotations. Nevertheless, there exists a constraint in quaternion parametrization which is known as unit norm constraint. One approach to deal with this constraint is using reduced quaternion model for control design [87]. In this approach the constraint will be satisfied in a natural way. However, there exists one point corresponding to the principle angle of π at which the reduced model is not valid. Another approach is performing a normalization on quaternion parameters to impose the constraint to be satisfied. This task must be carried out in each control design iteration. In this work the second approach is used in order to provide a universal design for the attitude control without any invalid point. Sun and star sensors can provide the data for inertial-pointing missions and according to [88] are compatible with inertial quaternions.

In the quaternion formulation, the quaternion vector is defined as

$$\overline{\mathbf{q}} = \begin{bmatrix} \mathbf{q} \\ q_4 \end{bmatrix} = \begin{bmatrix} \hat{\mathbf{I}} \cos\left(\frac{\Phi}{2}\right) \\ \sin\left(\frac{\Phi}{2}\right) \end{bmatrix} \tag{2.1}$$

where $\mathbf{q} = \begin{bmatrix} q_1 & q_2 & q_3 \end{bmatrix}^{\mathbf{T}}$, q_4 , Φ and $\hat{\mathbf{I}}$ are a vector part, a scalar part of quaternion, a principle angle and a principle line, respectively. There are two important operations corresponding to the quaternion, namely, an inverse quaternion and the quaternion multiplication which are given by equations (2.2), (2.3), respectively.

$$\overline{\mathbf{q}}^{-\mathbf{1}} = \begin{bmatrix} -\mathbf{q}^T & q_4 \end{bmatrix}, \tag{2.2}$$

and

$$\overline{\mathbf{q}}_{\mathbf{c}} = \overline{\mathbf{q}}_{\mathbf{a}} \otimes \overline{\mathbf{q}}_{\mathbf{b}}, \tag{2.3}$$

where the multiplication operator $\otimes$ is defined as

$$\overline{\mathbf{q}}\otimes = \begin{bmatrix} q_4 & q_3 & -q_2 & q_1 \\ -q_3 & q_4 & q_1 & q_2 \\ q_2 & -q_1 & q_4 & q_3 \\ -q_1 & -q_2 & -q_3 & q_4 \end{bmatrix}. \tag{2.4}$$

In the next section, the nonlinear dynamics and kinematic equations of a single satellite attitude motion using quaternion representation are discussed.

2.1.2 Nonlinear Dynamics and Kinematic Equations

The attitude measurements are made in the satellite body-fixed frame and it is required to consider its motion in this frame which we call hereby as "rotating coordinates".

The satellite kinematic will be obtained by taking the time derivative of the quaternion as discussed in [86]. Finally equations (2.5) and (2.6) describe the satellite kinematic equations.

$$\dot{\mathbf{q}} = -\frac{1}{2}\left[\omega\times\right]\mathbf{q} + \frac{1}{2}q_4\omega \tag{2.5}$$

$$\dot{q}_4 = -\frac{1}{2}\omega^T\mathbf{q}, \tag{2.6}$$

where $\mathbf{q}$ is the vector part of quaternion and $\omega = \begin{bmatrix} \omega_1 & \omega_2 & \omega_3 \end{bmatrix}^{\mathrm{T}}$ is the angular velocity of the satellite in the coordinate system defined above. The operation $[\omega\times]$ denotes a skew symmetric matrix and is defined as

$$[\omega\times] = \begin{bmatrix} 0 & -\omega_3 & \omega_2 \\ \omega_3 & 0 & -\omega_1 \\ -\omega_2 & \omega_1 & 0 \end{bmatrix}. \tag{2.7}$$

The foundation of attitude motion dynamics is based on the well-known Euler's moment equation (equation (2.8)). This equation describes the rate of change of any vector (A) in a fixed coordinate (I) in terms of the rate of change of that vector as observed in a rotating coordinate (B) plus a vector product involving angular velocity of the rotating coordinate (ω). [59]

$$\frac{d}{dt}A \mid_{\mathrm{I}} = \frac{dA}{dt} \mid_{\mathrm{B}} + \omega \times A, \tag{2.8}$$

This moment equation is used to derive an expression for the angular momentum of the entire system ($h \in \mathbb{R}^3$) as a function of the inertia matrix ($I_s \in \mathbb{R}^{3\times3}$) and the angular velocity of the rotating coordinate (equation (2.9)).

$$h = I_s\omega, \tag{2.9}$$

Also, the equation is used to obtain the rate of change of the angular momentum vector in fixed coordinates ($\dot{h}_{\mathrm{I}}$) to derive the satellite dynamics (equation (2.10)). Thus we have

$$T_e = \dot{h}_{\mathrm{I}} = \dot{h} + [\omega\times]\, h. \tag{2.10}$$

In equation (2.10), $T_e \in \mathbb{R}^3$ is the external torque and can be broken down into $T_c \in \mathbb{R}^3$ and $T_d \in \mathbb{R}^3$, which denote the external control moment (due to gas jets and magnetic coils) and the disturbance torques due to environmental effects, respectively. We are considering the case where the control torque is provided by reaction wheel (RW), which is one type of momentum exchange devices, instead of the propellant expelling thrusters. According to [85], the produced torque due to these devices is not an external torque and does not change the total angular momentum of the satellite. Consequently, the left hand side of the equation (2.10) is equal to T_d. A description of satellite disturbance torques is provided in Section 2.1.4.

The satellite dynamics, including the RW dynamics is subject to a slight modification. In this case the momentum of the entire system consists of the momentum of the rigid body, i.e., h_{B} and the momentum of the moment exchange devices, i.e., h_w, as follows

$$h = h_{\mathrm{B}} + h_w = I_s\omega + h_w. \tag{2.11}$$

Substituting for h from equation (2.11) in equation (2.10) yields

$$I_s\dot{\omega} + \dot{h_w} + [\omega\times]\,(I_s\omega) + [\omega\times]\,h_w = T_d, \tag{2.12}$$

where $h_w \in \mathbb{R}^3$ denotes the net angular momentum due to the rotation of the wheels relative to the spacecraft. Finally the satellite dynamics is expressed as

$$\dot{\omega} = -I_s^{-1}\,[\omega\times]\,(I_s\omega) - I_s^{-1}\,[\omega\times]\,h_w - I_s^{-1}\dot{h}_w + T_d \tag{2.13}$$

In the next section, the RW dynamics is included in the single satellite's dynamics expression.

2.1.2.1 Reaction Wheel (RW) Dynamics

The dynamics of the RW is considered to be nearly ideal [89]. The block diagram for the RW approximate model is shown in Figure 2.1.

The following differential equation holds for the wheel speed $\omega_w = \begin{bmatrix} \omega_{w1} & \omega_{w2} & \omega_{w3} \end{bmatrix}^T$.

$$\dot{\omega}_w = I_w^{-1}N_m - I_w^{-1}\tau_v\omega_w, \tag{2.14}$$

where $I_w \in \mathbb{R}^{3\times3}$ and $\tau_v \in \mathbb{R}^{3\times3}$ are diagonal matrices related to the wheels inertia and friction (viscous friction), and $N_m \in \mathbb{R}^3$ is the motor torque given by

$$N_m = G_dK_tu, \tag{2.15}$$

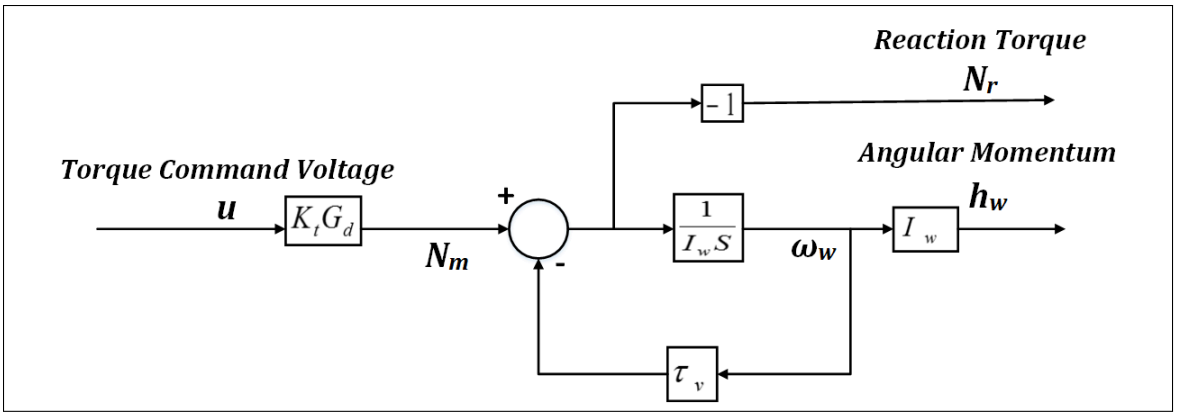

Figure 2.1: Nearly Ideal RW Block Diagram.

where $G_d \in \mathbb{R}^{3\times3}$ and $K_t \in \mathbb{R}^{3\times3}$ are diagonal matrices related to the driver gain and the motor torque constant associated with RW motor and $u \in \mathbb{R}^3$ is the controller torque command. Furthermore, the RW angular momentum is the product of the flywheel inertia and the wheel speed, i.e.

$$h_w = I_w \omega_w, \tag{2.16}$$

so that one gets

$$\dot{h}_w = I_w \dot{\omega}_w = N_m - \tau_v \omega_w. \tag{2.17}$$

Moreover, the reaction torque (produced torque) is opposite to the net torque and given by

$$N_r = -\dot{h_w}. \tag{2.18}$$

Substituting for N_m into equation (2.17) and then substituting for h_w and $\dot{h}_w$, from equations (2.16) and (2.17) into equation (2.13) yields the dynamics of a single satellite including its actuator dynamics given by

$$\dot{\omega} = -I_s^{-1} [\omega\times] (I_s\omega) - I_s^{-1} [\omega\times] I_w\omega_w + I_s^{-1}\tau_v\omega_w - I_s^{-1} G_d K_t u + T_d \tag{2.19}$$

2.1.3 Linearized Dynamics and Kinematic Equations

In this section, the satellites dynamics is linearized in a neighborhood of any arbitrary operating point. Let $\dot{x_j} = f(x_j, u_j)$ represent the satellite j nonlinear dynamics and kinematic equation where $x_j = \begin{bmatrix} \omega_j^{\mathrm{T}} & \mathbf{q}_j^{\mathrm{T}} & q_{4j} & \omega_{w_j}^{\mathrm{T}} \end{bmatrix}^{\mathrm{T}} \in \mathbb{R}^{10}$ and $u_j \in \mathbb{R}^3$ represent the single satellite state vector and the controller command which is input to each of the three RWs corresponding to the satellite's three axes (namely, pitch, yaw and roll) and the disturbance torques are neglected. Using the Jacobian and Tayor series expansion, in a neighborhood of any operating point $(\widehat{x}_j, \widehat{u}_j)$, one gets $f(x_j, u_j) = f(\widehat{x}_j, \widehat{u}_j) + \frac{\partial}{\partial x_j} f\,|_{(\widehat{x}_j, \widehat{u}_j)}\,(x_j - \widehat{x}_j) + \frac{\partial}{\partial u_j} f\,|_{(\widehat{x}_j, \widehat{u}_j)}\,(u_j - \widehat{u}_j) + h.o.t.$ Therefore, by neglecting the higher order terms, the linearized state-space equation for the absolute attitude dynamics will be expressed as

$$\delta\dot{x}_j = A_{c_j}\delta x_j + B_{c_j}\delta u_j \tag{2.20}$$

where

$$A_{c_j} = \frac{\partial}{\partial x_j} f\,|_{(\widehat{x}_j, \widehat{u}_j)} = \begin{bmatrix} -I_s^{-1}\big([\widehat{\omega}_j\times]I_s - [(I_s\widehat{\omega}_j)\times] - [(I_w\widehat{\omega}_{w_j})\times]\big) & 0 & 0 & I_s^{-1}\tau_v - I_s^{-1}[\widehat{\omega}_j\times]I_w \\ \frac{1}{2}[\widehat{\mathbf{q}}_j\times] + \frac{1}{2}\widehat{q}_{4j}\mathrm{E}_{3\times 3} & -\frac{1}{2}[\widehat{\omega}_j\times] & \frac{1}{2}\widehat{\omega}_j & 0 \\ -\frac{1}{2}\widehat{\mathbf{q}}_j^{\mathrm{T}} & -\frac{1}{2}\widehat{\omega}_j^{\mathrm{T}} & 0 & 0 \\ 0 & 0 & 0 & -I_w^{-1}\tau_v \end{bmatrix},$$

$$B_{c_j} = \frac{\partial}{\partial u_j} f\,|_{(\widehat{x}_j, \widehat{u}_j)} = \begin{bmatrix} -I_s^{-1}G_dK_t \\ 0 \\ 0 \\ I_w^{-1}G_dK_t \end{bmatrix} \tag{2.21}$$

where E denotes the identity matrix. Note that in the above expression δx_j and δu_j denote perturbation variables ($\delta x_j = x_j - \widehat{x}_j$ and $\delta u_j = u_j - \widehat{u}_j$). The difference equation representing the discrete-time linearized state equations of the continuous-

time linearized state space model over the sampling period T_s for nay satellite j is now obtained as

$$\delta x_j\left(k+1\right) = A_j \delta x_j\left(k\right) + B_j \delta u_j\left(k\right) \tag{2.22}$$

where

$$A_j = e^{A_{c_j} T_s}, \quad B_j = \int_0^{T_s} e^{A_{c_j}\lambda} B_{c_j} d\lambda \ . \tag{2.23}$$

2.1.4 Environmental Disturbances

Different forces/torques dominate in different space regions [85]. Aerodynamic disturbance torques due to aerodynamic forces dominate in the orbits close to the Earth. In larger distances from the Earth, these forces fall off and gravity gradient and magnetic field disturbance torques are larger. The other disturbance torque is the solar radiation disturbance which dominates in the interplanetary medium.

The aerodynamic torque depends on the orbital altitude and the satellite geometry. The magnitude of this disturbance torque can be obtained by $T_a = F\left(C_{pa} - C_g\right)$, where $F = 0.5\left(\rho C_d A V^2\right)$, and C_d denotes the drag coefficient (usually between 2 and 2.5), ρ denotes the atmospheric density, A represents the surface area and V denotes the satellite velocity, C_{pa} denotes the location of the satellite's center of aerodynamic pressure and C_g represents the location of the center of gravity [88]. The gravity gradient torque depends on the satellite inertias about its axis and also the orbital altitude. The maximum magnitude of this disturbance torque can be obtained by $T_g = \frac{3\mu}{2R^3}\left\|I_z - I_y\right\|$ for each satellite where $\mu = 3.988 \times 10^{14}\, m^3/s^2$ denotes the Earth's gravity constant and R denotes the orbital radius. The magnetic field disturbance can be obtained by $T_m = DB$ and therefore, is affected by the satellite's residual magnetic dipole D, where its typical value for a small sized satellite is $D = 1\ A.m^2$, and the Earth's magnetic field can be obtained by $B = \frac{2M}{R^3}$, where $M = 7.98 \times 10^{15}\, tesla.m^3$ denotes the magnetic moment of the Earth. Finally, the solar radiation disturbances

is affected by the satellite's geometry and surface reflectivity. The worst case of the solar radiation pressure torque can be obtained by $T_{sp} = F\left(C_{ps} - C_g\right)$. In this expression the maximum value of F can be obtained by $F = \frac{F_s}{c} A_s \left(1 + q\right)$, where $F_s = 1.367\, W/m^2$ denotes the solar constant, $c = 3 \times 10^8\, m/s$ denotes the speed of light, A_s denotes the surface area, C_{ps} denotes the location of the center of solar pressure, and q denotes the reflectance factor.

2.2 Formation Flying Satellites Relative Dynamic Equations

For the purpose of design of the MPC controller based on relative state measurements, the relative dynamic equations are needed in order to predict the future relative states. Chang *et al.* in [13] derived the linearized relative dynamic equations for the satellites formation flying. Their linearized relative dynamics neglected certain variables such as the absolute states by analyzing the relative dynamical behavior within the proximity of a certain operating condition. In this study, a generic relative dynamical modeling is obtained which is valid for any operating condition of the formation flying satellite system. Based on the problem objectives, both relative and absolute states must be predicted within the MPC framework. On the other hand, as will be shown in this subsection, a more precise relative state dynamics for the attitude motion relies on the absolute states. Combining both absolute and relative dynamics and by using a dynamic coupling approach enables one to satisfy the two objectives and at the same time benefit from a precise dynamical model for representing the attitude dynamics motion.

2.2.1 Nonlinear Relative Dynamic Equations

Consider the agents j and k, where $x_j = \begin{bmatrix} \omega_j^{\mathrm{T}} & \mathbf{q}_j^{\mathrm{T}} & q_{4j} & \omega_{w_j}^{\mathrm{T}} \end{bmatrix}^{\mathrm{T}} \in \mathbb{R}^{10}$, $x_k = \begin{bmatrix} \omega_k^{\mathrm{T}} & \mathbf{q}_k^{\mathrm{T}} & q_{4k} & \omega_{w_k}^{\mathrm{T}} \end{bmatrix}^{\mathrm{T}} \in \mathbb{R}^{10}$, represent their state vector and $u_j \in \mathbb{R}^3$ and $u_k \in \mathbb{R}^3$, represent their controller command which is input to each of the three RWs. In the relative attitude dynamics, the coordinates change. Relative quaternion can be obtained using the following operation

$$\overline{\mathbf{q}}_{jk} = \overline{\mathbf{q}}_j \otimes \overline{\mathbf{q}}_k^{-1} \tag{2.24}$$

Using equation (2.5) and (2.6) the kinematic equations for the relative attitude motion can be obtained as

$$\dot{\overline{\mathbf{q}}}_{jk} = \begin{bmatrix} \dot{\mathbf{q}}_{jk} \\ \dot{q}_{4jk} \end{bmatrix} = \begin{bmatrix} \frac{1}{2}\left(q_{4jk}\omega_{jk} - [\omega_{jk}\times]\,\mathbf{q}_{jk}\right) \\ -\frac{1}{2}\omega_{jk}^T\mathbf{q}_{jk} \end{bmatrix} \tag{2.25}$$

where $\overline{\mathbf{q}}_{jk} = \begin{bmatrix} \mathbf{q}_{jk}^{\mathrm{T}} & q_{4jk} \end{bmatrix}^{\mathrm{T}} = \begin{bmatrix} q_{1jk} & q_{2jk} & q_{3jk} & q_{4jk} \end{bmatrix}^{\mathrm{T}}$ and ω_{jk} represent the quaternion mapping of the satellite j body-fixed coordinate with respect to the satellite k body-fixed coordinate, and the angular velocity of the satellite j with respect to the satellite k, respectively. Relationships between the relative angular velocity of the satellites j and k and their absolute values can be described as

$$\omega_{jk} = \omega_j - C^{jk}\omega_k \tag{2.26}$$

where C^{jk} is the direction cosine matrix for the transformation from satellite k body-

fixed coordinates to satellite j body-fixed coordinates and can be obtained from

$$C^{jk} = \begin{bmatrix} 1-2\left(q_{2jk}^2+q_{3jk}^2\right) & 2\left(q_{1jk}q_{2jk}+q_{3jk}q_{4jk}\right) & 2\left(q_{1jk}q_{3jk}-q_{2jk}q_{4jk}\right) \\ 2\left(q_{1jk}q_{2jk}-q_{3jk}q_{4jk}\right) & 1-2\left(q_{1jk}^2+q_{3jk}^2\right) & 2\left(q_{2jk}q_{3jk}+q_{1jk}q_{4jk}\right) \\ 2\left(q_{1jk}q_{3jk}+q_{2jk}q_{4jk}\right) & 2\left(q_{2jk}q_{3jk}-q_{1jk}q_{4jk}\right) & 1-2\left(q_{1jk}^2+q_{2jk}^2\right) \end{bmatrix} \tag{2.27}$$

As can be observed from equation (2.26) corresponding to ω_{jk}, the matrix C^{jk} is involved in the equation, which is due to the change of coordinates. For deriving the relative states dynamics we need the derivative of equation (2.26), i.e.

$$\dot{\omega}_{jk} = \dot{\omega}_j - \dot{C}^{jk}\omega_k - C^{jk}\dot{\omega}_k \tag{2.28}$$

Based on the properties of the direction cosine matrix we have $\dot{C}^{jk} = -\left[\omega_{jk}\times\right]C^{jk}$. Substituting for $\dot{\omega}_j$ and $\dot{\omega}_k$ in equation (2.28) from their dynamics relationships and substituting for ω_k from equation (2.26) yields

$$\dot{\omega}_{jk} = f\left(\omega_j, \omega_{w_j}, \omega_{jk}, \overline{\mathbf{q}}_{jk}, \omega_{w_k}, u_j, u_k\right) \tag{2.29}$$

where $f(.)$ is a nonlinear function. As can be observed from equation (2.29), the absolute angular velocities appear in the relative dynamics equation. Thus, the linearized dynamics equation must include these terms as well as the relative states.

2.2.2 Relative States and Absolute States Linear Relation

In this subsection, the linear relation between absolute states and relative states is derived based on their nonlinear relation (equations (2.24) and (2.26)). We need this relation to further use it in similarity transformation.

For the purpose of model linearization, let the operating point for the absolute attitude state vector of satellite j and k be specified as $\widehat{x}_j = \begin{bmatrix} \widehat{\omega}_j^{\mathrm{T}} & \widehat{\mathbf{q}}_j^{\mathrm{T}} & \widehat{q}_{4j} & \widehat{\omega}_{w_j}^{\mathrm{T}} \end{bmatrix}^{\mathrm{T}}$

and $\widehat{x}_k = \begin{bmatrix} \widehat{\omega}_k^{\mathrm{T}} & \widehat{\mathbf{q}}_k^{\mathrm{T}} & \widehat{q}_{4k} & \widehat{\omega}_{w_k}^{\mathrm{T}} \end{bmatrix}^{\mathrm{T}}$. In this section, for each individual agent, the relative states will be derived as a linear combination of absolute states. We define the following two nonlinear functions that map the absolute states to the relative states

$$\overline{\mathbf{q}}_{jk} = \varphi_{\mathrm{q}}\left(\overline{\mathbf{q}}_j, \overline{\mathbf{q}}_k\right) = \overline{\mathbf{q}}_j \otimes \overline{\mathbf{q}}_k^{-1} = \begin{bmatrix} \mathbf{q}_{jk} \\ q_{4jk} \end{bmatrix} = \begin{bmatrix} \mathbf{q}_j \otimes \mathbf{q}_k + q_{4j}\left(-\mathbf{q}_k\right) + q_{4k}\left(\mathbf{q}_j\right) \\ \overline{\mathbf{q}}_j.\overline{\mathbf{q}}_k^{\mathrm{T}} \end{bmatrix} \tag{2.30}$$

$$\omega_{jk} = \varphi_{\omega}\left(\omega_j, \omega_k, \overline{\mathbf{q}}_j, \overline{\mathbf{q}}_k\right) = \omega_j - C^{jk}\omega_k \tag{2.31}$$

Due to the Jacobian and the Taylor series expansion for the equations (2.30) and (2.31), one gets

$$\overline{\mathbf{q}}_{jk} = \varphi_{\mathrm{q}}\left(\widehat{\overline{\mathbf{q}}}_j, \widehat{\overline{\mathbf{q}}}_k\right) + \begin{bmatrix} \frac{\partial}{\partial \overline{\mathbf{q}}_j}\varphi_{\mathrm{q}} & \frac{\partial}{\partial \overline{\mathbf{q}}_k}\varphi_{\mathrm{q}} \end{bmatrix} \begin{bmatrix} \overline{\mathbf{q}}_j - \widehat{\overline{\mathbf{q}}}_j \\ \overline{\mathbf{q}}_k - \widehat{\overline{\mathbf{q}}}_k \end{bmatrix} + h.o.t. \tag{2.32}$$

$$\omega_{jk} = \varphi_{\omega}\left(\widehat{\omega}_j, \widehat{\omega}_j, \widehat{\overline{\mathbf{q}}}_j, \widehat{\overline{\mathbf{q}}}_k\right) + \begin{bmatrix} \frac{\partial}{\partial \omega_j}\varphi_{\omega} & \frac{\partial}{\partial \omega_k}\varphi_{\omega} & \frac{\partial}{\partial \overline{\mathbf{q}}_j}\varphi_{\omega} & \frac{\partial}{\partial \overline{\mathbf{q}}_k}\varphi_{\omega} \end{bmatrix} \begin{bmatrix} \omega_j - \widehat{\omega}_j \\ \omega_k - \widehat{\omega}_k \\ \overline{\mathbf{q}}_j - \widehat{\overline{\mathbf{q}}}_j \\ \overline{\mathbf{q}}_k - \widehat{\overline{\mathbf{q}}}_k \end{bmatrix} + h.o.t.$$

where $\varphi_{\mathrm{q}}\left(\widehat{\overline{\mathbf{q}}}_j, \widehat{\overline{\mathbf{q}}}_k\right)$ is the vector function $\varphi_{\mathrm{q}}(.)$ which is evaluated at the operating point and $\frac{\partial}{\partial \overline{\mathbf{q}}_j}\varphi_{\mathrm{q}}$, $\frac{\partial}{\partial \overline{\mathbf{q}}_k}\varphi_{\mathrm{q}} \in \mathbb{R}^{4\times 4}$ represent the matrix derivatives of the vector function $\varphi_{\mathrm{q}}(.)$ evaluated at the operating point and $\frac{\partial}{\partial \omega_j}\varphi_{\omega}$, $\frac{\partial}{\partial \omega_k}\varphi_{\omega} \in \mathbb{R}^{3\times 3}$ and $\frac{\partial}{\partial \overline{\mathbf{q}}_j}\varphi_{\omega}$, $\frac{\partial}{\partial \overline{\mathbf{q}}_k}\varphi_{\omega} \in \mathbb{R}^{3\times 4}$ correspond to the vector function $\varphi_{\omega}(.)$. The matrix derivatives are obtained as follows

$$\begin{aligned} \frac{\partial}{\partial \overline{\mathbf{q}}_j}\varphi_{\mathrm{q}} &= \begin{bmatrix} \frac{\partial}{\partial \mathbf{q}_j}\mathbf{q}_{jk} & \frac{\partial}{\partial q_{4j}}\mathbf{q}_{jk} \\ \frac{\partial}{\partial \mathbf{q}_j}q_{4jk} & \frac{\partial}{\partial \mathbf{q}_{4j}}q_{4jk} \end{bmatrix} = \begin{bmatrix} -\left[\widehat{\mathbf{q}}_k\times\right] + \widehat{q}_{4k}\mathrm{E}_{3\times 3} & -\widehat{\mathbf{q}}_k \\ \widehat{\overline{\mathbf{q}}}_k^{T} \end{bmatrix}, \\ \frac{\partial}{\partial \overline{\mathbf{q}}_k}\varphi_{\mathrm{q}} &= \begin{bmatrix} \frac{\partial}{\partial \mathbf{q}_k}\mathbf{q}_{jk} & \frac{\partial}{\partial q_{4k}}\mathbf{q}_{jk} \\ \frac{\partial}{\partial \mathbf{q}_k}q_{4jk} & \frac{\partial}{\partial \mathbf{q}_{4k}}q_{4jk} \end{bmatrix} = \begin{bmatrix} \left[\widehat{\mathbf{q}}_j\times\right] - \widehat{q}_{4j}\mathrm{E}_{3\times 3} & \widehat{\mathbf{q}}_j \\ \widehat{\overline{\mathbf{q}}}_j^{T} \end{bmatrix}, \end{aligned} \tag{2.33}$$

$$\begin{array}{ll} \frac{\partial}{\partial \omega_j}\varphi_\omega = \mathrm{E}_{3\times 3}, & \frac{\partial}{\partial \omega_k}\varphi_\omega = -C_0^{jk}, \\ \frac{\partial}{\partial \overline{\mathbf{q}}_j}\varphi_\omega = -\widehat{\mathrm{C}}^{\prime\prime^{jk}}\left(\widehat{\overline{\mathbf{q}}}_{jk}, \widehat{\omega}_k\right)\frac{\partial}{\partial \overline{\mathbf{q}}_j}\varphi_{\mathrm{q}}, & \frac{\partial}{\partial \overline{\mathbf{q}}_k}\varphi_\omega = -\widehat{\mathrm{C}}^{\prime\prime^{jk}}\left(\widehat{\overline{\mathbf{q}}}_{jk}, \widehat{\omega}_k\right)\frac{\partial}{\partial \overline{\mathbf{q}}_k}\varphi_{\mathrm{q}} \end{array} \tag{2.34}$$

where $\widehat{C}^{jk}$ is the matrix C^{jk} evaluated at the operating point and $\widehat{\mathrm{C}}^{\prime\prime^{jk}}(.)$ is defined as follows:

The equation (2.31) has very high degree of non-linearity with respect to $\overline{\mathbf{q}}_j$ and $\overline{\mathbf{q}}_k$ because of the matrix C^{jk}. The partial derivatives of the matrix C^{jk} with respect to the partial elements of $\overline{\mathbf{q}}_{jk}$ (q_{1jk}, q_{2jk}, q_{3jk} and q_{4jk}) can be obtained as

$$C_1' = \frac{\partial}{\partial q_{1jk}}C^{jk} = \begin{bmatrix} 0 & 2\widehat{q}_{2jk} & 2\widehat{q}_{3jk} \\ 2\widehat{q}_{2jk} & -4\widehat{q}_{1jk} & 2\widehat{q}_{4jk} \\ 2\widehat{q}_{3jk} & -2\widehat{q}_{4jk} & -4\widehat{q}_{1jk} \end{bmatrix}, \quad C_2' = \frac{\partial}{\partial q_{2jk}}C^{jk} = \begin{bmatrix} -4\widehat{q}_{2jk} & 2\widehat{q}_{1jk} & -2\widehat{q}_{4jk} \\ 2\widehat{q}_{1jk} & 0 & 2\widehat{q}_{3jk} \\ 2\widehat{q}_{4jk} & 2\widehat{q}_{3jk} & -4\widehat{q}_{2jk} \end{bmatrix},$$

$$C_3' = \frac{\partial}{\partial q_{3jk}}C^{jk} = \begin{bmatrix} -4\widehat{q}_{3jk} & 2\widehat{q}_{4jk} & 2\widehat{q}_{1jk} \\ -2\widehat{q}_{4jk} & \widehat{q}_{3jk} & 2\widehat{q}_{2jk} \\ 2\widehat{q}_{1jk} & 2\widehat{q}_{2jk} & 0 \end{bmatrix}, \quad C_4' = \frac{\partial}{\partial q_{4jk}}C^{jk} = \begin{bmatrix} 0 & 2\widehat{q}_{3jk} & -2\widehat{q}_{2jk} \\ -2\widehat{q}_{3jk} & 0 & 2\widehat{q}_{1jk} \\ 2\widehat{q}_{2jk} & -2\widehat{q}_{1jk} & 0 \end{bmatrix}, \tag{2.35}$$

and $\widehat{C}^{\prime\prime^{jk}} \in \mathbb{R}^{3\times 4}$ is defined as a function of $\widehat{\overline{\mathbf{q}}}_{jk}$ and $\widehat{\omega}_k$ as follows

$$\widehat{\mathrm{C}}^{\prime\prime^{jk}}\left(\widehat{\overline{\mathbf{q}}}_{jk}, \widehat{\omega}_k\right) = \begin{bmatrix} C_1'\widehat{\omega}_k & C_2'\widehat{\omega}_k & C_3'\widehat{\omega}_k & C_4'\widehat{\omega}_k \end{bmatrix} \tag{2.36}$$

Finally, by neglecting the higher order terms, the slightly perturbed state vectors $\delta\overline{\mathbf{q}}_{jk} = \overline{\mathbf{q}}_{jk} - \widehat{\overline{\mathbf{q}}}_{jk}$ and $\delta\omega_{jk} = \omega_{jk} - \widehat{\omega}_{jk}$ will be expressed as

$$\delta\overline{\mathbf{q}}_{jk} = \begin{bmatrix} \delta\mathbf{q}_{jk} \\ \delta q_{4jk} \end{bmatrix} \approx \begin{bmatrix} \frac{\partial}{\partial \overline{\mathbf{q}}_j}\varphi_{\mathrm{q}} & \frac{\partial}{\partial \overline{\mathbf{q}}_k}\varphi_{\mathrm{q}} \end{bmatrix} \begin{bmatrix} \delta\overline{\mathbf{q}}_j \\ \delta\overline{\mathbf{q}}_k \end{bmatrix} \tag{2.37}$$

$$\delta\omega_{jk} \approx \begin{bmatrix} \frac{\partial}{\partial\omega_j}\varphi_\omega & \frac{\partial}{\partial\omega_k}\varphi_\omega & \frac{\partial}{\partial\overline{\mathbf{q}}_j}\varphi_\omega & \frac{\partial}{\partial\overline{\mathbf{q}}_k}\varphi_\omega \end{bmatrix} \begin{bmatrix} \delta\omega_j \\ \delta\omega_k \\ \delta\overline{\mathbf{q}}_j \\ \delta\overline{\mathbf{q}}_k \end{bmatrix} \tag{2.38}$$

Using equations (2.37) and (2.38), the relative angular velocity and attitude quaternion of the agent j and k can be derived as a linear combination of the absolute angular velocities and attitude quaternions as follows

$$\begin{bmatrix} \delta\omega_{jk} \\ \delta\overline{\mathbf{q}}_{jk} \end{bmatrix} = \underbrace{\begin{bmatrix} \frac{\partial}{\partial\omega_j}\varphi_\omega & \frac{\partial}{\partial\overline{\mathbf{q}}_j}\varphi_\omega & \frac{\partial}{\partial\omega_k}\varphi_\omega & \frac{\partial}{\partial\overline{\mathbf{q}}_k}\varphi_\omega \\ 0_{4\times3} & \frac{\partial}{\partial\overline{\mathbf{q}}_j}\varphi_{\mathrm{q}} & 0_{4\times3} & \frac{\partial}{\partial\overline{\mathbf{q}}_k}\varphi_{\mathrm{q}} \end{bmatrix}}_{T'_{jk}} \begin{bmatrix} \delta\omega_j \\ \delta\overline{\mathbf{q}}_j \\ \delta\omega_k \\ \delta\overline{\mathbf{q}}_k \end{bmatrix} \tag{2.39}$$

where T'_{jk} is a 7×14 matrix. The wheel angular velocity states is also included in order to use the matrix later in the dynamics equations, and therefore, equation (2.39) is written as

$$\begin{bmatrix} \delta\omega_{jk} \\ \delta\overline{\mathbf{q}}_{jk} \end{bmatrix} = \underbrace{\begin{bmatrix} \frac{\partial}{\partial\omega_j}\varphi_\omega & \frac{\partial}{\partial\overline{\mathbf{q}}_j}\varphi_\omega & 0_{3\times3} & \frac{\partial}{\partial\omega_k}\varphi_\omega & \frac{\partial}{\partial\overline{\mathbf{q}}_k}\varphi_\omega & 0_{3\times3} \\ 0_{4\times3} & \frac{\partial}{\partial\overline{\mathbf{q}}_j}\varphi_{\mathrm{q}} & 0_{4\times3} & 0_{4\times3} & \frac{\partial}{\partial\overline{\mathbf{q}}_k}\varphi_{\mathrm{q}} & 0_{4\times3} \end{bmatrix}}_{T''_{jk}} \begin{bmatrix} \delta\omega_j \\ \delta\overline{\mathbf{q}}_j \\ \delta\omega_{w_j} \\ \delta\omega_k \\ \delta\overline{\mathbf{q}}_k \\ \delta\omega_{w_k} \end{bmatrix} \tag{2.40}$$

It can be shown that the matrix $T''_{jk} \in \mathbb{R}^{7\times20}$ is a full-rank matrix because regardless of the operating-point, the first seven columns are linearly independent. Using this matrix, in the next section, we derive the linear relative dynamics equations.

2.2.3 Linearized Relative Dynamics Equations

Next, a similarity transformation is derived for representing the networked system in a new coordinate system which includes the absolute and the relative state vectors.

Problem A. *Given the augmented vector consisting of absolute state vectors of agents, defined as* $\begin{bmatrix} x_j^T & x_k^T \end{bmatrix}^T$*, there exists a similarity transformation* T *that transforms the coordinates to a new system of coordinates such that the transformed states become absolute state of one agent and their relative states, i.e.*

$$\begin{bmatrix} x_j \\ x_{jk} \end{bmatrix} = T \begin{bmatrix} x_j \\ x_k \end{bmatrix} \tag{2.41}$$

where $x_{jk} = \begin{bmatrix} \omega_{jk}^T & \overline{\mathbf{q}}_{jk}^T & \omega_{w_k}^T \end{bmatrix}^T \in \mathbb{R}^{10}$.

Given

$$\begin{aligned} \begin{bmatrix} x_j^{\mathrm{T}} & x_{jk}^{\mathrm{T}} \end{bmatrix}^{\mathrm{T}} &= \begin{bmatrix} \omega_j^{\mathrm{T}} & \overline{\mathbf{q}}_j^{\mathrm{T}} & \omega_{w_j}^{\mathrm{T}} & \omega_{jk}^{\mathrm{T}} & \overline{\mathbf{q}}_{jk}^{\mathrm{T}} & \omega_{w_k}^{\mathrm{T}} \end{bmatrix}^{\mathrm{T}} \quad \text{and} \\ \begin{bmatrix} x_j^{\mathrm{T}} & x_k^{\mathrm{T}} \end{bmatrix}^{\mathrm{T}} &= \begin{bmatrix} \omega_j^{\mathrm{T}} & \overline{\mathbf{q}}_j^{\mathrm{T}} & \omega_{w_j}^{\mathrm{T}} & \omega_k^{\mathrm{T}} & \overline{\mathbf{q}}_k^{\mathrm{T}} & \omega_{w_k}^{\mathrm{T}} \end{bmatrix}^{\mathrm{T}} \end{aligned} \tag{2.42}$$

and using equation (2.40), T can be written in the form of

$$T = \left[\begin{array}{ccc} \mathrm{E}_{10\times10} & 0_{10\times7} & 0_{10\times3} \\ \hline & T''_{jk} & \\ \hline 0_{3\times10} & 0_{3\times7} & \mathrm{E}_{3\times3} \end{array}\right]_{20\times20} \tag{2.43}$$

where E denotes the identity matrix and $T''_{jk} \in \mathbb{R}^{7\times20}$ was calculated in equation (2.40). As can be observed from equation (2.43), regardless of the operating point and given that the matrix T''_{jk} is full-rank, it can be concluded that the matrix T is invertible (linearly independent rows of the matrix).

Using T from equation (2.43), the dynamic equations in the new coordinate system

are obtained as

$$\begin{bmatrix} x_j(k+1) \\ x_{jk}(k+1) \end{bmatrix} = T \begin{bmatrix} A_j & 0 \\ 0 & A_k \end{bmatrix} T^{-1} \begin{bmatrix} x_j(k) \\ x_{jk}(k) \end{bmatrix} + T \begin{bmatrix} B_j & 0 \\ 0 & B_k \end{bmatrix} \begin{bmatrix} u_j(k) \\ u_k(k) \end{bmatrix} \quad (2.44)$$

where (A_j, B_j) and (A_k, B_k) are as specified in equation (2.23).

Remark 1. The state variables denote the perturbation variables.

Remark 2. The new coordinate system represents relative dynamics in a coupling manner as apposed to the original coordinate system in which agents were decoupled.

Next, we describe the information flow among the agents and follow the conventional method in the literature for representing the interactions and use a graph structure [90–93].

A simple fixed-undirected graph is represented by $g = (V, A)$ where V is the set of nodes and $A \subseteq V \times V$ is the set of edges. If $i \in V$ and $j \in V$ and the pair $(i, j) \in A$ then the nodes i and j are adjacent and we denote this by $i \sim j$.

An orientation in a graph is the assignment of a direction to each edge such that the positive direction of the arc (i, j) is from i to j. Let g^γ denote the graph g with an arbitrary orientation γ. The *incidence matrix* $B(g^\gamma)$ of a directed graph g^γ is the matrix with its rows and columns indexed by nodes and arcs of g^γ, respectively. The i , j entry of this matrix is equal to 1 if the edge j is incoming to the node i , -1 if the edge j is outgoing from the node i and 0 otherwise. The Laplacian of g is defined as the following symmetric matrix

$$L(g) = B(g) B(g)^T \quad (2.45)$$

$L(g)$ is always positive semi-definite and some important features about the graph can be captured from its eigenvalues. For a connected graph the number of zero eigenvalues are one and the second smallest eigenvalue, denoted by λ_2 is called algebraic

connectivity of the graph and is related to the structure of interconnections. Now we define a graph for our problem :

Definition 1. (Formation Neighboring Graph).

The formation neighboring graph $G_f\,(V_f, A_f)$ is an undirected graph which consists of a set of vertices V_f and a set of edges A_f such that:

1. $V_f = \{1, 2 \ldots, N_v\}$ is indexed by the agents in the team and N_v is the number of agents.

2. $A_f = \{(j,k) \in V_f \times V_f \mid j \sim k\}$ is the set of unordered pairs representing neighboring relations, where $j \sim k$ denotes neighboring nodes in the graph. Neighboring nodes represent the agents that share their relative state information.

Let $\widetilde{x}_j$ denote the vector of concatenation of all the relative states of agent j with respect to its neighbors, i.e. $\widetilde{x}_j = \{x_{jk} \in \mathbb{R}^{10} | \, (j,k) \in A_f\}$. Moreover, let the corresponding similarity transformation matrix be denoted by T_j, i.e. $\begin{bmatrix} x_j^{\mathrm{T}} & \widetilde{x}_j^{\mathrm{T}} \end{bmatrix}^{\mathrm{T}} = T_j \begin{bmatrix} x_j^{\mathrm{T}} & x_k^{\mathrm{T}} & \ldots \end{bmatrix}^{\mathrm{T}}$ and let the extended dynamic model described by equation (2.44), which includes the agent x_j and its neighbors ($\widetilde{x}_j$) in the model, be denoted by $\left(\overline{A}_j, \overline{B}_j\right) \in \mathbb{R}^{10N_v \times 10N_v \times 10N_v \times 3N_v}$, where $\overline{A}_j = T_j \begin{bmatrix} A_j & 0 & 0 \\ 0 & A_k & 0 \\ 0 & 0 & \ddots \end{bmatrix} T_j^{-1}$ and $\overline{B}_j = T_j \begin{bmatrix} B_j & 0 & 0 \\ 0 & B_k & 0 \\ 0 & 0 & \ddots \end{bmatrix}$.

The structure of the information flow (relative state information) in the team depends on the control strategy. In a centralized control strategy, the central controller has a global information about the team. Therefore, a neighboring formation graph and a neighboring relation is not specified for this case as all the agents are considered as neighbors. In a semi-decentralized control strategy each agent requires only a subset

of information exchange, which is denoted as exchange with its neighboring agents, and therefore a formation neighboring graph must be specified.

2.3 Fault Modeling

In Chapter 4 of this thesis, the satellite under fault condition is considered and a recovery approach is presented. Thus, one requires preliminary knowledge on the fault modeling. In this part, we focus on modeling two common faults in the satellites reaction wheels (RW), namely the reduction of motor torque constant or loss of effectiveness (LOE) fault and the friction fault. These faults were identified as sources of RW malfunction in two of the recent reports corresponding to Mars Odyssey and Dawn, NASA's spacecraft. Associated with any fault is a type, an extent and type of representing. The type of fault is a time-behavior description of it, which according to [94] for a physical system, can be categorized as abrupt, incipient or intermittent. Figure 2.2 shows a comparison of these types. Also different extent/severity levels can be considered for a fault ranging from a partial fault to a total failure. Finally, any fault can be represented in the system model parameters by multiplicative or additive terms. In this study we concentrate on the case where an abrupt partial fault of loss of effectiveness or fraction fault occurs. Both of the faults that are considered here are parametric faults of the state space model and thus are multiplicative faults.

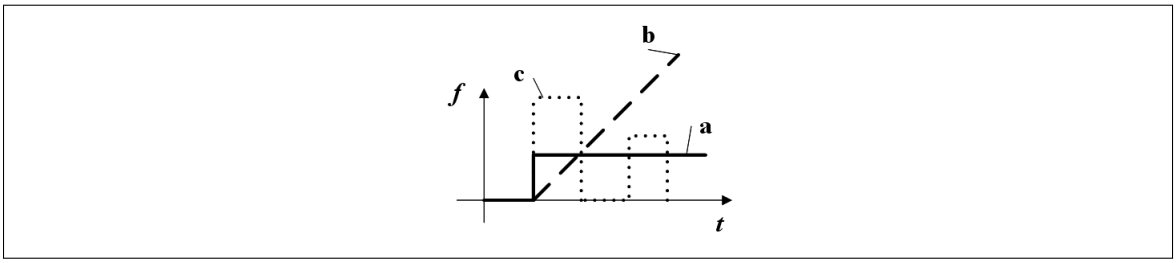

Figure 2.2: Time behavior of fault: (a) abrupt, (b) incipient, (c) intermittent.

2.3.1 Partial Loss of Effectiveness (LOE) Fault

Let the equation $x_j(k+1) = A_j x_j(k) + B_j u_j(k)$ describe the dynamics for any satellite j. Recall that based on the RW model presented in subsection 2.1.2.1, the controller command u_j is related to the RW produced torque by the motor torque constant (K_t) and the driver gain (G_d). The motor torque constant (K_t) is related to the magnetic flux linkage and the average phase current [95]. The magnetic flux linkage in motor might change abruptly. This fault usually occurs because of RW motor inefficiency. Under this fault condition, one will have

$$K_t' = \Gamma K_t \tag{2.46}$$

where $K_t' \in \mathbb{R}^{3\times 3}$ represents the motor torque constant under the fault condition and $\Gamma \in \mathbb{R}^3$ is the effectiveness matrix with the form

$$\Gamma = \begin{bmatrix} \Gamma_1 & 0 & 0 \\ 0 & \Gamma_2 & 0 \\ 0 & 0 & \Gamma_3 \end{bmatrix}, \tag{2.47}$$

where Γ_l for $1 \leq l \leq 3$ denotes the effectiveness corresponding to each of 3-axis RWs and has a value between zero and one. This fault causes the produced torque to be reduced by a certain value and is known as fault of loss of effectiveness.

2.3.2 Friction Fault

Recall that based on the RW model presented in section 2.1.2.1, the final reaction torque (N_r) is influenced by the existing viscous friction in the wheel bearing (τ_v). The viscous friction is the friction generated in the bearings due to bearing lubricant. Bearing lubricant is significantly sensitive to temperature and thus, the friction

constant (τ_v) is related to the temperature through the following relationship [89]

$$\tau_v = \left(0.049 - \frac{0.0002}{^\circ C}\left(T + 30^\circ C\right)\right)\frac{mN - m}{rad/sec} \tag{2.48}$$

Dramatic temperature changes ($\triangle T$) results in considerable change of friction constant (τ_v) in a way that the new friction constant will be given by

$$\tau_v' = \tau_v \pm \Pi, \tag{2.49}$$

where $\tau_v' \in \mathbb{R}^{3\times3}$ represents the friction constant in fault condition and $\Pi \in \mathbb{R}^{3\times3}$, the viscous friction loss/gain matrix, can be obtained by

$$\Pi = \left(\frac{0.0002}{^\circ C} \triangle T\right)\frac{mN - m}{rad/sec}, \tag{2.50}$$

where

$$\triangle T = \begin{bmatrix} \triangle T_1 & 0 & 0 \\ 0 & \triangle T_2 & 0 \\ 0 & 0 & \triangle T_3 \end{bmatrix} \in \mathbb{R}^{3\times3},$$

and $\triangle T_l$ for $1 \leq l \leq 3$ denotes the temperature change in the each of the 3-axis RWs. Consequently, the single satellite model in this fault situation can be described by the following equation

$$x_j\left(k+1\right) = \left(A_j \pm A_\Pi\right)x_j\left(k\right) + B_j\Gamma u_j\left(k\right) \tag{2.51}$$

where

$$A_\Pi = e^{\begin{bmatrix} 0_{3\times3} & 0_{3\times4} & I_s^{-1}\Pi \\ 0_{4\times3} & 0_{4\times4} & 0_{4\times3} \\ 0_{3\times3} & 0_{3\times4} & -I_w^{-1}\Pi \end{bmatrix}T_s}. \tag{2.52}$$

2.4 Model Predictive Control (MPC) Framework

In this section we introduce linear MPC method. MPC is an optimal control strategy. More specifically, it is a constrained finite-time optimal control (CFTOC). In the linear MPC, the future values of states of the system are predicted using the dynamic model of the system and the current states information. Therefore, a discrete-time setting is used and using the standard state-space formulation of system model and the current state information, the future states are predicted. The cost function is defined by equation (2.53) in the form of quadratic, where the time horizon for this cost function is finite and known as prediction horizon (N), that is

$$J(k) = \sum_{i=0}^{N-1} \{x^T(k+i|k)\, Qx(k+i|k) + u^T(k+i|k)\, Ru(k+i|k)\} + x^T(k+N|k)\, \overline{Q}x(k+N|k) \quad (2.53)$$

where $x(k+i|k) \in \mathbb{R}^n$ represents the prediction of the states vector at the time $k+i$ based on the measurements at the time k and $\{u(k|k), u(k+1|k), \ldots, u(k+M-1|k)\}$ are the set of designed inputs that minimize the objective function and the input to the system from the time M can be assumed to be constant. In that case M is the control horizon. $R \in \mathbb{R}^{l\times l}$ is a positive definite matrix representing the input penalty matrix and $Q \in \mathbb{R}^{n\times n}$ is a positive semi-definite matrix representing the state penalty matrix. The terminal cost is considered as a separate term ($\overline{Q} \in \mathbb{R}^{n\times n}$). As will be explained later and has been shown in the literature this weighting cost matrix can be designed in a way to provide the conditions for the system closed-loop stability.

Consider the following discrete-time state-space equation as the internal model of the system,

$$x(k+i+1|k) = Ax(k+i|k) + Bu(k+i|k) \qquad \text{for} \qquad i = 0, \ldots, N-1, \quad (2.54)$$

where $A \in \mathbb{R}^{n\times n}$ and $B \in \mathbb{R}^{n\times l}$ describe the internal linear model of the system.

Using the current state information at the instant k , i.e., $x(k)$ as the feedback from the system and equation (2.54) will enable us to calculate the predictions of the future value for the system as a function of a sequence of future control moves as follows

$$\begin{aligned} x(k|k) &= x(k) \\ x(k+1|k) &= Ax(k) + Bu(k|k) \\ &\vdots \\ \Rightarrow x(k+i|k) &= A^i x(k) + A^{i-1}Bu(k|k) + \ldots + Bu(k+i-1|k) \quad \text{for} \quad i = 0, \ldots, N \end{aligned} \tag{2.55}$$

Thus, the states predictions can be obtained by

$$\underbrace{\begin{bmatrix} x(k+1|k) \\ x(k+2|k) \\ \vdots \\ x(k+N|k) \end{bmatrix}}_{\mathbf{x}(k)} = \underbrace{\begin{bmatrix} A \\ A^2 \\ \vdots \\ A^N \end{bmatrix}}_{M} x(k) + \underbrace{\begin{bmatrix} B & 0 & \cdots & 0 \\ AB & B & \cdots & 0 \\ \vdots & \vdots & \ddots & \vdots \\ A^{N-1}B & A^{N-2}B & \cdots & B \end{bmatrix}}_{\Phi} \underbrace{\begin{bmatrix} u(k|k) \\ u(k+1|k) \\ \vdots \\ u(k+N-1|k) \end{bmatrix}}_{\mathbf{u}(k)} \tag{2.56}$$

which can be represented by the following compact form

$$\mathbf{x}(k) = Mx(k) + \Phi\mathbf{u}(k) \tag{2.57}$$

By substituting for $x(k+i|k)$ where $1 \leq i \leq N$ from equation (2.57) in equation (2.53), we obtain the cost function as

$$J(k) = \mathbf{u}^T(k) H\mathbf{u}(k) + 2x^T(k) F^T\mathbf{u}(k) + x^T(k) Gx(k) \tag{2.58}$$

where

$$\begin{aligned} H &= \Phi^T \widetilde{Q} \Phi + \widetilde{R} \qquad\qquad F = \Phi^T \widetilde{Q} M \\ G &= M^T \widetilde{Q} M + Q \end{aligned} \tag{2.59}$$

with

$$\widetilde{Q} = \begin{bmatrix} Q & 0 & \cdots & 0 \\ 0 & \ddots & & \vdots \\ \vdots & & Q & 0 \\ 0 & 0 & 0 & \overline{Q} \end{bmatrix}_{nN \times nN} \qquad \widetilde{R} = \begin{bmatrix} R & 0 & \cdots & 0 \\ 0 & \ddots & & \vdots \\ \vdots & & R & 0 \\ 0 & 0 & 0 & R \end{bmatrix}_{lN \times lN} \tag{2.60}$$

As can be observed from equation (2.58), the problem is converted to an optimization problem as a function of the input sequence. In the absence of constraints the optimal solution to this problem has a closed form which can be derived by taking the derivative of the cost function

$$\mathbf{u}^* (k) = \arg\min_{\mathbf{u}} J (k) \tag{2.61}$$

Given that H is a positive definite matrix, the condition $\nabla_{\mathbf{u}} J = 0$ yields that $\mathbf{u}^* (k)$ that is obtained below, minimizes the objective function [96].

$$\nabla_{\mathbf{u}} J = 2H\mathbf{u} + 2Fx = 0 \Rightarrow \mathbf{u}^* (k) = -H^{-1} F x (k) \tag{2.62}$$

In the presence of constraints there will be no analytical closed-form solution for $\mathbf{u}^* (k)$ with respect to the feedback signal. The inequality constraints represent feasible solution sets and are linear input and state constraints in the form of

$$\underline{u} \leq u (k + i \mid k) \leq \bar{u} \qquad \text{for} \quad i = 0, \ldots, N - 1 \tag{2.63}$$

$$\underline{x} \leq x\left(k+i \mid k\right) \leq \overline{x} \qquad \text{for} \quad i=1,\ldots,N \tag{2.64}$$

Where $\underline{u}$ and $\bar{u}$ represent the lower and the upper bound for the input and $\underline{x}$ and $\overline{x}$ represent the lower and upper bound for the state vector. By substituting $x\left(k+i \mid k\right)$ where $1 \leq i \leq N$ from equation (2.56) in equation (2.64) , the set of constraints can be rewritten in the following compact form

$$\begin{aligned}
&\begin{bmatrix} I \\ -I \end{bmatrix} \mathbf{u}\left(k\right) \leq \begin{bmatrix} 1\bar{u} \\ -1\underline{u} \end{bmatrix} \\
&\begin{bmatrix} \Phi_i \\ -\Phi_i \end{bmatrix} \mathbf{u}\left(k\right) \leq \begin{bmatrix} \overline{x} \\ -\underline{x} \end{bmatrix} + \begin{bmatrix} -A^i \\ A^i \end{bmatrix} x\left(k\right), \qquad i=1,\ldots,N
\end{aligned} \tag{2.65}$$

where $1 = \left[I_l \cdots I_l\right]^{\mathrm{T}} \in \mathbb{R}^{N.l \times l}$, and l is the dimension of u, and Φ_i are the i^{th} block row of Φ. Consequently the set of inequality constraints of equations (2.63) and (2.64) can be expressed as constraints on $\mathbf{u}\left(k\right)$ in the following form

$$A_{\Phi}\mathbf{u}\left(k\right) \leq b_0 + B_x x\left(k\right) \tag{2.66}$$

where A_{Φ}, b_0 and B_x are constant matrices. The problem can now be viewed as a quadratic programming, a special case of convex optimization, and numerical methods such as active-set, interior-point and trust-region can be employed to solve this problem [21, 97].

The following implementation remarks are of significance:

Remark 3. In the above MPC formulation the origin is shifted to the steady-state values of $x\left(k+i \mid k\right)$ and $u\left(k+i \mid k\right)$.

Remark 4. For a general nonlinear system the internal model of the system used in prediction equations will be the linearized state-space equations discretized using

the zero-order-hold method. However, one does not re-linearize the system at each sampling time and the same linearized model can be used for a number of control updates (sampling steps).

Remark 5. In this formulation, full-state measurements availability is assumed.

Remark 6. At each control update k (sampling step), using the states feedback provided to the controller, an open-loop optimal control problem, i.e., equation (2.61) is solved. The first element of the optimal solution, i.e., $u^*(k|k)$ is known as a receding horizon control law and will be implemented on the system during the following sampling interval.

Remark 7. The choice of the prediction horizon affects the performance of the system.

2.5 Linear Quadratic Regulator (LQR) Framework

Optimal control methods can be divided to two main groups. The methods that consider an infinite horizon cost function and the ones that consider a finite horizon cost function. If the problem constraints are going to be taken into consideration, solving an infinitely large-horizon optimal control will have a large computational cost. But in the case were the constraints are not being considered solving an infinite-horizon optimal control will make the problem simpler because of existence of an analytical solution which is dependent on the system parameters and can be calculated offline. This motivated us to compare the performance of these two approaches in fault-free situation for formation flying satellites and investigate their different properties. In this section the discrete-time LQR control approach and the necessary and sufficient conditions for obtaining a stable closed-loop system are presented. We focus on the discrete-time approach to keep consistency with the MPC approach.

Consider the following general linear system and the quadratic cost

$$x(k+1) = Ax(k) + Bu(k) \tag{2.67}$$

$$J = x(N)^{\mathrm{T}} Q_N x(N) + \sum_{k=0}^{N-1} \left\{ x(k)^{\mathrm{T}} Q x(k) + u(k)^{\mathrm{T}} R u(k) \right\} \tag{2.68}$$

where $x(k) \in \mathbb{R}^n$, $u(k) \in \mathbb{R}^m$, $A \in \mathbb{R}^{n\times n}$, $B \in \mathbb{R}^{n\times m}$, and matrices $Q_N \in \mathbb{R}^{n\times n}$, $Q \in \mathbb{R}^{n\times n}$ are positive semi-definite and $R \in \mathbb{R}^{m\times m}$ is a positive definite matrix.

Using dynamic programming and the algorithm based on cost-to-go, the input that minimizes the cost function at any time k can be obtained. In this algorithm the procedure starts at the terminal time N and proceeds backward. The following proposition provides the necessary and sufficient conditions for obtaining infinite-horizon discrete-time control law and the proof is provided in [98].

Proposition 1. *([98]) Let $Q = \mathbb{R}^{n\times n}$ and $R \in \mathbb{R}^{m\times m}$ denote a positive semi-definite symmetric matrix and a positive definite symmetric matrix, respectively. Consider the following discrete-time Ricatti equation,*

$$P_{k+1} = A^T \left(P_k - P_k B \left(B^T P_k B + R \right)^{-1} B^T P_k \right) A + Q. \qquad k = 0, 1, \ldots \tag{2.69}$$

Assume that the pair (A,B) is controllable. Assume also that we can measure all of the states. Then,

(a) There exists a positive definite symmetric matrix P such that for every positive semi-definite symmetric initial matrix P_0 we have $\lim_{k\to\infty} P_k = P$. Furthermore, P is the unique solution of the algebraic matrix equation (2.70) within the class of positive semi-definite symmetric matrices,

$$P = A^T \left(P - PB \left(B^T P B + R \right)^{-1} B^T P \right) A + Q. \tag{2.70}$$

(b) The corresponding closed-loop system is stable, that is, the eigen-values of the matrix $D = A + BL$, where

$$L = -\left(B^T P B + R\right)^{-1} B^T P A, \tag{2.71}$$

are strictly within the unit circle.

2.6 Conclusions

In this chapter the preliminary background for satellite dynamics modeling and control are presented and developed. Firstly, the modeling of a single satellite attitude dynamics is presented, that is, the linearized dynamic equation for a single satellite is obtained. The dynamics of the RW actuator is taken into account in this modeling. Next, using similarity transformations the relative dynamics equation for the satellite formation is derived and the information flow structure for formation satellites is provided. The mathematical modeling of certain RW faults are presented in this chapter and finally, the MPC and the LQR frameworks are discussed. The introduced notations will be used in the remainder of the thesis.

Chapter 3

Centralized, Semi-Decentralized and Decentralized Attitude Control Subject to Constraints

In this chapter, behavior-based formation control strategies are developed. The objectives of the behavior-based control are specified as: (a) goal seeking where a desirable orientation is assigned to each individual agent to track, and (b) formation keeping where the relative orientation of the agents is maintained to a desirable value. Associated with the second objective, the relative state measurements and the coupled dynamics model are used for achieving the desirable formation behavior. In other words, we propose to incorporate the interactions among the agents in the control design by using coupled dynamics model. The coupled dynamics model contributes to achieving a precise formation by (i) providing a precise knowledge through a relative attitude determination system [84] and (ii) development of a novel behavior-based control formulation based on coupled dynamic modeling.

The cooperative control of attitude motion of formation flying satellites can be accomplished by different control distribution schemes and hierarchies, namely,

centralized, semi-decentralized and decentralized schemes.

The centralized approach to solving the problem assumes that the central controller has a global information about the team and it determines the local agents inputs and communicates it to the local agents. This structure imposes stringent communication requirements on the system and the level of complexity for the control design is considerable due to solving a global problem of large size. Moreover, it inherits the problem of a single point of failure.

Dividing the centralized problem into sub problems of lower dimension, that is, developing a semi-decentralized scheme, allows addressing the aforementioned drawbacks of a centralized control scheme. In a semi-decentralize scheme, neighboring agents share their states information and each agent determines its optimal input.

On the other hand, a decentralized scheme implies independent operation of agents and therefore, the formation keeping objective cannot be satisfied by using this control scheme.

In the following sections, the centralized approach toward solving the formation problem is presented where the MPC and the LQR approaches for achieving the team objectives are provided. Next, the semi-decentralized solution of the problem is proposed that uses the MPC to achieve the team objectives and finally, a fully-decentralized non-cooperative scheme is presented. All the aforementioned MPC-based approaches take into account actuator constraints. The performance of the proposed semi-decentralized scheme is evaluated and compared with the other schemes by simulation studies.

3.1 Centralized MPC Control Scheme

This section presents the centralized solution to the MPC problem for formation flying of multi-agent systems. A behavior-based coordination method for the entire team is

developed with its desirable behaviors defined based on two objectives. The first objective is goal seeking where a desirable orientation is assigned to each individual agent to track. The second objective is formation keeping where the relative orientations of the agents with respect to each other are maintained to the desirable value. Note that the latter imposes interactions and coupling effects on the system. In the MPC control scheme, both absolute and relative state measurements are communicated from each agent to the central controller and the optimal input for each agent is determined by the controller through minimizing one global cost function, which is formed based on a behavior-based approach and then communicated to each agent.

In this structure the following dynamic equations govern the control design through performing the predictions based on the input dynamic information of all the agents. We concatenate the states, the inputs and the corresponding system models and obtain

$$\underbrace{\begin{bmatrix} x_1(k+1) \\ \widetilde{x}_1(k+1) \\ \hdashline \vdots \\ \hdashline x_{N_v}(k+1) \\ \widetilde{x}_{N_v}(k+1) \end{bmatrix}}_{x(k+1)} = \underbrace{\begin{bmatrix} \overline{A}_1 & 0 & 0 \\ 0 & \ddots & 0 \\ 0 & 0 & \overline{A}_{N_v} \end{bmatrix}}_{\overline{A}} \underbrace{\begin{bmatrix} x_1(k) \\ \widetilde{x}_1(k) \\ \hdashline \vdots \\ \hdashline x_{N_v}(k) \\ \widetilde{x}_{N_v}(k) \end{bmatrix}}_{x(k)} + \underbrace{\begin{bmatrix} \overline{B}_1 \\ \vdots \\ \overline{B}_{N_v} \end{bmatrix}}_{\overline{B}} \underbrace{\begin{bmatrix} u_1(k) \\ \vdots \\ u_{N_v}(k) \end{bmatrix}}_{u(k)} \tag{3.1}$$

where $x \in \mathbb{R}^{10N_v^2}$, $u \in \mathbb{R}^{3N_v}$ and $\left(\overline{A}, \overline{B}\right) \in \mathbb{R}^{10N_v^2 \times 10N_v^2 \times 10N_v^2 \times 3N_v}$.

Remark 1. Due to the centralized control structure, $\widetilde{x}_j$ represents the relative state of agent j with respect to all other agents, i.e., $\widetilde{x}_j = \{x_{jk} \in \mathbb{R}^{10} | k \in V_f - \{j\}\}$.

Remark 2. The concatenated dynamical model is composed of the agents absolute states dynamics and their relative states dynamics and therefore the model is of high dimensions as can be concluded from the dimensions specified above.

We are now in a position to formally state our centralized MPC-based control problem. We use the vector norm notation in the following formulation, i.e., $\|.\|_P^2$

denotes the vector norm, namely the $P-$weighted 2-norm ($\|x\|_P^2 = x^{\mathrm{T}}Px$).

Problem A. *At any time instant* t_k, $k \in \{0, 1, 2, \ldots\}$, *given* $x(k)$, *find the input sequence* $\{u(k|k), u(k+1|k), \ldots, u(k+m-1|k)\} \in \mathbb{R}^{3N_v}$, *that minimizes the cost function* J,

$$J = \min_{u(k|k),\ldots,u(k+m-1|k)} \sum_{l=0}^{N-1} \{\|x(k+l|k)\|_Q^2 + \|u(k+l|k)\|_R^2\} + \|x(k+N|k)\|_{\overline{Q}}^2 \tag{3.2}$$

where the prediction equations are as follows

$$\begin{cases} x(k+l+1 \mid k) = \overline{A}x(k+l \mid k) + \overline{B}u(k+l \mid k), \quad l = 0, \ldots, N-1 \\ x(k|k) = x(k) \end{cases} \tag{3.3}$$

Moreover, the constraints of the problem are given by

$$\begin{cases} x(k+l|k) \in X & l = 1, \ldots, N \\ u(k+l|k) \in U & l = 1, \ldots, M-1 \\ u(k+l|k) = u(k+M-1|k) & l \geq M \\ z^u(k+N|k) = \tilde{V}_u \begin{bmatrix} x(k+N|k) \end{bmatrix} = 0 \end{cases} \tag{3.4}$$

In this cost function, the first two terms are linked to minimizing the predicted $x(k+l \mid k)$ and the magnitude of the input $u(k+l \mid k)$, respectively, for $l = 0, \ldots, N-1$ and the last term reflects minimizing the terminal predicted states, $Q \in \mathbb{R}^{10N_v^2 \times 10N_v^2}$ denotes a positive definite matrix representing the state penalty matrix for the concatenated state vector and is considered constant over the prediction horizon, and $\overline{Q} \in \mathbb{R}^{10N_v^2 \times 10N_v^2}$ represents the penalty matrix for the terminal states. This matrix must be determined such that necessary conditions of the closed-loop system stability are satisfied. Moreover, $R \in \mathbb{R}^{3N_v \times 3N_v}$ denotes a positive definite matrix representing the input penalty matrix and is considered constant over the

prediction horizon. Also, $\overline{A}$ and $\overline{B}$ represent the linear state space model as given in equation (3.1). Finally, $X = \{x \mid \underline{x} \leq x \leq \overline{x}\}$ and $U = \{x \mid \underline{u} \leq x \leq \overline{u}\}$, represent the sets of linear constraints where $(\underline{x}, \overline{x})$, $\left(\widetilde{\underline{x}}, \widetilde{\overline{x}}\right)$ and $(\underline{u}, \overline{u})$ capture the lower and upper limits of the predicted states and the input, respectively, and $\tilde{V}_u$ must be determined such that the necessary conditions of the closed-loop system stability are satisfied (Theorem 1 in Subsection 3.3.1).

Here are some remarks on this optimization problem:

Remark 3. The objective in the above constrained minimization problem is state set-point tracking control, and for the sake of simplicity in the formulation, a shift of coordinates with respect to the desired set-point $\left(\widehat{x}_j, \widehat{\widetilde{x}}_j, \widehat{u}_j, \widehat{\widetilde{u}}_j\right)$ is performed.

Remark 4. The available algorithms for solving the above constrained optimization problem include interior point, active set and trust-region reflective

We present the implementation algorithm for our proposed control approach in Algorithm 3.1.

Algorithm 3.1 Centralized MPC Scheme

1. At any time t_k, $k \in \{0, 1, 2, \ldots\}$:
   - For any agent j:
     (a) Measure $x_j(k)$ and $\widetilde{x}_j(k)$.
     (b) Communicate $x_j(k)$ and $\widetilde{x}_j(k)$ to the central controller.
   - The central controller:
     (a) Receives the state $x(k)$.
     (b) Solves Problem A by using any available algorithm such as the interior point, etc. yielding $u^*(k+l \mid k)$ for $l = 0, 1, \ldots, M-1$.
     (c) Communicates $u_j^*(k \mid k)$ to each corresponding agent j.
2. Over any interval $[t_k, t_{k+1})$, $k \in \{0, 1, 2, \ldots\}$:
   - For any agent j:
     Apply $u_j^*(k \mid k)$.

In the next section, we provide coping the problem using another relevant optimal

control method, namely, the LQR.

3.2 Centralized LQR Control Scheme

As explained in Section 3.1, the following linear model, governs the control design in the centralized control scheme,

$$\underbrace{\begin{bmatrix} x_1(k+1) \\ \widetilde{x}_1(k+1) \\ \hdashline \vdots \\ \hdashline x_{N_v}(k+1) \\ \widetilde{x}_{N_v}(k+1) \end{bmatrix}}_{x(k+1)} = \underbrace{\begin{bmatrix} \overline{A}_1 & 0 & 0 \\ 0 & \ddots & 0 \\ 0 & 0 & \overline{A}_{N_v} \end{bmatrix}}_{\overline{A}} \underbrace{\begin{bmatrix} x_1(k) \\ \widetilde{x}_1(k) \\ \hdashline \vdots \\ \hdashline x_{N_v}(k) \\ \widetilde{x}_{N_v}(k) \end{bmatrix}}_{x(k)} + \underbrace{\begin{bmatrix} \overline{B}_1 \\ \vdots \\ \overline{B}_{N_v} \end{bmatrix}}_{\overline{B}} \underbrace{\begin{bmatrix} u_1(k) \\ \vdots \\ u_{N_v}(k) \end{bmatrix}}_{u(k)} \tag{3.5}$$

$$y(k) = \underbrace{\begin{bmatrix} \overline{C}_1 & 0 & 0 \\ 0 & \ddots & 0 \\ 0 & 0 & \overline{C}_1 \end{bmatrix}}_{\overline{C}} \underbrace{\begin{bmatrix} x_1(k) \\ \widetilde{x}_1(k) \\ \hdashline \vdots \\ \hdashline x_{N_v}(k) \\ \widetilde{x}_{N_v}(k) \end{bmatrix}}_{x(k)} \tag{3.6}$$

where an output vector is also considered for the purpose of control of an error vector. Matrix $\overline{C} \in \mathbb{R}^{3N_v \times 10N_v^2}$ is chosen such that the outputs are quaternion vectors for each satellite i.e.,

$$\overline{C}_1 = \begin{bmatrix} C_2 & 0_{3\times 10(N_v-1)} \end{bmatrix}, \quad \text{and} \quad C_2 = \begin{bmatrix} 0 & 0 & 0 & 1 & 0 & 0 & 0 & 0 & 0 & 0 \\ 0 & 0 & 0 & 0 & 1 & 0 & 0 & 0 & 0 & 0 \\ 0 & 0 & 0 & 0 & 0 & 1 & 0 & 0 & 0 & 0 \end{bmatrix}. \tag{3.7}$$

By using the controller Hessenberg canonical decomposition form, the control of

the controllable subsystem is addressed,

$$\begin{bmatrix} x_{co}(k+1) \\ x_{\overline{co}}(k+1) \end{bmatrix} = \begin{bmatrix} \overline{A}_{co} & \overline{A}_{12} \\ 0 & \overline{A}_{\overline{co}} \end{bmatrix} \begin{bmatrix} x_{co}(k) \\ x_{\overline{co}}(k) \end{bmatrix} + \begin{bmatrix} \overline{B}_{co} \\ 0 \end{bmatrix} u(k) \tag{3.8}$$

Remark 5. The concatenated dynamical model in equation (3.5) is of high dimensions as was specified before. However, the only controllable modes are related to the agents absolute dynamics. As will be shown in Subsection 3.3.1, if one considers the arbitrary point of $\begin{bmatrix} 0 & 0 & 0 & \widehat{\overline{\mathbf{q}}}^{\mathrm{T}} & \widehat{\omega}_w^{\mathrm{T}} \end{bmatrix}^{\mathrm{T}}$ as the operating point condition, a single satellite is uncontrollable and its controllable subsystem is a 6-order subsystem. Therefore, the dimension of the controllable subsystem for the concatenated dynamical model is obtained as $x_{co} \in \mathbb{R}^{24}$, (that is $4 \times 6 = 24$).

One of the conventional methods for providing set-point tracking property for the system is employing an integrator. The input to the integrator is the error between measured output and the desired set-point. The tracking objective will be achieved by designing a proper proportional compensator for the integrator. Therefore, by adding the extra error dynamics the tracking performance will be improved. Then both objectives can be fulfilled by designing an LQR state feedback control law for the augmented states as follows.

Let the 24-dimensional discrete-time controllable-subsystem state equation for the system described in equation (3.8) be obtained as follows

$$\begin{aligned} x_{co}(k+1) &= \overline{A}_{co} x_{co}(k) + \overline{B}_{co} u(k) \\ y(k) &= y_{co}(k) + y_{\overline{co}}(k) = \overline{C}_{co} x_{co}(k) + \overline{C}_{\overline{co}} x_{\overline{co}}(k) \end{aligned} . \tag{3.9}$$

And the state space formulation after augmenting with the integral of error is

expressed as

$$\begin{array}{c} x_{co}(k+1) = \overline{A}_{co} x_{co}(k) + \overline{B}_{co} u(k) \\ e_I(k+1) = e_I(k) + T_s e(k) = e_I(k) + T_s (r_{co} - y_{co}(k)) \end{array}, \tag{3.10}$$

where T_s denotes the sampling period. Thus the standard augmented state space representation will be obtained as

$$\underbrace{\begin{bmatrix} x_{co}(k+1) \\ e_I(k+1) \end{bmatrix}}_{x_{au}(k+1)} = \underbrace{\begin{bmatrix} \overline{A}_{co} & 0 \\ -T_s \overline{C}_{co} & I \end{bmatrix}}_{A_{au}} \underbrace{\begin{bmatrix} x_{co}(k) \\ e_I(k) \end{bmatrix}}_{x_{au}(k)} + \underbrace{\begin{bmatrix} \overline{B}_{co} \\ 0 \end{bmatrix}}_{B_{au}} u(k) + \begin{bmatrix} 0 \\ T_s I \end{bmatrix} r_{co}, \tag{3.11}$$

Where r_{co} denotes the desirable controllable output set-point which is transformed to new coordinates corresponding to the controller Hessenberg canonical decomposition form. The design of the state-feedback $u(k)$, such that the augmented closed-loop system becomes stable, yields an improved reference tracking performance and can be accomplished by LQR method. Finally, the state-feedback will be in the form of :

$$u(k) = L x_{au}(k) = \begin{bmatrix} L_P & L_I \end{bmatrix} \begin{bmatrix} x_{co}(k) \\ e_I(k) \end{bmatrix} \tag{3.12}$$

The following LQR formulation (Problem B) introduces the set-point tracking problem using the centralized LQR control scheme [98].

Problem B. *Given the controllable pair* (A_{au}, B_{au}), *find the matrix* L, *such that* $u(k) = L x_{au}(k)$ *minimizes the following cost function* J,

$$J = \sum_{k=0}^{\infty} \left\{ x_{au}(k)^T Q x_{au}(k) + u(k)^T R u(k) \right\}. \tag{3.13}$$

In equation (3.13), the first term is linked to minimizing the states $x_{au}(k)$ and the second term is linked to the size of control input $u(k)$ for $k = 0, \ldots, \infty$. Q and R

denote a positive semi-definite and a positive definite matrix, respectively, with proper dimensions. According to [98], if we obtain the unique solution P of the following algebraic matrix equation (3.14) within the class of positive semi-definite symmetric matrices,

$$P = A_{au}^{\mathrm{T}} \left(P - PB_{au} \left(B_{au}^{\mathrm{T}} PB_{au} + R \right)^{-1} B_{au}^{\mathrm{T}} P \right) A_{au} + Q, \tag{3.14}$$

and if we let

$$L = - \left(B_{au}^{\mathrm{T}} PB_{au} + R \right)^{-1} B_{au}^{\mathrm{T}} PA_{au}, \tag{3.15}$$

then the eigen-values of the matrix $D = A_{au} + B_{au}L$, are strictly within the unit circle which implies the stability of the corresponding closed-loop system.

Remark 6. The objective in this minimization problem is state set-point tracking control, and for the sake of simplicity in the formulation, a shift of coordinates with respect to the desired set-points is performed.

3.3 Semi-Decentralized MPC Control Scheme

In this section, the semi-decentralized solution of the problem is proposed in which only neighboring agents share their relative state measurements and each agent determines its optimal input based on a behavior-based approach. A behavior-based coordination method for each individual agent is developed where the first objective is goal seeking and the second objective is formation keeping where the relative orientation of the agents with respect to their neighbors is maintained to the desirable value. Our objective here is to obtain a coupled dynamic equation such that the effects of each individual input is reflected in the relative states. We demonstrate this approach by using an example:

Example 1. Consider the communication topology that is depicted in Figure 3.1. The specified graph describes a connected graph (its Laplacian has only one zero

eigenvalue), with $V_f = \{1, 2, 3, 4\}$ and $A_f = \{(1, 2), (1, 3), (2, 4), (3, 4)\}$.

Given that for each individual agent, the effects of its input are reflected in the states of the agent and also relative states, we use the following definition to design each local controller such that the predictions are performed based on the input activity information of each individual agent.

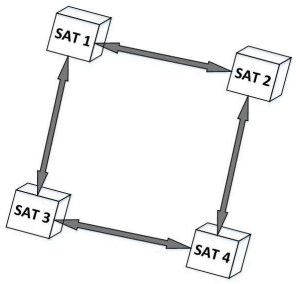

Figure 3.1: A Semi-Decentralized Communication Topology.

Definition 1. (Coupled Subsystem). A coupled subsystem j is a subsystem with the state vector that is composed of $x_j^{(j)}$and $\widetilde{x}_j^{(j)}$ defined as responses of the states x_j and $\widetilde{x}_j$ to the input u_j. We represent this vector response by superscripts to distinguish it from the overall state of the system. The coupling equation is now given by

$$\begin{bmatrix} x_j^{(j)}(k+1) \\ \widetilde{x}_j^{(j)}(k+1) \end{bmatrix} = \overline{A}_j \begin{bmatrix} x_j^{(j)}(k) \\ \widetilde{x}_j^{(j)}(k) \end{bmatrix} + \underline{B}_j u_j(k) \tag{3.16}$$

where the pair $\left(\overline{A}_j, \underline{B}_j\right)$ is obtained as follows:

The following similarity transformation exists for the augmented state vector corresponding to the subsystem 1, i.e., agent 1 in the Example 1, namely $\begin{bmatrix} x_1^{(1)^{\mathrm{T}}} & \widetilde{x}_1^{(1)^{\mathrm{T}}} \end{bmatrix}^{\mathrm{T}} = \begin{bmatrix} x_1^{(1)^{\mathrm{T}}} & x_{12}^{(1)^{\mathrm{T}}} & x_{13}^{(1)^{\mathrm{T}}} \end{bmatrix}^{\mathrm{T}} = T_1 \begin{bmatrix} x_1^{(1)^{\mathrm{T}}} & x_2^{(1)^{\mathrm{T}}} & x_3^{(1)^{\mathrm{T}}} \end{bmatrix}^{\mathrm{T}}$. T_1 can be found as

$$T_1 = \begin{bmatrix} I_{10\times 10} & 0_{10\times 7} & 0_{10\times 3} & 0_{10\times 7} & 0_{10\times 3} \\ T''_{12}(1:10) & T''_{12}(11:20) & 0_{7\times 3} & 0_{7\times 7} & 0_{7\times 3} \\ 0_{3\times 10} & 0_{3\times 7} & I_{3\times 3} & 0_{3\times 7} & 0_{3\times 3} \\ T''_{13}(1:10) & 0_{7\times 7} & 0_{7\times 3} & 0_{7\times 7} & T''_{13}(11:20) \\ 0_{3\times 10} & 0_{3\times 7} & 0_{3\times 3} & 0_{3\times 7} & I_{3\times 3} \end{bmatrix},$$

where $T''_{jk}(n_1 : n_2)$ denotes the columns n_1 to n_2 of the matrix T''_{jk}, which is given in equation (2.40), for any $(j,k) \in A_f$. Thus, the pair $\left(\overline{A}_j, \underline{B}_j\right)$ in equation (3.16) for the subsystem 1 in Example 1 is obtained as

$$\overline{A}_1 = T_1 \begin{bmatrix} A_1 & 0 & 0 \\ 0 & A_2 & 0 \\ 0 & 0 & A_3 \end{bmatrix} T_1^{-1} \quad \text{and} \quad \underline{B}_1 = T_1 \begin{bmatrix} B_1 \\ 0 \\ 0 \end{bmatrix}. \tag{3.17}$$

The objective here is simultaneous control of absolute states of a given agent and its relative states with respect to the neighbors (semi-decentralized control). In the remainder of this section, and for the sake of simplicity, we focus on design of the control law governing the behavior of the agent j. The same design strategy is applied to all other agents.

In this structure for any agent j, the following dynamic equation governs the control design through performing the predictions based on the input dynamic information of each agent, that is

$$\begin{bmatrix} x_j(k+1) \\ \widetilde{x}_j(k+1) \end{bmatrix} = \overline{A}_j \begin{bmatrix} x_j(k) \\ \widetilde{x}_j(k) \end{bmatrix} + \underline{B}_j u_j(k), \tag{3.18}$$

which corresponds to the model in equation (3.16) where for the sake of brevity, the superscripts are omitted. We are now in a position to formally state our semi-decentralized MPC-based control problem.

Problem C. *For every agent $j \in V_f$ and at any time instant t_k, $k \in \{0, 1, 2, \ldots\}$, given $x_j(k)$ and $\widetilde{x}_j(k)$, i.e. the agent j absolute and relative states measurements, find the input sequence $\{u_j(k|k), u_j(k+1|k), \ldots, u_j(k+m-1|k)\} \in \mathbb{R}^3$ that minimizes the cost function J_j,*

$$J_j = \sum_{l=0}^{N-1} \{\|x_j(k+l|k)\|^2_{Q_j} + \|\tilde{x}_j(k+l|k)\|^2_{\widetilde{Q}_j} + \|u_j(k+l|k)\|^2_{R_j}\} + \\ \|x_j(k+N|k)\|^2_{\overline{Q}_j} + \|\tilde{x}_j(k+N|k)\|^2_{\overline{\widetilde{Q}}_j},$$

where the prediction equations are as follows

$$\begin{cases} \begin{bmatrix} x_j(k+l+1|k) \\ \widetilde{x}_j(k+l+1|k) \end{bmatrix} = \overline{A}_j \begin{bmatrix} x_j(k+l|k) \\ \widetilde{x}_j(k+l|k) \end{bmatrix} + \underline{B}_j u_j(k+l|k), \quad l = 0, \ldots, N-1 \\ x_j(k|k) = x_j(k) \\ \widetilde{x}_j(k|k) = \widetilde{x}_j(k) \end{cases}$$

Moreover, the constraints of the problem are given by

$$\begin{cases} x_j(k+l|k) \in X_j & l = 1, \ldots, N \\ \widetilde{x}_j(k+l|k) \in \widetilde{X_j} & l = 1, \ldots, N \\ u_j(k+l|k) \in U_j & l = 1, \ldots, M-1 \\ u_j(k+l|k) = u_j(k+M-1|k) & l \geq M \\ z^u_j(k+N|k) = \tilde{V}_{u_j} \begin{bmatrix} x_j(k+N|k) \\ \widetilde{x}_j(k+N|k) \end{bmatrix} = 0 \end{cases}$$

In this cost function, $Q_j \in \mathbb{R}^{10\times10}$ and $\widetilde{Q}_j$ denote positive definite matrices representing the state penalty matrices for the absolute states and relative states, respectively,

and are considered constant over the prediction horizon, and $\overline{Q}_j \in \mathbb{R}^{10\times10}$ and $\overline{\widetilde{Q}}_j$ represent the penalty matrices for the terminal states. These matrices must be determined such that necessary conditions of the closed-loop system stability are satisfied. The dimensions of $\widetilde{Q}_j$ and $\overline{\widetilde{Q}}_j$ depend on the communication topology, $R_j \in \mathbb{R}^{3\times3}$ denotes a positive definite matrix representing the input penalty matrix and is considered constant over the prediction horizon. Also, $\overline{A}_j$ and $\underline{B}_j$ represent the linear state space model as given in equation (3.18). The dimensions of $\overline{A}_j$ and $\underline{B}_j$ depend on the communication topology. Finally, $X_j = \left\{x \mid \underline{x}_j \leq x \leq \overline{x}_j\right\}$, $\widetilde{X}_j = \left\{x \mid \underline{\widetilde{x}}_j \leq x \leq \overline{\widetilde{x}}_j\right\}$ and $U_j = \left\{x \mid \underline{u}_j \leq x \leq \overline{u}_j\right\}$, represent the sets of linear constraints where $\left(\underline{x}_j, \overline{x}_j\right)$, $\left(\underline{\widetilde{x}}_j, \overline{\widetilde{x}}_j\right)$ and $\left(\underline{u}_j, \overline{u}_j\right)$ capture the lower and upper limits of the predicted absolute states, predicted relative states and the input, respectively, and $\tilde{V}_{u_j}$ must be determined such that the necessary conditions of the closed-loop system stability are satisfied.

Here are some remarks on the above optimization problem:

Remark 7. The objective in the above constrained minimization problem is state set-point tracking control, and for the sake of simplicity in the formulation, a shift of coordinates with respect to the desired set-point$\left(\widehat{x}_j, \widehat{\widetilde{x}}_j, \widehat{u}_j\right)$ is performed.

Remark 8. The available algorithm for solving this constrained optimization problem include interior point, active set and trust-region reflective.

We present the implementation algorithm for our proposed control approach in Algorithm 3.2. In the following subsection, we also discuss the stability issues for the formulated MPC problem.

3.3.1 Stability Analysis

Early versions of the MPC method did not ensure stability and relied on tuning. After 1990, the MPC algorithm was developed to guarantee stability. Indeed the stability issue resulted in new formulations for the MPC method. A comprehensive survey [99] discussed the stability issues of the MPC. Based on this survey Keerthi

Algorithm 3.2 Semi-Decentralized MPC Scheme for any agent $j \in V_f$

1. At any time t_k, $k \in \{0, 1, 2, \ldots\}$:
   (a) Measure the current absolute state $x_j(k)$ and measure or receive current relative states $\widetilde{x}_j(k)$.
   (b) Solve Problem C for agent j by using any available algorithm such as the interior point, etc., yielding $u_j^*(k+l \mid k)$ for $l = 0, 1, \ldots, M-1$.
2. Over any interval $[t_k, t_{k+1})$, $k \in \{0, 1, 2, \ldots\}$:
   Apply $u_j^*(k \mid k)$.

and Gilbert in 1988 [100] and Mayne and Michalska in [101] established the stability of nonlinear constrained MPC for the first time. They used Lyapunov analysis and selected value function of the MPC as the Lyapunov function and employed terminal equality constraint for establishing its closed-loop stability. Muske and Rawlings in 1993 proved nominal constrained stability for the linear constrained receding horizon regulator with perfect measurement of the states at each sampling step [102].

Recall that the linear discrete-time model, based on which the semi-decentralized MPC control was developed was as follows:

$$\begin{bmatrix} x_j(k+1) \\ \tilde{x}_j(k+1) \end{bmatrix} = \overline{A}_j \begin{bmatrix} x_j(k) \\ \tilde{x}_j(k) \end{bmatrix} + \overline{B}_j u_j(k) \tag{3.19}$$

The overall system behavior is shaped from the collective responses of the local controllers. This collective response, based on the principle of superposition, is obtained as the the following dynamical model

$$\begin{bmatrix} x_j(k+1) \\ x_k(k+1) \\ \vdots \end{bmatrix} = \begin{bmatrix} A_j & 0 & 0 \\ 0 & A_k & 0 \\ 0 & 0 & \ddots \end{bmatrix} \begin{bmatrix} x_j(k) \\ x_k(k) \\ \vdots \end{bmatrix} + \begin{bmatrix} B_j & 0 & 0 \\ 0 & B_k & 0 \\ 0 & 0 & \ddots \end{bmatrix} \begin{bmatrix} u_j(k) \\ u_k(k) \\ \vdots \end{bmatrix}. \tag{3.20}$$

Therefore, the stability properties of the system can be analyzed by evaluating

the stability properties for a single satellite. Recall from Chapter 2 that any single satellite (i.e., agent j) with the nonlinear model $\dot{x}_j = f(x_j, u_j)$, in the neighborhood of any operating point $(\widehat{x}_j, \widehat{u}_j)$ with $\widehat{x}_j = \begin{bmatrix} \widehat{\omega}^{\mathrm{T}} & \widehat{\mathbf{q}}^{\mathrm{T}} & \widehat{q}_4 & \widehat{\omega}_w^{\mathrm{T}} \end{bmatrix}^{\mathrm{T}}$ has the following linear form:

$$x_j(k+1) = A_j x_j(k) + B_j u_j(k) \tag{3.21}$$

where

$$A_j = e^{A_{c_j} T_s}, B_j = \int_0^{T_s} e^{A_{c_j}\lambda} B_{c_j} d\lambda \tag{3.22}$$

and

$$A_{c_j} = \begin{bmatrix} -I_s^{-1}\big([\widehat{\omega}_j\times]I_s - [(I_s\widehat{\omega}_j)\times] - [(I_w\widehat{\omega}_{w_j})\times]\big) & 0 & 0 & I_s^{-1}\tau_v - I_s^{-1}[\widehat{\omega}_j\times]I_w \\ \frac{1}{2}[\widehat{\mathbf{q}}_j\times] + \frac{1}{2}\widehat{q}_{4j}\mathrm{E}_{3\times 3} & -\frac{1}{2}[\widehat{\omega}_j\times] & \frac{1}{2}\widehat{\omega}_j & 0 \\ -\frac{1}{2}\widehat{\mathbf{q}}_j^T & -\frac{1}{2}\widehat{\omega}_j^T & 0 & 0 \\ 0 & 0 & 0 & -I_w^{-1}\tau_v \end{bmatrix}, \quad B_{c_j} = \begin{bmatrix} -I_s^{-1}G_d K_t \\ 0 \\ 0 \\ I_w^{-1}G_d K_t \end{bmatrix} \tag{3.23}$$

The first condition that we must verify for using the stability result in [102] is whether the considered models are stabilizable and detectable. We are assuming availability of full state measurements, thus the condition of detectability is verified. For the purpose of evaluating the stabilizability property of a single agent, the operating point must be specified. Note that our control problem is a set-point tracking problem. Any set-point $(\widehat{x}_j, \widehat{u}_j)$ with $\widehat{x}_j = \begin{bmatrix} \widehat{\omega}_j^{\mathrm{T}} & \widehat{\mathbf{q}}_j^{\mathrm{T}} & \widehat{q}_{4j} & \widehat{\omega}_{w_j}^{\mathrm{T}} \end{bmatrix}^{\mathrm{T}}$ must satisfy the equilibrium condition which is $f(\widehat{x}_j, \widehat{u}_j) = 0$. The pair $(\widehat{x}_j, \widehat{u}_j)$ consists of the equilibrium state and the equilibrium input. As a result, from the kinematic equation (2.5) and dynamic equation (2.14), one will obtain

$$\begin{aligned} \widehat{\omega}_j &= \begin{bmatrix} 0 & 0 & 0 \end{bmatrix}^T, \\ \widehat{u}_j &= \frac{\tau_v \widehat{\omega}_{w_j}}{G_d K_t}, \end{aligned} \tag{3.24}$$

In other words, a set-point tracking problem can only be solved for applications where the desired behavior of satellites is defined as inertial-pointing condition, that is, the condition where the desired value for the angular velocity ($\widehat{\omega}_j$) is zero. Note also that in this equilibrium-point, the torque applied by the RW balances the drag torque caused by the bearing friction [103]. In the inertial-pointing operating condition which is the condition for the set-point regulation problem, $\begin{bmatrix} \widehat{\mathbf{q}}_j^{\mathrm{T}} & \widehat{q}_{4j} \end{bmatrix}$ can be any arbitrary desired set-point vector satisfying unit-norm constraint of quaternion and $\widehat{\omega}_{w_j}^{\mathrm{T}}$ can be any arbitrary desired set-point vector. The top left 3×3 matrix of A_{c_j} will be the following matrix

$$I_s^{-1} \begin{bmatrix} 0 & -I_{w_3}\widehat{\omega}_{w_{3j}} & I_{w_2}\widehat{\omega}_{w_{2j}} \\ I_{w_3}\widehat{\omega}_{w_{3j}} & 0 & -I_{w_1}\widehat{\omega}_{w_{1j}} \\ -I_{w_2}\widehat{\omega}_{w_{2j}} & I_{w_1}\widehat{\omega}_{w_{1j}} & 0 \end{bmatrix} = \begin{bmatrix} 0 & -I_{s_1}^{-1}I_{w_3}\widehat{\omega}_{w_{3j}} & I_{s_1}^{-1}I_{w_2}\widehat{\omega}_{w_{2j}} \\ I_{s_2}^{-1}I_{w_3}\widehat{\omega}_{w_{3j}} & 0 & -I_{s_2}^{-1}I_{w_1}\widehat{\omega}_{w_{1j}} \\ -I_{s_3}^{-1}I_{w_2}\widehat{\omega}_{w_{2j}} & I_{s_3}^{-1}I_{w_1}\widehat{\omega}_{w_{1j}} & 0 \end{bmatrix}, \tag{3.25}$$

and one gets the characteristic polynomial of this matrix as

$$\lambda^3 + \alpha_1\lambda + \alpha_2 = 0 \tag{3.26}$$

where

$$\alpha_1 = I_{s_3}^{-1}I_{s_2}^{-1}I_{w_1}^2\widehat{\omega}_{w_{1j}}^2 + I_{s_3}^{-1}I_{s_1}^{-1}I_{w_2}^2\widehat{\omega}_{w_{2j}}^2 + I_{s_2}^{-1}I_{s_1}^{-1}I_{w_3}^2\widehat{\omega}_{w_{3j}}^2 \geq 0, \tag{3.27}$$

$$\alpha_2 = I_{s_1}^{-1}I_{s_2}^{-1}I_{s_2}^{-1}I_{w_1}I_{w_2}I_{w_3}\widehat{\omega}_{w_{2j}}\widehat{\omega}_{w_{2j}}\widehat{\omega}_{w_{2j}} - I_{s_1}^{-1}I_{s_2}^{-1}I_{s_2}^{-1}I_{w_1}I_{w_2}I_{w_3}\widehat{\omega}_{w_{2j}}\widehat{\omega}_{w_{2j}}\widehat{\omega}_{w_{2j}} = 0, \tag{3.28}$$

therefore, the three eigenvalues are $\lambda_1 = 0$, $\lambda_2 = i\sqrt{\sigma}$ and $\lambda_3 = -i\sqrt{\sigma}$, where $\sigma \geq 0$ is a function of I_s, I_w and $\widehat{\omega}_{w_j}$. The Jordan canonical form of the matrix A_{c_j} is evaluated to be

$$\mathcal{J}\left(A_{c_j}\right) = \left[\begin{array}{cc:ccccc:ccc} 0 & 1 & 0 & 0 & 0 & 0 & 0 & 0 & 0 & 0 \\ 0 & 0 & 0 & 0 & 0 & 0 & 0 & 0 & 0 & 0 \\ \hdashline 0 & 0 & & & & 0 & 0 & 0 & 0 & 0 \\ 0 & 0 & & -I_w^{-1}\tau_v & & 0 & 0 & 0 & 0 & 0 \\ 0 & 0 & & & & 0 & 0 & 0 & 0 & 0 \\ \hdashline 0 & 0 & 0 & 0 & 0 & i\sqrt{\sigma} & 0 & 0 & 0 & 0 \\ 0 & 0 & 0 & 0 & 0 & 0 & -i\sqrt{\sigma} & 0 & 0 & 0 \\ \hdashline 0 & 0 & 0 & 0 & 0 & 0 & 0 & 0 & 0 & 0 \\ 0 & 0 & 0 & 0 & 0 & 0 & 0 & 0 & 0 & 0 \\ 0 & 0 & 0 & 0 & 0 & 0 & 0 & 0 & 0 & 0 \end{array}\right], \tag{3.29}$$

and finding the Jordan canonical form corresponding to the discrete-time model A_j yields

$$\mathcal{J}\left(A_j\right) = \left[\begin{array}{cc:ccccc:ccc} 1 & T_s & 0 & 0 & 0 & 0 & 0 & 0 & 0 & 0 \\ 0 & 1 & 0 & 0 & 0 & 0 & 0 & 0 & 0 & 0 \\ \hdashline 0 & 0 & & & & 0 & 0 & 0 & 0 & 0 \\ 0 & 0 & & e^{-I_w^{-1}\tau_v T_s} & & 0 & 0 & 0 & 0 & 0 \\ 0 & 0 & & & & 0 & 0 & 0 & 0 & 0 \\ \hdashline 0 & 0 & 0 & 0 & 0 & e^{i\sqrt{\sigma}T_s} & 0 & 0 & 0 & 0 \\ 0 & 0 & 0 & 0 & 0 & 0 & e^{-i\sqrt{\sigma}T_s} & 0 & 0 & 0 \\ \hdashline 0 & 0 & 0 & 0 & 0 & 0 & 0 & 1 & 0 & 0 \\ 0 & 0 & 0 & 0 & 0 & 0 & 0 & 0 & 1 & 0 \\ 0 & 0 & 0 & 0 & 0 & 0 & 0 & 0 & 0 & 1 \end{array}\right], \tag{3.30}$$

and therefore, for each agent, there exist two modes on the unit circle crossing the positive real axis, with the associated Jordan block of order two, and two modes on the unit circle in the complex plane, that imply instability of the open-loop system.

Based on the controllability matrix for the pair (A_j, B_j), it follows that it is not full rank, and thus the pair (A_j, B_j) is not controllable. This problem arises because of including higher order dynamics of the system, in particular, ω_w. We now obtain the controller Hessenberg canonical decomposition form, the form that decomposes the system into controllable and uncontrollable subsystems, by finding the corresponding similarity transformation matrix and use staircase algorithm proposed by Rosenbrock [104] to calculate this matrix.

Consider the single satellite (i.e agent j) state equation

$$x_j(k+1) = A_j x_j(k) + B_j u_j(k) \tag{3.31}$$

By using the corresponding transformation matrix, the equation (3.31) will be transformed into

$$\begin{bmatrix} x_{j_{co}}(k+1) \\ x_{j_{\overline{co}}}(k+1) \end{bmatrix} = \begin{bmatrix} A_{j_{co}} & A_{12} \\ 0 & A_{j_{\overline{co}}} \end{bmatrix} \begin{bmatrix} x_{j_{co}}(k) \\ x_{j_{\overline{co}}}(k) \end{bmatrix} + \begin{bmatrix} B_{j_{co}} \\ 0 \end{bmatrix} u_j(k) \tag{3.32}$$

where $A_{j_{co}} \in \mathbb{R}^{6\times 6}$ and $A_{j_{\overline{co}}} \in \mathbb{R}^{4\times 4}$ and the 6-dimensional sub equation of equation (3.32) is controllable:

$$x_{j_{co}}(k+1) = A_{j_{co}} x_{j_{co}}(k) + B_{j_{co}} u_j(k) \tag{3.33}$$

After forming the staircase-form, one observes that the controllable and uncontrollable subsystems have the following Jordan forms:

$$\mathcal{J}\left(A_{j_{co}}\right)=\left[\begin{array}{ccc:cc:c} & & & 0 & 0 & 0 \\ & e^{-I_w^{-1}\tau_v T_s} & & 0 & 0 & 0 \\ & & & 0 & 0 & 0 \\ \hdashline 0 & 0 & 0 & e^{i\sqrt{\sigma}T_s} & 0 & 0 \\ 0 & 0 & 0 & 0 & e^{-i\sqrt{\sigma}T_s} & 0 \\ \hdashline 0 & 0 & 0 & 0 & 0 & 1 \end{array}\right] \tag{3.34}$$

and

$$\mathcal{J}(A_{j_{\overline{co}}})=\left[\begin{array}{cccc} 1 & 0 & 0 & 0 \\ 0 & 1 & 0 & 0 \\ 0 & 0 & 1 & 0 \\ 0 & 0 & 0 & 1 \end{array}\right] \tag{3.35}$$

Obviously, the eigenvalues of the matrix $\mathcal{J}(A_{j_{\overline{co}}})$ are composed of four simple eigenvalues on the unit circle crossing the positive real axis only. Thus, the uncontrollable subsystem is stable and the system is stabilizable [105].

Muske and Rawling in 1993 discussed implementing linear model MPC for unstable but stabilizable plants. According to [102], for unstable modes the input sequence in the optimization problem must be selected in a way such that the predictions of those modes at the time instant $k+N$ are zero (appending terminal equality constraints in the framework). We refer to the following theorem for proving the stability of MPC and use results of their work for achieving a stable closed-loop performance in fault-free conditions.

Theorem 1. *([102]) For the internal model*

$$x\left(k+i+1|k\right)=Ax\left(k+i|k\right)+Bu\left(k+i|k\right) \qquad \text{for} \qquad i=0,\ldots,N-1 \tag{3.36}$$

where A is unstable. Provided (A,B) is stabilizable and $N \geq r$, in which r is the

number of unstable modes of A, $x(k) = 0$ is an asymptotically stable solution of the closed-loop MPC with feasible constraints equations (3.38), (3.39), and objective function given as equation (3.37) for $R > 0$ and $Q \geq 0$, that is

$$J(k) = \sum_{i=0}^{N-1} \{x^T(k+i|k)\, Qx(k+i|k) + u^T(k+i|k)\, Ru(k+i|k)\} + x^T(k+N|k)\, \overline{Q} x(k+N|k) \quad (3.37)$$

The initial state must satisfy $x_0 \in \mathbf{X}_N$ where $\mathbf{X}_N$ denotes the set of x_0 for which there exists an input sequence $\{u(0), u(1|0), \ldots, u(N-1|0)\}$ satisfying the following inequality constraints:

$$\underline{u} \leq u(k+i \mid k) \leq \bar{u} \qquad \text{for} \qquad i = 0, \ldots, N-1 \quad (3.38)$$

$$\underline{x} \leq x(k+i \mid k) \leq \overline{x} \qquad \text{for} \qquad i = 1, \ldots, N \quad (3.39)$$

Moreover, x_0 must satisfy the following equality constraints:

$$z^u(k+N|k) = \tilde{V}_u x(k+N|x) = 0 \quad (3.40)$$

where $\tilde{V}_u$ is determined from Jordan decomposition of A as below

$$A = V \mathcal{J} V^{-1} = \begin{bmatrix} V_u & V_s \end{bmatrix} \begin{bmatrix} J_u & 0 \\ 0 & J_s \end{bmatrix} \begin{bmatrix} \tilde{V}_u \\ \tilde{V}_s \end{bmatrix} \quad (3.41)$$

Furthermore, the terminal state penalty must be determined from

$$\overline{Q} = \tilde{V}_s^T \Sigma \tilde{V}_s \quad (3.42)$$

$$\Sigma = \sum_{i=0}^{\infty} J_s^{T^i} V_s{}^T Q V_s J_s^i = V_s{}^T Q V_s + J_s^T \Sigma J_s \tag{3.43}$$

Proof: The proof of this theorem can be found in [102].

3.4 Decentralized MPC Control Scheme

In this section, the decentralized solution to the problem of formation flying of multi-agent systems is provided. A decentralized scheme is defined as a scheme where the agents do not share any information with each other. Therefore, the only objective for each individual agent is their goal seeking. In this scheme, any agent j uses the previously specified linear discrete-time dynamic model of single satellite j, i.e.,

$$x_j\left(k+1\right) = A_j x_j\left(k\right) + B_j u_j\left(k\right), \tag{3.44}$$

where $A_j \in R^{10\times 10}$, $B_j \in R^{10\times 3}$, $x_j = \left[\begin{array}{ccc} \omega_\alpha^{\mathrm{T}} & \overline{\mathbf{q}}_\alpha^{\mathrm{T}} & \omega_{w_\alpha}^{\mathrm{T}} \end{array}\right]^{\mathrm{T}}$ and $u_j \in \mathbb{R}^3$ indicates the controller command which is input to each of three RWs corresponding to three-axis of any satellite $j \in V_f$ where V_f denotes the set of agents in the team.

We now state the set-point tracking problem for the agent j using the decentralized control scheme.

Problem D. *For every agent $j \in V_f$ and at any time instant t_k, $k \in \{0, 1, 2, \ldots\}$, given $x_j\left(k\right)$, i.e. the agent j absolute states measurements, find the input sequence $\{u_j\left(k|k\right), u_j\left(k+1|k\right), \ldots, u_j\left(k+m-1|k\right)\} \in \mathbb{R}^3$ that minimizes the cost function J_j,*

$$J_j = \textstyle\sum_{l=0}^{N-1} \left\{ \left\| x_j\left(k+l|k\right)\right\|_{Q_j}^2 + \left\| u_j\left(k+l|k\right)\right\|_{R_j}^2 \right\} + \left\| x_j\left(k+N|k\right)\right\|_{\overline{Q}_j}^2 \tag{3.45}$$

where the prediction equations are as follows

$$\begin{cases} x_j\left(k+l+1|k\right) = A_j x_j\left(k+l|k\right) + B_j u_j\left(k+l|k\right) & l = 0, \ldots, N-1 \\ x_j\left(k|k\right) = x_j\left(k\right) \end{cases} \tag{3.46}$$

Moreover, the constraints of the problem are given by

$$\begin{cases} x_j\left(k+l|k\right) \in X_j & l = 1, \ldots, N \\ u_j\left(k+l|k\right) \in U_j & l = 0, \ldots, M-1 \\ u_j\left(k+l|k\right) = u_j\left(k+M-1|k\right) & l \geq M \\ z_j^u\left(k+N|k\right) = \tilde{V}_{u_j} x_j\left(k+N|k\right) = 0 \end{cases} \tag{3.47}$$

In this cost function, the terms are linked to minimizing the predicted $x_j\left(k+l \mid k\right)$, the size of control input $u_j\left(k+l \mid k\right)$ for $l = 0, \ldots, N-1$ and minimizing the terminal predicted states respectively.

Remark 9. The objective in the above constrained minimization problem is state set-point tracking control where, and for the sake of simplicity in the formulation, a shift of coordinates with respect to the desired set-point $(\widehat{x}_j, \widehat{u}_j)$ is performed.

Remark 10. The available algorithm for solving this constrained optimization problem include interior point, active set and trust-region reflective.

Remark 11. Only x_j is incorporated in the cost function and the control input involved in this cost function for the agent j is only the input for the agent j, therefore, the controller has a decentralized design scheme.

We present the implementation algorithm for the decentralized control approach in Algorithm 3.3.

In can be noticed that the equation (3.44) governing the control law in this decentralized control is stabilizable and detectable. Hence, the same theorem stated

Algorithm 3.3 Decentralized MPC scheme for any individual agent j

1. At any time t_k, $k \in \{0, 1, 2, \ldots\}$:
   (a) Measure current absolute state $x_j(k)$.
   (b) Solve Problem D for the agent j by using any available algorithm such as the interior point, etc., yielding $u_j^*(k+l \mid k)$ for $l = 0, 1, \ldots, M-1$.
2. Over any interval $[t_k, t_{k+1})$, $k \in \{0, 1, 2, \ldots\}$:
   Apply $u_j^*(k \mid k)$.

for the semi-decentralized case can be employed here.

3.5 Simulation Results

In this section, the performance of our proposed control strategies are analyzed through simulations. A team of four coordinating satellites is considered and their communication topology for the semi-decentralized case is the one which is depicted in Figure 3.2. The considered graph is connected and symmetric. These properties are desirable for formation applications. Moreover, the graph is not fully connected and therefore, does not impose significant communication requirements. The data communication is assumed to be ideal with zero time delay and loss. Table 3.3 shows the parameters that are considered for modeling the satellites and also saturation constraints and other details related to the RW parameters. Table 3.1 summarizes the initial state values for each agent and Table 3.2 summarizes the operating point information corresponding to the mission specified as an inertial-pointing formation of satellites. The satellites are assumed to be launched into a low Earth orbit and the orbital altitude is specified in Table 3.3.

The dominant environmental disturbance torques corresponding to this orbital altitude include gravity gradient, magnetic field and solar radiation disturbances. The aerodynamic torque is negligible in the orbits with altitude above 500 km. We

assume $2\,m$ by $1.5\,m$ cross section satellites with the center of solar pressure to center of gravity difference of $0.3\,m$ and reflectance factor of $q = 0.6$. The cumulative disturbance torques are calculated for all satellites and provided in Table 3.4. The cumulative disturbance torque acting on each satellite is modeled as zero-mean Gaussian white-noises with standard deviation of $\sigma_{T_d} = \begin{bmatrix} Td & Td & Td \end{bmatrix} (N.m)$. The measurements vector is also modeled as $x = \begin{bmatrix} \omega^{\mathrm{T}} & \overline{\mathbf{q}}^{\mathrm{T}} & \omega_w^{\mathrm{T}} \end{bmatrix}^{\mathrm{T}} + \varepsilon$, where ε denotes the measurements error and modeled as zero-mean Gaussian white-noise with standard deviation of $\sigma_\varepsilon = \begin{bmatrix} 0.1 \times 10^{-4}\, rad/sec & 0.35\, mrad & 0.1 \times 10^{-5}\, rad/sec \end{bmatrix}$, in which the attitude measurements error can be translated to quaternion and obtained as $\begin{bmatrix} 1.7 \times 10^{-4} & 1.7 \times 10^{-4} & 1.7 \times 10^{-4} & 4.5 \times 10^{-8} \end{bmatrix}$.

The controller parameters are summarized in Table 3.5. We do not consider any constraint on states and rate of change of inputs. The optimization problem is solved by using the interior point method. In order to perform a quantitative analysis and comparison of the behavior of the system, particularly steady state and transient behavior, the following performance indices (PIs) are defined,

$$\begin{aligned} \widetilde{J}_{tr_j} &= \textstyle\int_{t=0}^{\widetilde{t}_{s_j}} \widetilde{z}_j^2\,(t)\,dt & \widetilde{J}_{tr} &= \tfrac{1}{2}\textstyle\sum_{j=1}^{4} \widetilde{J}_{tr_j} \\ J_{ss_j} &= z_j^2\,(t_s) & J_{ss} &= \textstyle\sum_{j=1}^{4} J_{ss_j} \\ \widetilde{J}_{ss_j} &= \widetilde{z}_j^2\left(\widetilde{t}_{s_j}\right) & \widetilde{J}_{ss} &= \textstyle\sum_{j=1}^{4} \widetilde{J}_{ss_j} \\ t_s &= \tfrac{1}{4}\textstyle\sum_{j=1}^{4} t_{s_j} & \widetilde{t}_s &= \tfrac{1}{4}\textstyle\sum_{j=1}^{4} \widetilde{t}_{s_j} \end{aligned} \tag{3.48}$$

$$J_{u_{j_l}} = \textstyle\int_{t=0}^{t_{u_j}} u_{jl}^2\,(t)\,dt \qquad J_{u_j} = \textstyle\sum_{l=x,y,z} J_{u_{jl}} \qquad J_u = \textstyle\sum_{j=1:4} J_{u_j} \tag{3.49}$$

where z_j represents either the first, second or the third component of the absolute attitude quaternion vector and $\widetilde{z}_j$ denotes the corresponding components for the relative attitude quaternion vector with respect to one neighboring agent associated with the agent j, t_{s_j} and $\widetilde{t}_{s_j}$indicate their corresponding settling times and u_{jl} represents the control input for the l-axis RW, and t_{u_j} denotes the settling time for this control input.

Note that since in the transient condition only the formation performance is important, this transient-behavior PI targets only relative attitude quaternion variables. The upper limits of the PIs J_{ss} and $\widetilde{J}_{ss}$, namely $J_{ss} \leq \varepsilon$ and $\widetilde{J}_{ss} \leq \widetilde{\varepsilon}$, are selected to be as follows based on the desirable specifications for the steady-state performance of the formation flying system.

$$\begin{aligned} \varepsilon &= 5 \times 10^{-4} \\ \widetilde{\varepsilon} &= 5 \times 10^{-11}, \end{aligned} \tag{3.50}$$

The computational complexity of the control schemes are compared by examining the average number of required iterations ($ITER$) and the average time (t_{solv}) that is taken by the solver to compute the optimal solution at each control update. For the case of the semi-decentralized control scheme, these measures are quite similar to one another for all the agents. The optimization is solved by the FMINCON function of MATLAB and the processor is 4-cored operating at 2.80 GHz, and is managed by a 64-bit operating system.

The following comparisons are made to evaluate the effectiveness of the proposed semi-decentralized approach.

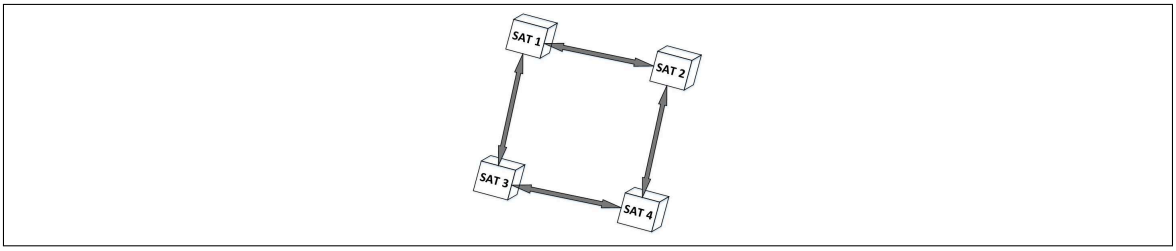

Figure 3.2: Communication Topology (Semi-Decentralized Control)

Table 3.1: Initial State Values

SAT 1				SAT 2			
ω_0 *rad/sec*	$\overline{\mathbf{q}}_0$	ω_{w_0} *rad/sec*	N_{m_0} *N.m*	ω_0 *rad/sec*	$\overline{\mathbf{q}}_0$	ω_{w_0} *rad/sec*	N_{m_0} *N.m*
$\begin{bmatrix} 0 \\ 0 \\ 0 \end{bmatrix}$	$\begin{bmatrix} 0.47 \\ 0.47 \\ 0.47 \\ 0.58 \end{bmatrix}$	$\begin{bmatrix} 2400 \\ 2400 \\ 2400 \end{bmatrix}$	$\begin{bmatrix} 0.5 \\ 0.5 \\ 0.5 \end{bmatrix}$	$\begin{bmatrix} 0 \\ 0 \\ 0 \end{bmatrix}$	$\begin{bmatrix} 0.43 \\ 0.43 \\ 0.43 \\ 0.67 \end{bmatrix}$	$\begin{bmatrix} 2400 \\ 2400 \\ 2400 \end{bmatrix}$	$\begin{bmatrix} 0.5 \\ 0.5 \\ 0.5 \end{bmatrix}$
SAT 3				SAT 4			
ω_0 *rad/sec*	$\overline{\mathbf{q}}_0$	ω_{w_0} *rad/sec*	N_{m_0} *N.m*	ω_0 *rad/sec*	$\overline{\mathbf{q}}_0$	ω_{w_0} *rad/sec*	N_{m_0} *N.m*
$\begin{bmatrix} 0 \\ 0 \\ 0 \end{bmatrix}$	$\begin{bmatrix} 0.5 \\ 0.5 \\ 0.5 \\ 0.5 \end{bmatrix}$	$\begin{bmatrix} 2400 \\ 2400 \\ 2400 \end{bmatrix}$	$\begin{bmatrix} 0.5 \\ 0.5 \\ 0.5 \end{bmatrix}$	$\begin{bmatrix} 0 \\ 0 \\ 0 \end{bmatrix}$	$\begin{bmatrix} 0.45 \\ 0.45 \\ 0.45 \\ 0.63 \end{bmatrix}$	$\begin{bmatrix} 2400 \\ 2400 \\ 2400 \end{bmatrix}$	$\begin{bmatrix} 0.5 \\ 0.5 \\ 0.5 \end{bmatrix}$

Table 3.2: Operating Point

$\widehat{\omega}_{jk}$ for $1 \leq j \leq 4$and $1 \leq k \leq 4$	$\begin{bmatrix} 0 & 0 & 0 \end{bmatrix}^{\mathrm{T}}$ *rad/sec*
$\widehat{\mathbf{q}}_{jk}$ for $1 \leq j \leq 4$and $1 \leq k \leq 4$	$\begin{bmatrix} 0 & 0 & 0 \end{bmatrix}^{\mathrm{T}}$
$\widehat{\omega}_j$ for $1 \leq j \leq 4$	$\begin{bmatrix} 0 & 0 & 0 \end{bmatrix}^{\mathrm{T}}$ *rad/sec*
$\widehat{\overline{\mathbf{q}}}_j$ for $1 \leq j \leq 4$	$\begin{bmatrix} 0.5866 & 0.5816 & 0.5743 & 0.039 \end{bmatrix}^{\mathrm{T}}$
$\widehat{\omega}_{w_j}$ for $1 \leq j \leq 4$	$\begin{bmatrix} 2500 & 2500 & 2500 \end{bmatrix}^{\mathrm{T}}$ *rad/sec*
$\widehat{N}_{m_j}$ for $1 \leq j \leq 4$	$\begin{bmatrix} 0.5 & 0.5 & 0.5 \end{bmatrix}^{\mathrm{T}}$ *N.m*

Table 3.3: Parameters of the System

Angular velocity of the satellite with respect to the Earth associated with altitude of $981.39Km$ [59] (all SATs)	$\omega_0 = 0.001\ rad/sec$
Principal moments of inertia for SAT 1	$I = \text{diag}\begin{bmatrix} 41.2 & 39.6 & 38.4 \end{bmatrix} N.m.s^2$
Principal moments of inertia for SAT 2	$I = \text{diag}\begin{bmatrix} 40.4 & 40.8 & 39.2 \end{bmatrix} N.m.s^2$
Principal moments of inertia for SAT 3	$I = \text{diag}\begin{bmatrix} 40.8 & 40.4 & 41.2 \end{bmatrix} N.m.s^2$
Principal moments of inertia for SAT 4	$I = \text{diag}\begin{bmatrix} 40.4 & 40.8 & 38.8 \end{bmatrix} N.m.s^2$
Flywheel inertia (all SATs)	$I_W = \text{diag}\begin{bmatrix} 0.007 & 0.007 & 0.007 \end{bmatrix} N.m.s^2$
RW driver gain (all SATs)	$G_d = 0.19\ A/V$
Motor torque constant (all SATs)	$K_t = 0.029\ N.m/A$
Viscous friction (all SATs)	$\tau_d = 0.2\ \frac{mN.m}{rad/sec}$
Maximum limit on torque produced by the RW [106] (all SATs)	$N_m = 1\ N.m$
Sampling Time (all SATs)	$T_s = 0.25\ sec$

Table 3.4: Satellites Disturbance Torques

	SAT 1	SAT 2	SAT 3	SAT 4
T_d	4.18×10^{-5}	4.24×10^{-5}	4.06×10^{-5}	4.30×10^{-5}

Table 3.5: MPC Controller Parameters (Consistent for All of the Satellites)

Absolute state penalty matrix	$Q = \text{diag}\left[\begin{array}{cccccccccc} 2{\times}10^4 & 2{\times}10^4 & 2{\times}10^4 & 5{\times}10^4 & 5{\times}10^4 & 5{\times}10^4 & 5{\times}10^4 & 10^{-4} & 10^{-4} & 10^{-4} \end{array}\right]^{\mathrm{T}}$
Absolute terminal state penalty matrix	$\bar{Q} = \text{diag}\left[\begin{array}{cccccccccc} 2{\times}10^4 & 2{\times}10^4 & 2{\times}10^4 & 5{\times}10^4 & 5{\times}10^4 & 5{\times}10^4 & 5{\times}10^4 & 10^{-4} & 10^{-4} & 10^{-4} \end{array}\right]^{\mathrm{T}}$
Relative state penalty matrix	$\widetilde{Q} = \text{diag}\left[\begin{array}{cccccccccc} 2{\times}10^4 & 2{\times}10^4 & 2{\times}10^4 & 5{\times}10^5 & 5{\times}10^5 & 5{\times}10^5 & 5{\times}10^5 & 10^{-4} & 10^{-4} & 10^{-4} \end{array}\right]^{\mathrm{T}}$
Relative terminal state penalty matrix	$\bar{\widetilde{Q}} = \text{diag}\left[\begin{array}{cccccccccc} 2{\times}10^4 & 2{\times}10^4 & 2{\times}10^4 & 5{\times}10^5 & 5{\times}10^5 & 5{\times}10^5 & 5{\times}10^5 & 10^{-4} & 10^{-4} & 10^{-4} \end{array}\right]^{\mathrm{T}}$
Input penalty matrix	$R = 10^{-5} \times \mathrm{I}^{3\times 3}$
Prediction horizon	$N = 5$
Control horizon	$m = 1$

3.5.1 Semi-Decentralized MPC Scheme vs. Centralized MPC Scheme

The first comparative study is performed between a centralized control scheme and a semi-decentralized control scheme. The x-axis absolute attitude quaternion of all the satellites, the relative attitude quaternion and the corresponding control torques for the semi-decentralized and centralized control schemes are shown in Figures 3.3, 3.4 and 3.5, respectively. The response characteristics are summarized in Table 3.6. Figure 3.4 and also the PI $\widetilde{J}_{tr}$ show that the relative states in the semi-decentralized case shows a fairly similar behavior with the centralized scheme but without imposing significant computational complexity due to solving one problem of higher dimensions, as shown by comparing t_{solv} and $ITER$ in Table 3.6, and without imposing significant communication requirements associated with the centralized scheme. Figure 3.5 shows that the RW constraints are satisfied in these control design schemes and the RW torque never exceeded the specified threshold. The cumulative control effort costs (J_u) for the two schemes show that the centralized scheme yields a lower control effort cost. This feature is related to the global optimization problem that is solved for the entire team in this centralized scheme.

Table 3.6: Goal-Seeking/Formation Performance and Time Response for the x-axis, Control Effort Costs and Computational Efforts in Semi-Decentralized and Centralized Schemes

	$\widetilde{J}_{tr}$	J_{ss}	$\widetilde{J}_{ss}$	J_u	$\widetilde{t}_s$	t_s	t_{solv}	$ITER$
Semi-Dec. MPC	0.158	2.7×10^{-4}	1.4×10^{-11}	494.09	6.93	12.58	0.31	21
Centralized MPC	0.082	4.5×10^{-4}	4×10^{-11}	380.44	8.68	16.75	3.41	83

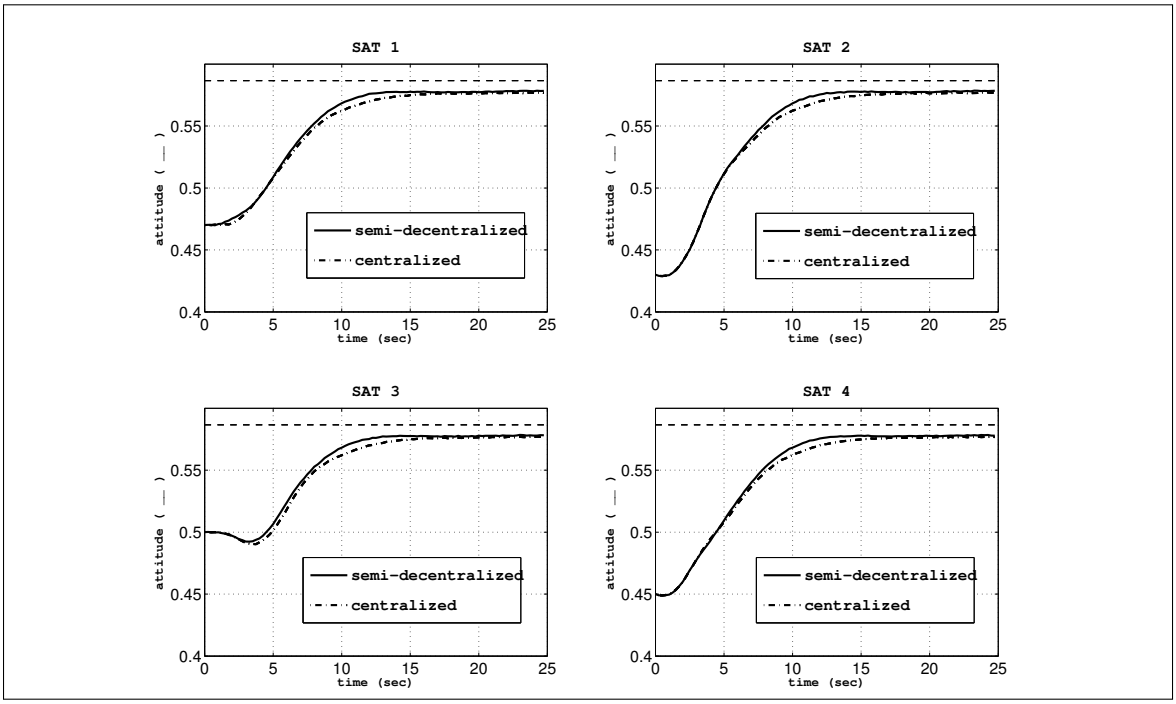

Figure 3.3: X-axis Attitude Quaternion.

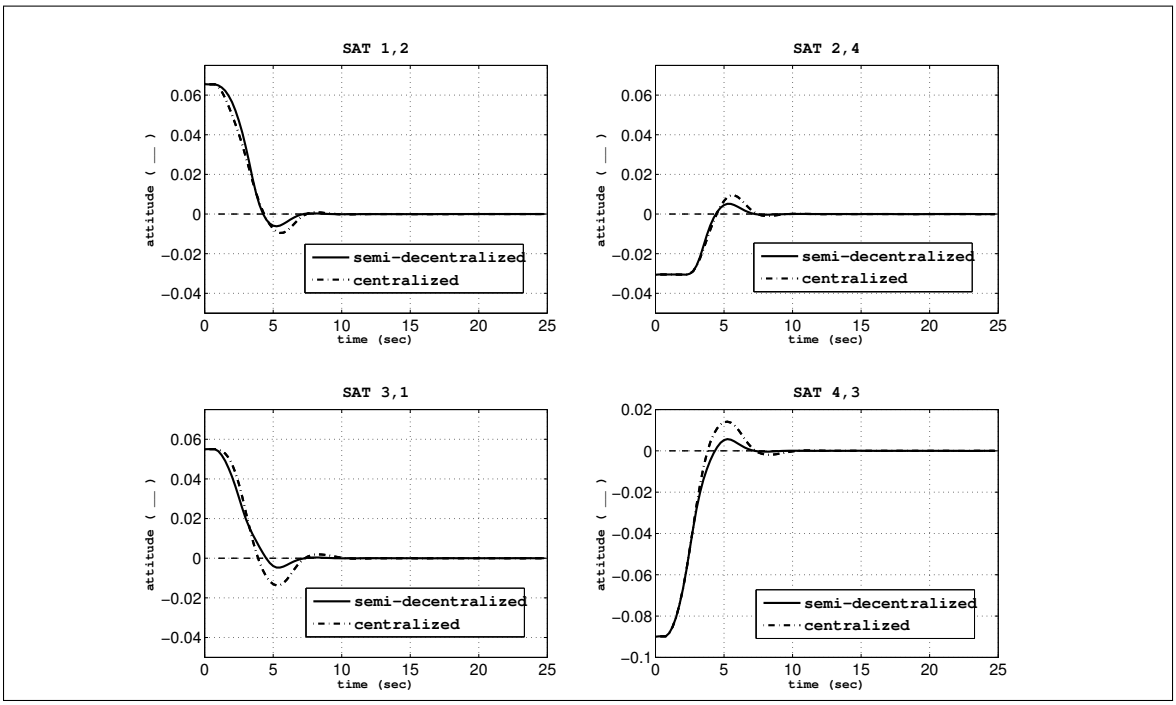

Figure 3.4: X-axis Relative Attitude Quaternion.

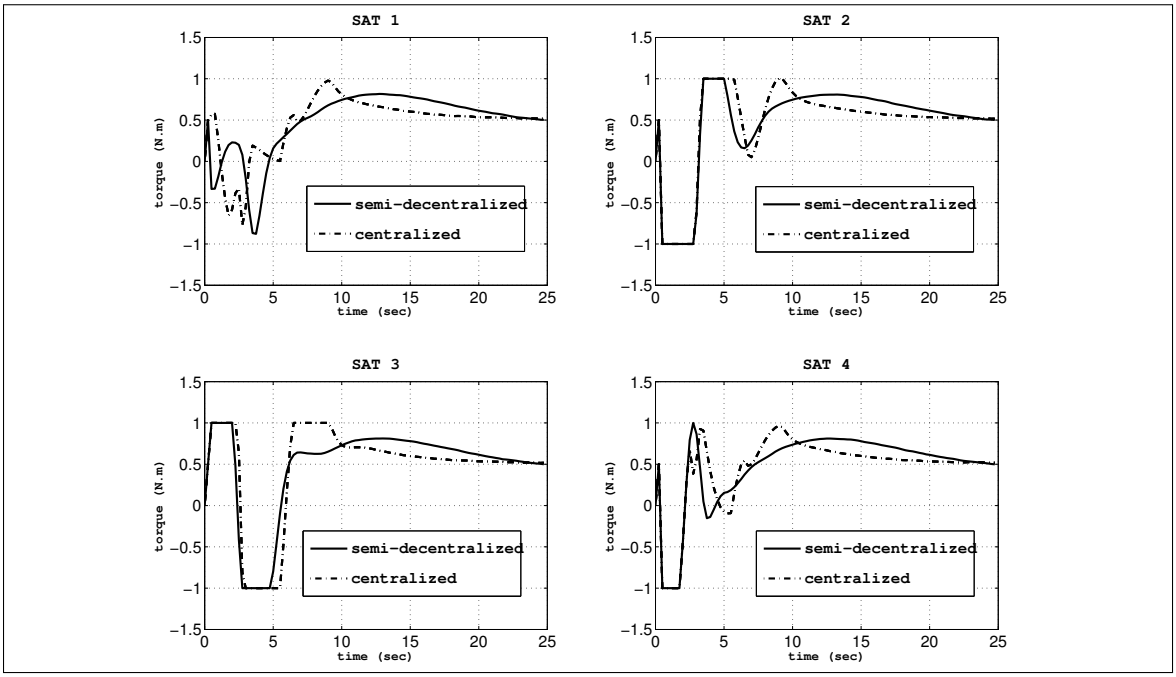

Figure 3.5: X-axis RW Torque.

3.5.2 Semi-Decentralized MPC Scheme vs. Decentralized MPC Scheme

The second comparative study is performed between semi-decentralized and decentralized control schemes. The x-axis absolute attitude quaternion of all the satellites, the relative attitude quaternion and the corresponding control torques for the semi-decentralized and decentralized control schemes are shown in Figures 3.6, 3.7 and 3.8, respectively. The response characteristics are summarized in Table 3.7. By comparing the evolution of relative attitude in Figure 3.7, it can be concluded that the proposed semi-decentralized scheme enhances the formation performance as the agent are reaching their final goal. Also evaluating the PI $\widetilde{J}_{tr}$ for these two scheme verify this enhancement as $\widetilde{J}_{tr}$ in the cooperative case is calculated to be 0.158 while in the non-cooperative case calculated to be 0.385. This result highlights the effectiveness of the proposed cooperative formation keeping scheme. The results reveal an improved absolute steady-state performance J_{ss} in the decentralized case but the magnitude of absolute state error, i.e., the tracking performance for the goal seeking remains acceptable in the semi-decentralized scheme as well. Moreover, the relative steady-state tracking error $\widetilde{J}_{ss}$ achieved from the decentralized scheme is shown to be larger than the required specifications.

Table 3.7: Goal Seeking/Formation Performance and Time Response for the x-axis, and Control Effort Costs in Semi-Decentralized and Decentralized Schemes

	$\widetilde{J}_{tr}$	J_{ss}	$\widetilde{J}_{ss}$	J_u	$\widetilde{t}_s$	t_s
Decentralized MPC	0.385	1.64×10^{-4}	1.7×10^{-7}	533.05	15.6	14.03
Semi-Dec. MPC	0.158	2.7×10^{-4}	1.4×10^{-11}	494.09	6.93	12.58

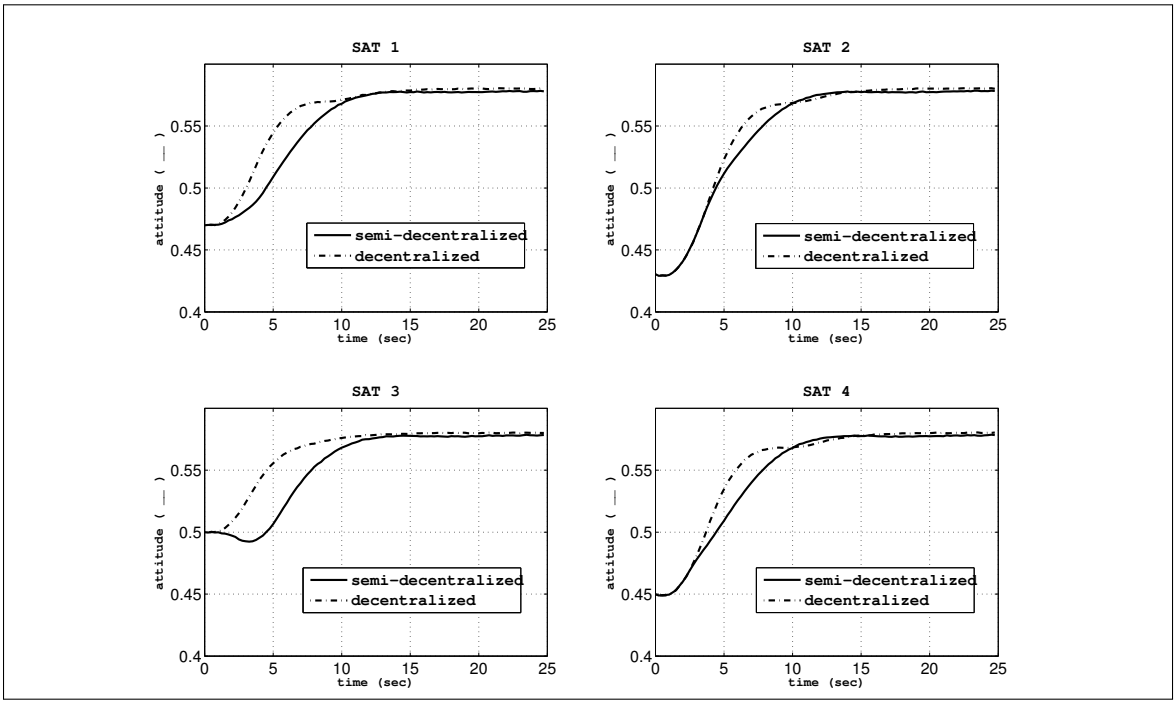

Figure 3.6: X-axis Attitude Quaternion.

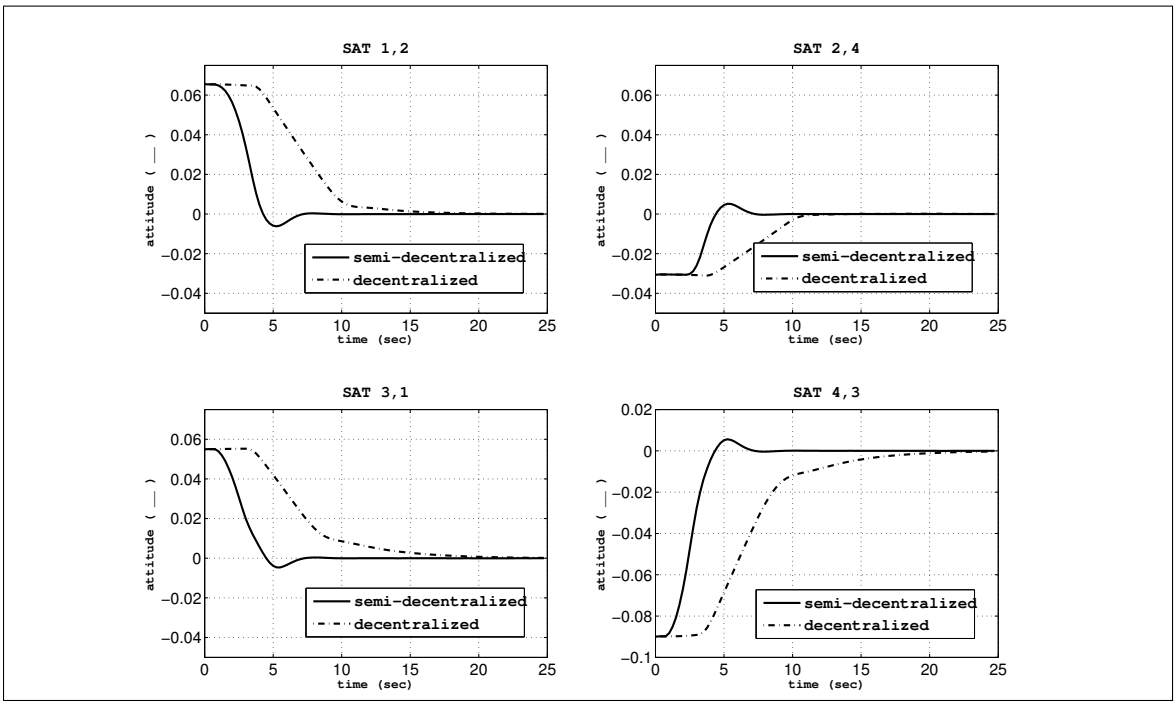

Figure 3.7: X-axis Relative Attitude Quaternion.

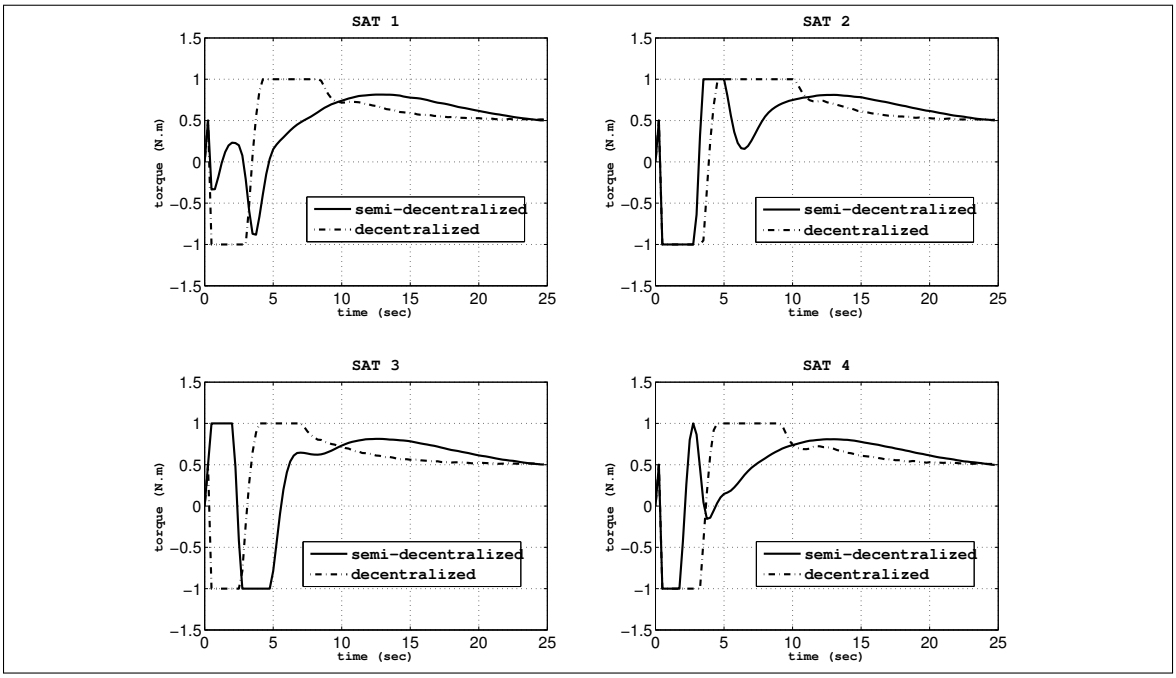

Figure 3.8: X-axis RW Torque.

Table 3.8: Cumulative Control Effort Cost in MPC Schemes

	Decentralized	Semi-decentralized	Centralized
J_u	533.05	494.09	380.44

3.5.3 Centralized MPC Scheme vs. Centralized LQR Scheme

The third comparative study is performed between centralized MPC and centralized LQR control schemes. The x-axis absolute attitude quaternion of all the satellites, the relative attitude quaternion and the corresponding control torques for the semi-decentralized and decentralized control schemes are shown in Figures 3.9, 3.10 and 3.11, respectively. The response characteristics are summarized in Table 3.9. Figure 3.10 and also the PI $\widetilde{J}_{tr}$ show that formation performance in the LQR scheme is not as accurate as in the MPC case. Whereas by incorporating the error integral in this control scheme, the individual steady-state performances is improved in the LQR scheme. The relative steady-state tracking error $\widetilde{J}_{ss}$ is shown to be larger than the required specifications by using the LQR method. The LQR method requires tuning such that the input does not exceed the threshold because input constraints can not be incorporated into the design directly. The input limit imposes larger settling-time for the control variable in this scheme as given in Table 3.9. However the LQR design can be performed offline which reduces the on-board computational burdens.

Table 3.9: Goal Seeking/Formation Performance and Time Response for the x-axis, and Control Effort Costs in Centralized LQR and MPC Schemes

	$\widetilde{J}_{tr}$	J_{ss}	$\widetilde{J}_{ss}$	J_u	$\widetilde{t}_s$	t_s
Centralized LQR	0.1	3.04×10^{-4}	7.05×10^{-8}	501.25	20.5	13.9
Centralized MPC	0.082	4.5×10^{-4}	4×10^{-11}	380.44	8.68	16.75

Table 3.10: LQR Controller Parameters (Consistent for all the Satellites)

Q (controllable modes and integral of output error)	$Q = \text{diag}\left[\begin{array}{cccccccccc} 2\times10^5 & 2\times10^5 & 2\times10^5 & 5\times10^4 & 5\times10^4 & 5\times10^4 & 5\times10^4 & 10^{-4} & 10^{-4} & 10^{-4} \end{array}\right]^{\mathrm{T}}$
R	$R = 0.8 \times \mathrm{I}^{3\times3}$

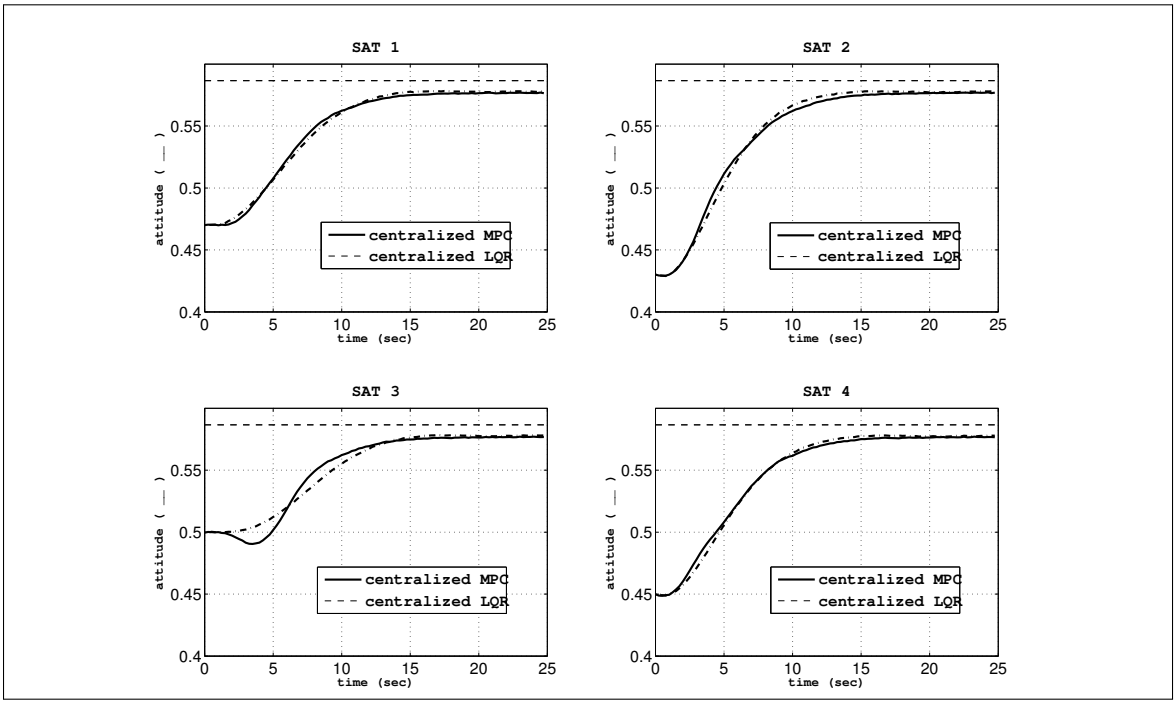

Figure 3.9: X-axis Attitude Quaternion.

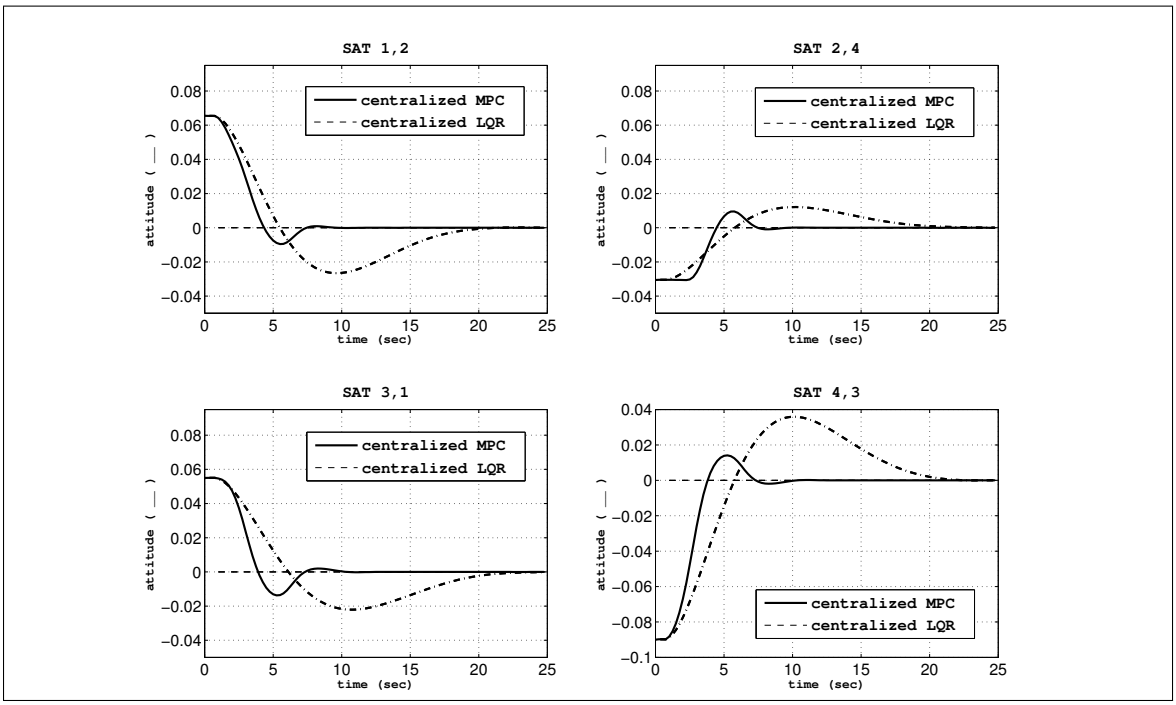

Figure 3.10: X-axis Relative Attitude Quaternion.

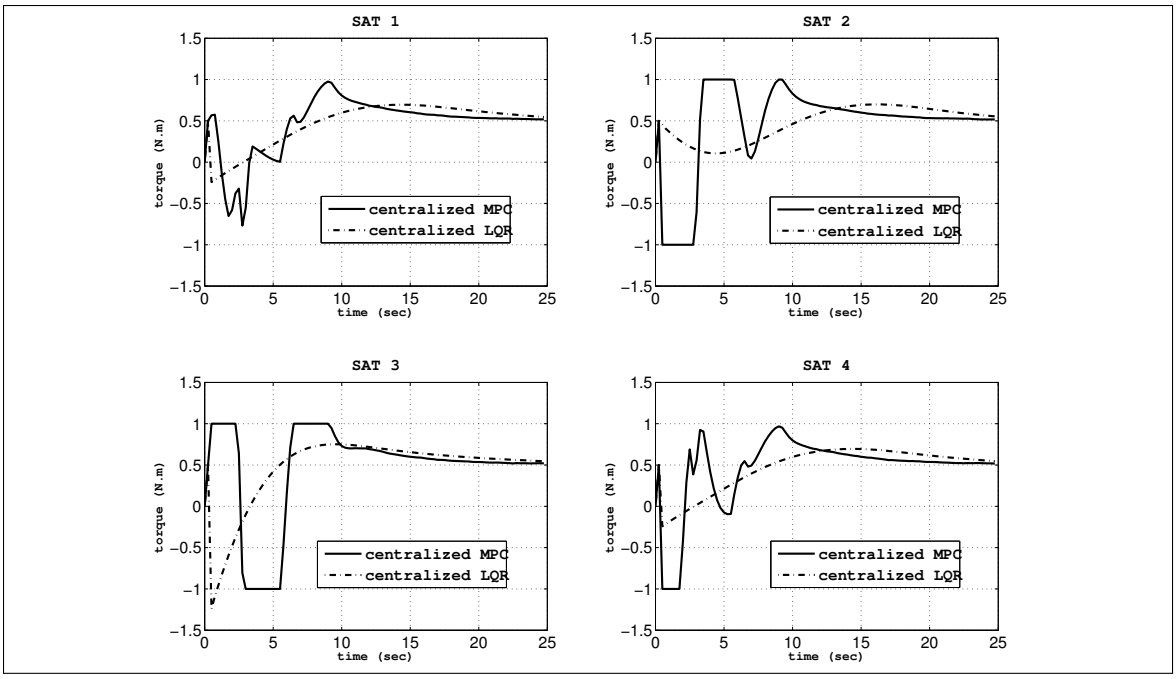

Figure 3.11: X-axis RW Torque.

3.6 Conclusions

In this chapter, a behavior-based formation flying control using a semi-decentralized control scheme is developed for a team of cooperative agents. In this control scheme, the control objective is achieved with an MPC-based control law that incorporates the actuator saturation constraints and it is shown that the proposed control scheme, which utilizes relative state measurements and the coupled dynamical model, maintains the agents in formation while reaching the final goal. It is shown that the proposed semi-decentralized strategy yields a quite satisfactory formation performance such that the team fairly behaves similar to a centralized MPC control scheme but without imposing significant computational complexity (based on the performance indices t_{solv} and $ITER$) and stringent communication requirements of the centralized approach. A comparison of response characteristics for the three control schemes, namely decentralized, semi-decentralized and centralized is presented below to demonstrate the effectiveness of the proposed semi-decentralized scheme. The following summarizes

the performance evaluation we have obtained:

1. Absolute States Steady-State Tracking Error

   In the decentralized scheme, as the only objective criteria is defined as goal seeking for each individual vehicle, the best absolute states steady-state tracking performance is achieved (based on the performance index J_{ss}). This characteristic is compromised within a semi-decentralized scheme due to incorporating the formation keeping objective.

2. Formation Behavior

   The formation behavior achieved by the centralized scheme is shown to be the best among other control structures (based on the performance indices $\widetilde{J}_{ss}$ and $\widetilde{J}_{tr}$) which is due to solving a global optimization problem. However, the formation behavior achieved by the semi-decentralized scheme is fairly comparable with the centralized structure.

3. Control Effort Costs

   The cumulative control effort cost for all of the three schemes are calculated, which shows that the centralized scheme yields the lowest control effort cost (based on the performance index J_u). This feature is related to the global optimization problem solved for the entire team in this architecture. By comparing the semi-decentralized and the decentralized schemes, one observes that the cumulative control cost is lower in the semi-decentralized scheme, which is due to an enhanced closed-loop performance in this scheme that yields saving costs.

4. Time Response

   One of the main advantages of the proposed semi-decentralized scheme is its improvement in the sense of fast time-response. Specially the length of the time

taken to achieve formation is significantly improved in this scheme compared with the centralized and decentralized schemes (based on the performance index $\widetilde{t}_s$).

The MPC method is compared with another relevant optimal control method, namely LQR. The main advantage of the MPC is its capability to handle actuator constraints within the design whereas in the LQR this must performed by tuning the controller gains. The second advantage of the MPC is the improved formation keeping performance which is mainly due to failure of the LQR to incorporate uncontrollable modes which correspond to the attitude kinematics. Moreover, the results show a lower convergence time for the MPC method and a lower cumulative control effort cost. However, the LQR method reduces online-computational burden significantly through the offline control design capability.

Chapter 4

Centralized, Semi-Decentralized and Decentralized Fault Accommodation

In the previous chapter, formation control strategies namely decentralized, semi-decentralized and centralized strategies were introduced. The MPC method was employed to design the controller for each of the strategies which handled reaction wheel (RW) constraints as opposed to an LQR-based approach. Fault occurrence in a component of an agent causes the individual tracking performance of the agent to become deteriorated and due to the agents' interactions, failure to consider an automatic system recovery in a cooperative control scheme leads to an undesirable team behavior. Therefore, proper fault management would assist in obtaining an acceptable recovery performance for both formation and individual behavior. Satellite attitude control subsystem (ACS) instrumentation including sensors and actuators are prone to develop a malfunction. Actuators are heavy and it is impossible for certain applications to provide the system with redundant actuators. Thus, studying its fault and analytic redundancy is of importance. In this work, we focus on two

common faults on the satellites RW, namely loss of effectiveness and friction faults. These faults were identified as sources of RW malfunction in two of the recent reports corresponding to Mars Odyssey and Dawn, NASA's spacecraft.

In this chapter, active system recovery strategies are proposed that use on-line fault information in the centralized, semi-decentralized and decentralized control designs to compensate for the identified characteristic losses. Each of the aforementioned control structures requires different amounts of fault information communicated among agents. In the decentralized control scheme, one fault in one agent does not influence other agents performance and therefore, in a decentralized recovery scheme (Section 4.4), each individual faulty agent recovers its decentralized control scheme. On the other hand, in the semi-decentralized control scheme fault occurrence in one agent influences the performance of other agents. In this case, the healthy neighboring agents face conflicting goals in terms of formation keeping goal and individual tracking goal. Therefore, an active control recovery that incorporates the neighboring agents fault information into the control design, provides an improved team performance and saving costs (Section 4.3). Finally, in a centralized control reconfiguration through the centralized control scheme, the central controller requires the fault information from all the agents (Section 4.2).

In general, a semi-decentralized control scheme provides more reliability in faulty cases as compared with centralized schemes, which is due to exploiting parallelism [107]. At the end of this chapter, the performance of the proposed semi-decentralized recovery scheme is evaluated and compared with the centralized and decentralized system recovery schemes in the simulation studies. Below, as a preliminary criteria for the fault accommodation problem, we define an acceptable degraded performance.

Definition 1. Given the criteria for an acceptable performance specified by two

previously defined Performance Indices (PI) of

$$\begin{aligned} J_{ss_j} &= z_j^2\left(t_{ss}\right) & J_{ss} &= \textstyle\sum_{j=1}^{4} J_{ss_j} \\ \widetilde{J}_{ss_j} &= \widetilde{z}_j^2\left(t_{ss}\right) & \widetilde{J}_{ss} &= \textstyle\sum_{j=1}^{4} \widetilde{J}_{ss_j} \end{aligned} \tag{4.1}$$

with the condition to satisfy the criterion

$$\begin{aligned} J_{ss} &\leq \varepsilon_n \\ \widetilde{J}_{ss} &\leq \widetilde{\varepsilon}_n \end{aligned}, \tag{4.2}$$

where z_j represent either the first, second or the third component of the absolute attitude quaternion vector and $\widetilde{z}_j$ denotes the corresponding component for the relative attitude quaternion vector with respect to one neighboring agent associated with the vehicle j, the acceptable degraded performance for each vehicle j is defined by new lower bounds specified for the maximum PIs and satisfying this new criterion.

$$\begin{aligned} J_{ss} &\leq \varepsilon_f \\ \widetilde{J}_{ss} &\leq \widetilde{\varepsilon}_f, \end{aligned} \tag{4.3}$$

Particularly $\varepsilon_f \geq \varepsilon_n$ and $\varepsilon_f \geq \widetilde{\varepsilon}_n$. In other words, the steady-state tracking performances are degraded under fault conditions. Note that the performance indices only target the steady-state attitude values.

4.1 MPC Fault Recovery Subject to Loss of Effectiveness (LOE) and Friction Faults

Followed by fault occurrence, the system deviates from the nominal operating point (input and state). A fault accommodating MPC controller must determine the new control parameters to drive the system to a condition where an acceptable performance

is achieved [108]. The parameters that are configurable in an MPC design are (a) the internal model, (b) the input set-point, (c) the input constraints, and (d) the penalty matrices in the cost function. In general, our MPC recovery strategy targets three reconfigurations as follows. The first one guarantees the MPC problem feasibility, the second one reduces the offset from the desirable state set-point, and the third one enhances the agents recovery performance in a semi-decentralized control recovery scheme (Section 4.3). In the following analysis in Subsection 4.1.1, due to the change of the operating condition in the faulty case, the variables denote the original state variables rather than the perturbation variables as were considered in the previous chapter.

4.1.1 Problem Feasibility

Recall from the previous chapter that the input constraints set for solving the optimization problem for any agent j was given by $U_j = \left\{x \mid \underline{u}_j \leq x \leq \overline{u}_j\right\}$. Without loss of generality let $\underline{u}_j = -\overline{u}_j$. Two important factors that determine this set are process requirement and feasibility. The physical interpretation of these factors can be stated as follows.

The former, process requirement, places an upper bound on this set to prevent physical saturation, which is one of the drawbacks of RW [61], [62], i.e.,

$$\text{(i)} \qquad \overline{u}_j \leq u_s,$$

where u_s denotes the input upper saturation limit in the nominal condition. Assume that the maximum level of torque that can be provided by the RW is $N_s\,[N.m]$ and therefore, $N_m = G_d K_t u_j < N_s\,[N.m]$ where N_m denotes the torque produced by the motor. Hence, $u_s = \frac{N_s}{G_d K_t}$, where u_s denotes the input saturation limit in the nominal condition.

The latter constraints set determination factor, which is feasibility, places a lower bound on this set as follows. The necessary condition in a set-point tracking problem states that the set-point must be a feasible point of the optimization problem and must satisfy its constraints. i.e.,

$$\text{(ii)} \qquad \underline{u}_j < \widehat{u}_j < \overline{u}_j.$$

Given $\widehat{u}_j = \frac{\tau_v \widehat{\omega}_{w_j}}{G_d K_t} < u_s$, and by letting $\overline{u}_j = -\underline{u}_j = u_s$, the conditions (i), i.e., $\overline{u}_j \leq u_s$, and (ii), i.e., $\underline{u}_j < \widehat{u}_j < \overline{u}_j$ are satisfied in the nominal condition.

The previous conditions (i) and (ii), which were specified for the healthy case will be translated into the following conditions in the faulty cases, namely

$$\text{(iii)} \qquad \overline{u}_{f_j} \leq u_{f_s},$$
$$\text{(iv)} \qquad \underline{u}_{f_j} < u_{j_{f_e}} < \overline{u}_{f_j},$$

where $u_{j_{f_e}}$ denotes the equilibrium point in the faulty cases. We differentiate the notation of the faulty case equilibrium point with the healthy case equilibrium point because the fault might drive the system to a condition where in contrast to the healthy case, its equilibrium point does not remain at our disposal by adjusting the input set-point.

In order to maintain the constraint set feasible after fault occurrence, a reconfiguration and obtaining the new set $U_{f_j} = \left\{ x \mid \underline{u}_{f_j} \leq x \leq \overline{u}_{f_j} \right\}$ is required as follows.

In the case of LOE fault, the produced torque by the actuator will reduce in accordance with the magnitude of fault and the saturation limit will increase accordingly to $u_{f_s} = \frac{N_s}{G_d K_t'} = \frac{N_s}{G_d(\Gamma^* K_t)}$, where Γ^* denotes the process LOE fault. It can be easily shown that given the condition (i) was satisfied in the healthy case and by letting $\overline{u}_{f_j} = -\underline{u}_{f_j} = \frac{\overline{u}_j}{\Gamma} - \frac{\Pi \widehat{\omega}_{w_j}}{G_d(\Gamma K_t)}$, where the matrices Γ and Π are estimated by the FDI module, and by assuming that the corresponding Γ estimate inaccuracies to be severity

under-estimation, i.e., $\Gamma^* < \Gamma$, the condition (iii) is met for the faults of *reduced* friction and LOE. Moreover, the equilibrium point must satisfy $u_{j_{f_e}} < \overline{u}_{f_j}$, so that the condition (iv) is satisfied.

Remark 1. Under severe LOE fault conditions, the FDI accuracy level must be higher so that the value assigned to the $\overline{u}_{f_j}$ be a large value and the desirable equilibrium point lies in the interior of the specified feasible solution set so that the problem converges to this desirable equilibrium point.

Remark 2. The friction fault estimate inaccuracy does not violate the feasibility conditions. Therefore, inaccurate friction fault does not lead to loss of convergence. The only influence of this fault is injecting offset to the steady-state values as will be discussed in the subsequent Subsection 4.1.2.

4.1.2 Tracking Performance

The input-set point and the internal model of the optimal control design influence the steady-state values of the states of the system under control. Depending on the structure of the fault, the input set-point that drives the system to the desired state set-point might need reconfiguration. Therefore, once a fault of LOE or friction fault occurs, this value for the input set-point must change accordingly to $\widehat{u}_{f_j} = \frac{\tau_v' \widehat{\omega}_{w_j}}{G_d K_t'}$ where the matrices $\tau_v' = \tau_v \pm \Pi$ and $K_t' = \Gamma K_t$ are estimated by the FDI module.

The mismatch between the real system and the internal model results in an undesirable offset in the states steady-state values when set-point tracking is performed. Availability of an accurate linear model approximation for the system, reduces this offset. Therefore, availability of an accurate diagnostics of the fault contributes to removing this offset. As stated earlier, the expression $x_j(k+1) = A_j x_j(k) + B_j u_j(k)$ represents the internal model for any agent j. As far as two previously explained faults are concerned, provided the diagnostics data from the FDI module, this model will be modified to

$$x_j(k+1) = \underbrace{\left(A_j \pm A_{\Pi_j}\right)}_{A_{f_j}} x_j(k) + \underbrace{B_j\Gamma_j}_{B_{f_j}} u_j(k), \tag{4.4}$$

where the matrices A_{Π_j} and Γ_j are estimated by the FDI module.

Remark 3. The integration of the recovery with the FDI module is an important issue. Our recovery approach is based on [57] where a relation is established between the FDI module and the controller as follows. Once the fault is diagnosed by the FDI module, the recovery module uses the FDI module information to perform the fault accommodation through the controller reconfiguration. The FDI module information accuracy and the fault detection time-delay are two conditions that affect the integration of the FDI module and recovery module and therefore, influence the recovery reliability. If one assumes the condition where the FDI module information is ideal, that is, perfect accuracy and zero time-delay, then the problem is reduced to analyzing the ability of the control system to control the system in the new, given condition, and generally, the fault might change the system characteristic in a way that the MPC solution is undesirable. On the other hand, if one assumes the realistic condition, in which two practical aspects of inaccuracy in diagnostics and the time required for fault detection (t_d) are taken into account, one must analyze the effects of the discrepancy in the real process and the controller design parameters. In this thesis, the impacts of the FDI information inaccuracy and the fault detection time delay on the formation system performance is investigated in simulation studies.

4.2 Centralized Fault Accommodation Approach Using the Centralized MPC-based Formation Control

Given the reconfiguration procedure for an MPC control subject to faults of LOE and friction fault, we can now address the centralized recovery of the faulty formation system through the centralized formation control approach. In this scheme, due to the centralized nature of the controller, the reconfiguration also needs to be performed in a centralized manner. In other words, the fault information needs to be communicated to the central controller, and the corresponding reconfiguration be performed accordingly.

The previously developed centralized approach is reconfigured in the fault conditions. In other words, provided the information about the fault by the FDI module, it is possible to reconfigure MPC in such a way that cooperative task is not lost and an acceptable performance is achieved.

Recall from the previous chapter that the internal model employed in the centralized approach was a concatenated, coupled model as follows

$$\underbrace{\begin{bmatrix} x_1(k+1) \\ \widetilde{x}_1(k+1) \\ \hdashline \vdots \\ \hdashline x_{N_v}(k+1) \\ \widetilde{x}_{N_v}(k+1) \end{bmatrix}}_{x(k+1)} = \underbrace{\begin{bmatrix} \overline{A}_1 & 0 & 0 \\ 0 & \ddots & 0 \\ 0 & 0 & \overline{A}_{N_v} \end{bmatrix}}_{\overline{A}} \underbrace{\begin{bmatrix} x_1(k) \\ \widetilde{x}_1(k) \\ \hdashline \vdots \\ \hdashline x_{N_v}(k) \\ \widetilde{x}_{N_v}(k) \end{bmatrix}}_{x(k)} + \underbrace{\begin{bmatrix} \overline{B}_1 \\ \vdots \\ \overline{B}_{N_v} \end{bmatrix}}_{\overline{B}} \underbrace{\begin{bmatrix} u_1(k) \\ \vdots \\ u_{N_v}(k) \end{bmatrix}}_{u(k)}, \quad (4.5)$$

where

$$\overline{A}_j = T_j \begin{bmatrix} A_j & 0 & 0 \\ 0 & A_k & 0 \\ 0 & 0 & \ddots \end{bmatrix} T_j^{-1} \quad \text{and} \quad \overline{B}_j = T_j \begin{bmatrix} B_j & 0 & 0 \\ 0 & B_k & 0 \\ 0 & 0 & \ddots \end{bmatrix}. \tag{4.6}$$

Therefore, under the fault conditions one gets

$$\underbrace{\begin{bmatrix} x_1(k+1) \\ \widetilde{x}_1(k+1) \\ \hdashline \vdots \\ \hdashline x_{N_v}(k+1) \\ \widetilde{x}_{N_v}(k+1) \end{bmatrix}}_{x(k+1)} = \underbrace{\begin{bmatrix} \overline{A}_{f_1} & 0 & 0 \\ 0 & \ddots & 0 \\ 0 & 0 & \overline{A}_{f_{N_v}} \end{bmatrix}}_{\overline{A}_f} \underbrace{\begin{bmatrix} x_1(k) \\ \widetilde{x}_1(k) \\ \hdashline \vdots \\ \hdashline x_{N_v}(k) \\ \widetilde{x}_{N_v}(k) \end{bmatrix}}_{x(k)} + \underbrace{\begin{bmatrix} \overline{B}_{f_1} \\ \vdots \\ \overline{B}_{f_{N_v}} \end{bmatrix}}_{\overline{B}_f} \underbrace{\begin{bmatrix} u_1(k) \\ \vdots \\ u_{N_v}(k) \end{bmatrix}}_{u(k)}, \tag{4.7}$$

where

$$\overline{A}_{f_j} = T_j \begin{bmatrix} A_{f_j} & 0 & 0 \\ 0 & A_{f_k} & 0 \\ 0 & 0 & \ddots \end{bmatrix} T_j^{-1} \quad \text{and} \quad \overline{B}_{f_j} = T_j \begin{bmatrix} B_{f_j} & 0 & 0 \\ 0 & B_{f_k} & 0 \\ 0 & 0 & \ddots \end{bmatrix}. \tag{4.8}$$

The following problem (Problem A) introduces the centralized recovery scheme through the centralized MPC-based control scheme. For the sake of simplicity in the formulation, a shift of coordinates with respect to the reconfigured desired set-point $(\widehat{x}, \widehat{u}_f)$ is performed. The fault is assumed to occur at the time instant t_f and the fault detection time delay is assumed to be t_d.

Problem A. *At any time instant $t_k \mid t_k \geq t_f + t_d$, given $x(k)$ and also given the FDI information about the faults for any agent $j \in V_f$, namely, A_{Π_j} and Γ_j, find the input sequence $\{u(k|k), u(k+1|k), \ldots, u(k+m-1|k)\} \in \mathbb{R}^{3N_v}$, that minimizes the cost*

function J,

$$J = \sum_{l=0}^{N-1} \{ \| x\,(k+l|k) \|_{Q}^{2} + \| u\,(k+l|k) \|_{R}^{2} \} + \| x\,(k+N|k) \|_{\overline{Q}}^{2}, \quad (4.9)$$

where the prediction equations are as follows

$$\begin{cases} x\,(k+l+1 \mid k) = \overline{A}_f x\,(k+l \mid k) + \overline{B}_f u\,(k+l \mid k), \quad l = 0, \ldots, N-1 \\ x\,(k|k) = x\,(k) \end{cases} \quad (4.10)$$

and the constraints of the problem are given by

$$\begin{cases} x\,(k+l|k) \in X & l = 1, \ldots N \\ u\,(k+l|k) \in U_f & l = 0, \ldots, M-1 \\ u\,(k+l|k) = u\,(k+M-1|k) & l \geq M \\ z^{u}\,(k+N|k) = \tilde{V}_u \left[\; x\,(k+N|k) \; \right] = 0 \end{cases} \quad (4.11)$$

In the above cost function, the first two terms are linked to minimizing the predicted $x\,(k+l \mid k)$ and the magnitude of the input $u\,(k+l \mid k)$, respectively, for $l = 0, \ldots, N-1$ and the last term reflects minimizing the terminal predicted states, $Q \in \mathbb{R}^{10N_v^2 \times 10N_v^2}$ denotes a positive definite matrix representing the state penalty matrix for the concatenated state vector and is considered constant over the prediction horizon, and $\overline{Q} \in \mathbb{R}^{10N_v^2 \times 10N_v^2}$ represents the penalty matrix for the terminal states. This matrix must be determined such that necessary conditions of the closed-loop system stability are satisfied. Moreover, $R \in \mathbb{R}^{3N_v \times 3N_v}$ denotes a positive definite matrix representing the input penalty matrix and is considered constant over the prediction horizon. Also, $\overline{A}_f$ and $\overline{B}_f$ represent the linear state space model as given in equation (4.7). Finally, $X = \{x \mid \underline{x} \leq x \leq \overline{x}\}$ and $U_f = \left\{ x \mid \underline{u}_f \leq x \leq \overline{u}_f \right\}$, represent the sets of linear constraints where $(\underline{x}, \overline{x})$, $\left(\underline{\tilde{x}}, \overline{\tilde{x}}\right)$ and $\left(\underline{u}_f, \overline{u}_f\right)$ capture the lower and

upper limits of the predicted states and the input, respectively, and $\tilde{V}_u$ must be determined such that the necessary conditions of the closed-loop system stability are satisfied.

The implementation algorithm for our proposed system recovery approach subject to the LOE and friction fault using the MPC and based on the centralized control approach is presented in Algorithm 4.1.

Algorithm 4.1 Centralized System Recovery

1. At any time $t_k \mid t_k \geq t_f + t_d$
   - For any agent j:
     (a) Measure $x_j(k)$ and $\widetilde{x}_j(k)$.
     (b) Communicate $x_j(k)$ and $\widetilde{x}_j(k)$ to the central controller.
     (c) Communicate the estimated local faults, i.e., A_{Π_j} and Γ_j to the central controller.
   - The central controller:
     (a) Receives the state $x(k)$.
     (b) Receives all the estimated local faults and reconfigures the internal model $(\overline{A}_f, \overline{B}_f)$, the input set-point $(\widehat{u}_f)$ and the control input constraints (U_f) according to the information which is collected from the local FDIs
     (c) Solves Problem A by using any available algorithm such as the interior point, etc. yielding $u^*(k+l \mid k)$ for $l = 0, 1, \ldots, M-1$.
     (d) Communicates $u_j^*(k \mid k)$ to each corresponding agent j.
2. Over any interval $[t_k, t_{k+1})$, $k \in \{0, 1, 2, \ldots\}$:
   - For any agent j:
     Apply $u_j^*(k \mid k)$.

4.3 Semi-Decentralized Fault Accommodation Approach using the Semi-Decentralized MPC-Based Formation Control

In this section, the semi-decentralized recovery of the faulty formation system through the semi-decentralized formation control approach is addressed. To this end, a two level system recovery approach is proposed. At the first level, the faulty agent is recovered locally by reconfiguring its local control design. Given that the behavior of neighbors of the faulty agent influence the faulty agent behavior, at the second level we propose to reconfigure the neighboring agents controller such that they maintain their nominal attitude rather than keeping an strict formation with the faulty agent and this way they provide a desirable reference for the faulty agent behavior. It is shown that providing such system recovery for the healthy neighboring agents enhances the recovery performance of the team. Therefore, the proposed semi-decentralized system recovery is performed in two levels, namely, (i) local control recovery of the faulty agent, and (ii) improvement of the recovery performance by using the formation level fault recovery.

4.3.1 Local Fault Recovery

Recall form the previous chapter that, in the semi-decentralized formation control structure, for any agent j, the following dynamic equation governs the control design through performing the predictions based on the input dynamic information of each agent, that is

$$\begin{bmatrix} x_j(k+1) \\ \tilde{x}_j(k+1) \end{bmatrix} = \overline{A}_j \begin{bmatrix} x_j(k) \\ \widetilde{x}_j(k) \end{bmatrix} + \underline{B}_j u_j(k) \tag{4.12}$$

Let the agent j'th actuator be faulty. Based on the prediction equations (4.12), an

LOE fault in this agent influences the matrix $\underline{B}_j = T_j \begin{bmatrix} B_j \\ 0 \\ \vdots \\ 0 \end{bmatrix}$. On the other hand, the friction fault influences the matrix $\overline{A}_j = T_j \begin{bmatrix} A_j & 0 & 0 \\ 0 & A_k & 0 \\ 0 & 0 & \ddots \end{bmatrix} T_j^{-1}$. The steady-state behavior of the system is influenced by the controllable subsystem and therefore, once a friction fault occurs in agent j, matrix $\overline{A}_j$ must be reconfigured.

Now consider the dynamic equation that governs the control design and predictions for agent k, where $(j,k) \in A_f$, that is

$$\overline{A}_k = T_k \begin{bmatrix} A_k & 0 & 0 \\ 0 & A_j & 0 \\ 0 & 0 & \ddots \end{bmatrix} T_k^{-1} \quad \text{and} \quad \underline{B}_k = T_k \begin{bmatrix} B_k \\ 0 \\ \vdots \\ 0 \end{bmatrix}. \tag{4.13}$$

Due to the structure of the semi-decentralized control scheme, an LOE fault in agent j can not be incorporated in the agent k internal model. Moreover, the uncontrollable subsystem of the model $\left(\overline{A}_k, \underline{B}_k\right)$ does not influence the steady-state behavior of the system and therefore, once a friction fault occurs in agent j, it does not influence the steady-state offset through the coupled subsystem k dynamical model.

Consequently, we attribute the internal model reconfigurations in the semi-decentralized control scheme, to the reconfiguration of the absolute state component of the faulty agent's coupled subsystem model. Therefore, when a fault occurs in agent j, the

coupled subsystem j dynamical model will be given by

$$\overline{A}_{f_j} = T_j \begin{bmatrix} A_{f_j} & 0 & 0 \\ 0 & A_k & 0 \\ 0 & 0 & \ddots \end{bmatrix} T_j^{-1} \quad \text{and} \quad \underline{B}_{f_j} = T_j \begin{bmatrix} B_{f_j} \\ 0 \\ \vdots \\ 0 \end{bmatrix}, \tag{4.14}$$

and any coupled subsystem k dynamical model will remain unchanged. In subsequent Subsection 4.3.2, the system recovery for agent k, where $(j,k) \in A_f$ is proposed.

The following MPC formulation (Problem B) introduces the set-point tracking problem for the faulty agent j using the semi-decentralized control. The fault is assumed to occur at the time instant t_f in agent j and the fault detection time delay is assumed to be t_d. For the sake of simplicity in the formulation, a shift of coordinates with respect to the reconfigured desired set-point $\left(\widehat{x}_j, \widehat{\widetilde{x}}_j, \widehat{u}_{j_f}\right)$ is performed.

Problem B. *For any agent $j \in V_f$ and at any time instant $t_k \mid t_k \geq t_f + t_d$, given $x_j(k)$ and $\widetilde{x}_j(k)$, i.e. the agent j absolute and relative states measurements and also given the FDI information about the faults in the agent j, namely, A_{Π_j} and Γ_j, find the input sequence $\{u_j(k|k), u_j(k+1|k), \ldots, u_j(k+m-1|k)\} \in \mathbb{R}^3$ that minimizes the cost function J_j,*

$$J_j = \sum_{l=0}^{N-1} \{\|x_j(k+l|k)\|_{Q_j}^2 + \|\tilde{x}_j(k+l|k)\|_{\widetilde{Q}_j}^2 + \|u_j(k+l|k)\|_{R_j}^2\} + \\ \|x_j(k+N|k)\|_{\overline{Q}_j}^2 + \|\tilde{x}_j(k+N|k)\|_{\overline{\widetilde{Q}}_j}^2, \tag{4.15}$$

where the prediction equations are as follows

$$\begin{cases} \begin{bmatrix} x_j\left(k+l+1|k\right) \\ \widetilde{x}_j\left(k+l+1|k\right) \end{bmatrix} = \overline{A}_{f_j} \begin{bmatrix} x_j\left(k+l|k\right) \\ \widetilde{x}_j\left(k+l|k\right) \end{bmatrix} + \underline{B}_{f_j} u_j\left(k+l|k\right) \quad l=0,\ldots,N-1 \\ x_j\left(k|k\right) = x_j\left(k\right) \\ \widetilde{x}_j\left(k|k\right) = \widetilde{x}_j\left(k\right) \end{cases} \tag{4.16}$$

and the constraints of the problem are given by

$$\begin{cases} x_j\left(k+l|k\right) \in X_j & l=1,\ldots,N \\ \widetilde{x}_j\left(k+l|k\right) \in \widetilde{X_j} & l=1,\ldots,N \\ u_j\left(k+l|k\right) \in U_{f_j} & l=0,\ldots,M-1 \\ u_j\left(k+l|k\right) = u_j\left(k+M-1|k\right) & l \geq M \\ z_j^u\left(k+N|k\right) = \tilde{V}_{u_j} \begin{bmatrix} x_j\left(k+N|k\right) \\ \widetilde{x}_j\left(k+N|k\right) \end{bmatrix} = 0 & \end{cases} \tag{4.17}$$

In equation (4.15), the first three terms are linked to minimizing the predicted $x_j\left(k+l \mid k\right)$, the predicted $\tilde{x}_j\left(k+l \mid k\right)$ and the size of control input $u_j\left(k+l \mid k\right)$ respectively for $l=0,\ldots,N-1$ and the last two terms reflect minimizing the terminal predicted states. $\widetilde{Q}_j$ and $Q_j \in \mathbb{R}^{10\times 10}$ denote positive definite matrices representing state penalty matrices for relative states and absolute states respectively and are considered constant over the prediction horizon. The dimension of $\widetilde{Q}_j$ depends of the communication topology. $\overline{\widetilde{Q}}_j$ and $\overline{Q}_j \in \mathbb{R}^{10\times 10}$ represent the corresponding penalty matrices for the terminal state. As explained in Section 3.3.1, these matrices must be determined such that necessary conditions of the stability are satisfied. The dimension of $\overline{\widetilde{Q}}_j$ depends on the communication topology. $R_j \in \mathbb{R}^{3\times 3}$ is a positive definite matrix representing input penalty matrix and is considered constant over

the prediction horizon. $\overline{A}_{f_j}$ and $\underline{B}_{f_j}$ represent the linear states space model in the equation (4.14). The dimensions of $\overline{A}_{f_j}$ and $\underline{B}_{f_j}$ depend on the communication topology. $\widetilde{X}_j = \left\{x \mid \underline{\widetilde{x}}_j \leq x \leq \overline{\widetilde{x}}_j\right\}$, $X_j = \left\{x \mid \underline{x}_j \leq x \leq \overline{x}_j\right\}$ and $U_{f_j} = \left\{x \mid \underline{u}_{f_j} \leq x \leq \overline{u}_{f_j}\right\}$ represent sets of linear constraints where $\left(\underline{\widetilde{x}}_j, \overline{\widetilde{x}}_j\right)$, $\left(\underline{x}_j, \overline{x}_j\right)$ and $\left(\underline{u}_{f_j}, \overline{u}_{f_j}\right)$ indicate the lower and upper limit for predicted relative states, predicted absolute states and the control input respectively. $\tilde{V}_{u_j}$ must be determined such that necessary conditions of stability are satisfied.

Remark 4. The proposed local level recovery strategy is based on the local FDI module information, that is, once a fault occurs in any agent $j \in V_f$, only the local controller is reconfigured and communicating the fault information among agents is not required, and therefore, no excessive bandwidth requirement is imposed on the system. However, if an enhanced recovery performance is desirable, then a formation level recovery strategy must be implemented in which the fault information must be communicated from the faulty agent to the neighboring agents as will be described in the subsequent section.

4.3.2 Formation Level Fault Recovery

The above procedure targeted recovering the individual performance of the faulty agent by reconfiguring its internal model, its input set-point and input constraints. However, it is important to note that another factor that can influence the recovery performance of the faulty agent is the healthy neighboring agent performances. By forcing those neighbors to maintain their nominal behavior in the faulty case, the faulty agent will be reinforced to reach the same behavior through its baseline formation control law. Recall from the previous chapter that the control law for any each agent

k ($(j,k) \in A_f$) was determined based on minimizing the cost function J_k :

$$J_k = \sum_{l=0}^{N-1} \{\|x_k(k+l|k)\|^2_{Q_k} + \|\tilde{x}_k(k+l|k)\|^2_{\widetilde{Q}_k} + \|u_k(k+l|k)\|^2_{R_k}\} + \|x_k(k+N|k)\|^2_{\overline{Q}_k} + \|\tilde{x}_k(k+N|k)\|^2_{\widetilde{\overline{Q}}_k} .$$

Given that the desirable optimal solution under fault condition is that healthy agents maintain their nominal attitude and the faulty agent keeps the formation, by relaxing the formation performance criteria for the neighboring agents in the faulty case, the optimal solution converges to the desirable equilibrium point. Note that the more sever the fault, the more the performance degrades and therefore, the formation criteria of the neighboring agent must be relaxed to prevent their absolute performance degradations. Therefore, by letting

$$\widetilde{Q}_{f_k} = \Lambda_j \widetilde{Q}_k \tag{4.18}$$

where $\Lambda_j \in \mathbb{R}$ denotes the fault severity index and $0 \leq \Lambda_j \leq 1$, the aforementioned objective is satisfied and the neighboring formation keeping criteria is reconfigured based on the magnitude of the performance degradation. In the case of LOE fault, we let $\Lambda_j = \Gamma_{lj}$, and in the case of reduced friction fault, we let $\Lambda_j = \frac{\tau_{v_{lj}} - \Pi_{lj}}{\tau_{v_{lj}}}$, where the $l-$axis RW of the agent j is assumed to be faulty.

The following MPC formulation (Problem C) introduces the set-point tracking problem for any healthy agent $k \mid (j,k) \in A_f$ using the semi-decentralized control. The fault is assumed to occur at the time instant t_f in agent j and the fault detection time delay is assumed to be t_d. For the sake of simplicity in the formulation, a shift of coordinates with respect to the reconfigured desired set-point $\left(\widehat{x}_k, \widehat{\tilde{x}}_k, \widehat{u}_k\right)$ is performed.

Problem C. *For any agent $k \mid (j,k) \in A_f$ and at any time instant $t_k \mid t_k \geq t_f + t_d$, given $x_k(k)$ and $\widetilde{x}_k(k)$, i.e. the agent k absolute and relative states measurements*

and also given the FDI information about the faults in the agent j, namely, Π_j and Γ_j, find the input sequence $\{u_k(k|k), u_k(k+1|k), \ldots, u_k(k+m-1|k)\} \in \mathbb{R}^3$ that minimizes the cost function J_k,

$$J_k = \sum_{l=0}^{N-1} \{\|x_k(k+l|k)\|^2_{Q_k} + \|\tilde{x}_k(k+l|k)\|^2_{\widetilde{Q}_{f_k}} + \|u_k(k+l|k)\|^2_{R_k}\} + \|x_k(k+N|k)\|^2_{\overline{Q}_k} + \|\tilde{x}_k(k+N|k)\|^2_{\widetilde{\overline{Q}}_{f_k}}, \quad (4.19)$$

where the prediction equations are as follows

$$\begin{cases} \begin{bmatrix} x_k(k+l+1|k) \\ \tilde{x}_k(k+l+1|k) \end{bmatrix} = \overline{A}_k \begin{bmatrix} x_k(k+l|k) \\ \tilde{x}_k(k+l|k) \end{bmatrix} + \underline{B}_k u_k(k+l|k) \quad l = 0, \ldots, N-1 \\ x_k(k|k) = x_k(k) \\ \tilde{x}_k(k|k) = \tilde{x}_k(k) \end{cases} \quad (4.20)$$

and the constraints of the problem are given by

$$\begin{cases} x_k(k+l|k) \in X_k & l = 1, \ldots, N \\ \tilde{x}_k(k+l|k) \in \widetilde{X}_k & l = 1, \ldots, N \\ u_k(k+l|k) \in U_k & l = 0, \ldots, M-1 \\ u_k(k+l|k) = u_k(k+M-1|k) & l \geq M \\ z^u_k(k+N|k) = \tilde{V}_{u_k} \begin{bmatrix} x_k(k+N|k) \\ \tilde{x}_k(k+N|k) \end{bmatrix} = 0 \end{cases} \quad (4.21)$$

In equation (4.19), the first three terms are linked to minimizing the predicted $x_k(k+l \mid k)$, the predicted $\tilde{x}_k(k+l \mid k)$ and the size of control input $u_k(k+l \mid k)$ respectively for $l = 0, \ldots, N-1$ and the last two terms reflect minimizing the terminal

predicted states. $\widetilde{Q}_{f_k}$ and $Q_k \in \mathbb{R}^{10\times10}$ denote positive definite matrices representing state penalty matrices for relative states and absolute states respectively and are considered constant over the prediction horizon. $\widetilde{Q}_{f_k}$ is obtained from equation (4.18) and its dimension depends of the communication topology. $\overline{\widetilde{Q}}_{f_k}$ and $\overline{Q}_k \in \mathbb{R}^{10\times10}$ represent the corresponding penalty matrices for the terminal state. As explained in Section 3.3.1, these matrices must be determined such that necessary conditions of the stability are satisfied. The dimension of $\overline{\widetilde{Q}}_{f_k}$ depends on the communication topology. $R_k \in \mathbb{R}^{3\times3}$ is a positive definite matrix representing input penalty matrix and is considered constant over the prediction horizon. $\overline{A}_k$ and $\underline{B}_k$ represent the linear states space models and were specified earlier. The dimensions of $\overline{A}_k$ and $\underline{B}_k$ depend on the communication topology. $\widetilde{X}_k = \left\{x \mid \underline{\widetilde{x}}_k \leq x \leq \overline{\widetilde{x}}_k\right\}$, $X_k = \{x \mid \underline{x}_k \leq x \leq \overline{x}_k\}$ and $U_k = \{x \mid \underline{u}_k \leq x \leq \overline{u}_k\}$ represent sets of linear constraints where $\left(\underline{\widetilde{x}}_k, \overline{\widetilde{x}}_k\right)$, $(\underline{x}_k, \overline{x}_k)$ and $(\underline{u}_k, \overline{u}_k)$ indicate the lower and upper limit for predicted relative states, predicted absolute states and the control input respectively. $\tilde{V}_{u_k}$ must be determined such that necessary conditions of stability are satisfied.

Remark 5. The proposed formation level fault recovery implies that the healthy neighboring agents participate in the fault accommodation, rather than passively relying on the baseline coordination laws without any explicit control reconfiguration.

We present the implementation algorithm for our proposed semi-decentralized recovery approach in Algorithm 4.2.

Remark 6. Under the partial LOE and friction fault conditions, the open-loop stability properties of the system remain similar to the healthy condition because the unstable modes are independent of the fault parameters. Furthermore, the controllability properties are only influenced if the LOE severity is a total loss which makes the unstable but controllable modes, uncontrollable.

Algorithm 4.2 Semi-Decentralized System Recovery for Faulty Agent $j \in V_f$ and any Agent $k \mid (k,j) \in A_f$

1. At any time $t_k \mid t_k \geq t_f + t_d$:
   - Agent j:
     (a) Measures the current absolute state $x_j(k)$ and measures or receives current relative states $\widetilde{x}_j(k)$.
     (b) Obtains the fault information from the local FDI and reconfigures the internal model $(\overline{A}_{f_j}, \underline{B}_{f_j})$, the input set-point $(u_{j_{f_e}})$ and the control input constraints (U_{f_j}) accordingly.
     (c) Solves Problem B by using any available algorithm such as the interior point, etc., yielding $u_j^*(k+l \mid k)$ for $l = 0, 1, \ldots, M-1$.
     (d) Communicates the estimated local faults, i.e., Π_j and Γ_j to any agent $k \mid (k,j) \in A_f$.
   - For any agent $k \mid (k,j) \in A_f$:
     (a) Measure the current absolute state $x_k(k)$ and measure or receive current relative states $\widetilde{x}_k(k)$.
     (b) Receive the fault information from the neighboring agents FDIs and reconfigure the penalty matrices $\widetilde{Q}_{f_k}$ and $\overline{\widetilde{Q}}_{f_k}$.
     (c) Solve Problem C for agent k by using any available algorithm such as the interior point, etc., yielding $u_k^*(k+l \mid k)$ for $l = 0, 1, \ldots, M-1$.
2. Over any interval $[t_k, t_{k+1})$, $k \in \{0, 1, 2, \ldots\}$:
   - Agent j: Applies $u_j^*(k \mid k)$.
   - For any agent $k \mid (k,j) \in A_f$: Apply $u_k^*(k \mid k)$.

4.4 Decentralized Fault Accommodation Approach Using the Decentralized MPC-based Formation Control

In this section, the decentralized recovery of the faulty formation system through the decentralized formation control approach is addressed. Recall form the previous chapter that in the decentralized formation control structure any agent j uses its dynamical model for the state predictions, that is

$$x_j(k+1) = A_j x_j(k) + B_j u_j(k), \tag{4.22}$$

In the decentralized control scheme, one fault in an agent does not influence other agents performances and therefore, in a decentralized recovery scheme, each individual faulty agent recovers its decentralized control scheme. An LOE fault in agent j influences the matrix B_j, and a friction fault influences the matrix A_j of the prediction equations. Therefore, under fault conditions one gets

$$x_j(k+1) = A_{f_j} x_j(k) + B_{f_j} u_j(k), \tag{4.23}$$

where $\left(A_{f_j}, B_{f_j}\right)$ are obtained from equation (4.4). The following MPC formulation (Problem D) introduces the set-point tracking problem for the faulty agent j using the decentralized control with the decentralized recovery scheme. The fault is assumed to occur at the time instant t_f and the fault detection time-delay is assumed to be t_d. For the sake of simplicity in the formulation, a shift of coordinates with respect to the reconfigured desired set-point $\left(\widehat{x}_j, \widehat{u}_{j_f}\right)$ is performed.

Problem D. *For any agent $j \in V_f$ and at any time instant $t_k \mid t_k \geq t_f + t_d$, given $x_j(k)$, i.e. the agent j absolute states measurements and also given the FDI*

information about the faults in the agent j, namely, A_{Π_j} and Γ_j, find the input sequence $\{u_j(k|k), u_j(k+1|k), \ldots, u_j(k+m-1|k)\} \in \mathbb{R}^3$ *that minimizes the cost function* J_j,

$$J_j = \sum_{l=0}^{N-1} \{\|x_j(k+l|k)\|^2_{Q_j} + \|u_j(k+l|k)\|^2_{R_j}\} + \|x_j(k+N|k)\|^2_{\overline{Q}_j}, \quad (4.24)$$

where the prediction equations are as follows

$$\begin{cases} x_j(k+l+1|k) = A_{f_j} x_j(k+l|k) + B_{f_j} u_j(k+l|k) & l = 0, \ldots, N-1 \\ x_j(k|k) = x_j(k) \end{cases} \quad (4.25)$$

and the constraints of the problem are given by

$$\begin{cases} x_j(k+l|k) \in X_j & l = 1, \ldots, N \\ u_j(k+l|k) \in U_{f_j} & l = 0, \ldots, M-1 \\ u_j(k+l|k) = u_j(k+M-1|k) & l \geq M \\ z^u_j(k+N|k) = \tilde{V}_{u_j} x_j(k+N|k) = 0 \end{cases} \quad (4.26)$$

In equation (4.24), the terms are linked to minimizing the predicted $x_j(k+l \mid k)$, the size of control input $u_j(k+l \mid k)$ for $l = 0, \ldots, N-1$ and minimizing the terminal predicted states respectively. $X_j = \left\{x \mid \underline{x}_j \leq x \leq \overline{x}_j\right\}$ and $U_{f_j} = \left\{x \mid \underline{u}_{f_j} \leq x \leq \overline{u}_{f_j}\right\}$ represent sets of linear constraints where $\left(\underline{x}_j, \overline{x}_j\right)$ and $\left(\underline{u}_{f_j}, \overline{u}_{f_j}\right)$ indicate the lower and upper limit for predicted relative states, predicted absolute states and the control input respectively. $\tilde{V}_{u_j}$ must be determined such that necessary conditions of stability are satisfied.

We present the implementation algorithm for the presented recovery approach in Algorithm 4.3.

Algorithm 4.3 Decentralized Local System Recovery for Any Agent $j \in V_f$

1. At any time $t_k \mid t_k \geq t_f + t_d$:
   (a) Measure the current absolute state $x_j(k)$.
   (b) Obtain the fault information from the local FDI and reconfigure the internal model (A_{f_j}, B_{f_j}), the input set-point $(u_{j_{f_e}})$ and the control input constraints (U_{f_j}) accordingly.
   (c) Solve Problem D for agent j by using any available algorithm such as the interior point, etc., yielding $u_j^*(k+l \mid k)$ for $l = 0, 1, \ldots, M-1$.
2. Over any interval $[t_k, t_{k+1})$, $k \in \{0, 1, 2, \ldots\}$:
   Apply $u_j^*(k \mid k)$.

4.5 Simulation Results

In this section, the performance of our proposed recovery strategies are analyzed through simulations. Similar to the previous chapter simulation studies, a team of four coordinating satellites is considered and their communication topology for the semi-decentralized control is the one depicted in Figure 3.2. The data communication is assumed to be ideal with zero communication time delay and loss.

The parameters that are considered for modeling the satellites and also the saturation constraints, other details related to the RW parameters and disturbance and noise characteristics are similar to the previous chapter simulation studies. The controller weightings are also selected to be similar to those selected in the previous chapter except one which is reconfigured under fault condition as it was outlined in Section 4.3.2. We do not consider any constraint on states and rate of change of inputs. The optimization problem is solved by using interior point method. In order to perform a quantitative analysis and comparison of the behavior of the system after fault occurrence, the previously defined PIs (defined in the previous chapter simulation studies) are employed. The upper limits of the PIs J_{ss} and $\widetilde{J}_{ss}$, namely $J_{ss} \leq \varepsilon_f$ and $\widetilde{J}_{ss} \leq \widetilde{\varepsilon}_f$, are selected to be $\varepsilon_f = 10 \times 10^{-4}$ and $\widetilde{\varepsilon}_f = 10 \times 10^{-5}$, based on

acceptable degraded specifications for the steady-state performance of the formation flying system.

The faults are injected to the system at the time $t_f = 25\,sec$. The fault scenarios are described in the following and for each scenario the maximum FDI information inaccuracy that does not violate the acceptable degraded performance specifications in terms of the tracking performance is evaluated by the simulations and provided.

- **Scenario a.1**: A high severity LOE fault with the magnitude of 90% is considered in this scenario. The maximum FDI information under-estimation inaccuracy that provides an acceptable degraded performance after fault recovery is evaluated to be 5% .

- **Scenario a.2**: A moderate magnitude LOE fault with the magnitude of 70% is considered in this scenario. The maximum FDI information under-estimation inaccuracy that provides an acceptable degraded performance after fault recovery is evaluated to be 30%.

- **Scenario a.3**: A low severity LOE fault with the magnitude of 15% is considered in this scenario. The nominal control schemes can handle this fault and recover the system without the need for employing any system recovery scheme.

- **Scenario b.1**: A high severity reduced friction fault with the magnitude of 90% is considered in this scenario. The maximum FDI information under-estimation inaccuracy that provides an acceptable degraded performance after fault recovery is evaluated to be 50%.

- **Scenario b.2**: A moderate magnitude reduced friction fault with the magnitude of 50% is considered in this scenario. The nominal control schemes can handle this fault and recover the system without the need for employing any system recovery scheme.

4.5.1 Semi-Decentralized Two-Level Recovery Scheme

In this subsection, the recovery performance of the proposed two-level semi-decentralized recovery strategy under the fault scenarios a.1 and b.1 is evaluated. The FDI fault detection time delays for both scenarios are assumed to be $t_d = 5\ sec$. In Section 4.5.4 we consider the effects of different time delays on the performance of the recovery system.

4.5.1.1 LOE Fault - Scenario a.1

In this subsection, we compare the performance of one-level (local) recovery scheme with the two-level scheme under fault scenario a.1. Figure 4.1 and also the PI J_{ss} for the two recovery schemes verify that the desirable set-point tracking after fault recovery is satisfied by using the one-level recovery scheme but without imposing communication requirements in terms of fault information associated with the two-level recovery scheme. However, the absolute attitude quaternions in the one-level semi-decentralized recovery scheme show an oscillatory recovery behavior with a longer settling time characteristic. This behavior arises due to the larger input signal overshoot of the faulty agent in the one-level semi-decentralized recovery scheme, compared with the two-level semi-decentralized recovery scheme as shown in Figure 4.3. Furthermore, the input signals corresponding to the neighboring healthy agents in the one-level recovery scheme show a lower overshoot whereas in the two-level scheme the over-shoots are increased.

Figure 4.2 and also the PI $\widetilde{J}_{ss}$ shows that the formation behavior are fairly comparable in these two scheme and both are satisfactory according to the required specifications.

Figure 4.3 also shows that in the one-level recovery scheme, the healthy agents input signals are violated once the fault occurs, which reveals the behavior-based nature of our semi-decentralized control approach.

Table 4.1: Goal Seeking/Formation Performance, Time Response for the x-axis, and Control Effort Costs, Computational Efforts after One-Level and Two-Level Semi-Decentralized Fault Recovery, 90% LOE Fault with 5% FDI Inaccuracy

	$\widetilde{J}_{tr}$	J_{ss}	$\widetilde{J}_{ss}$	J_u	$\widetilde{t}_s$	t_s	t_{solv}	$ITER$
Two-level recovery	0.158	2.9×10^{-4}	2.6×10^{-5}	815.18	45.4	72.17	0.32	20
One-level recovery	0.158	8.31×10^{-4}	1.75×10^{-5}	1005.8	41.6	74.23	0.32	21

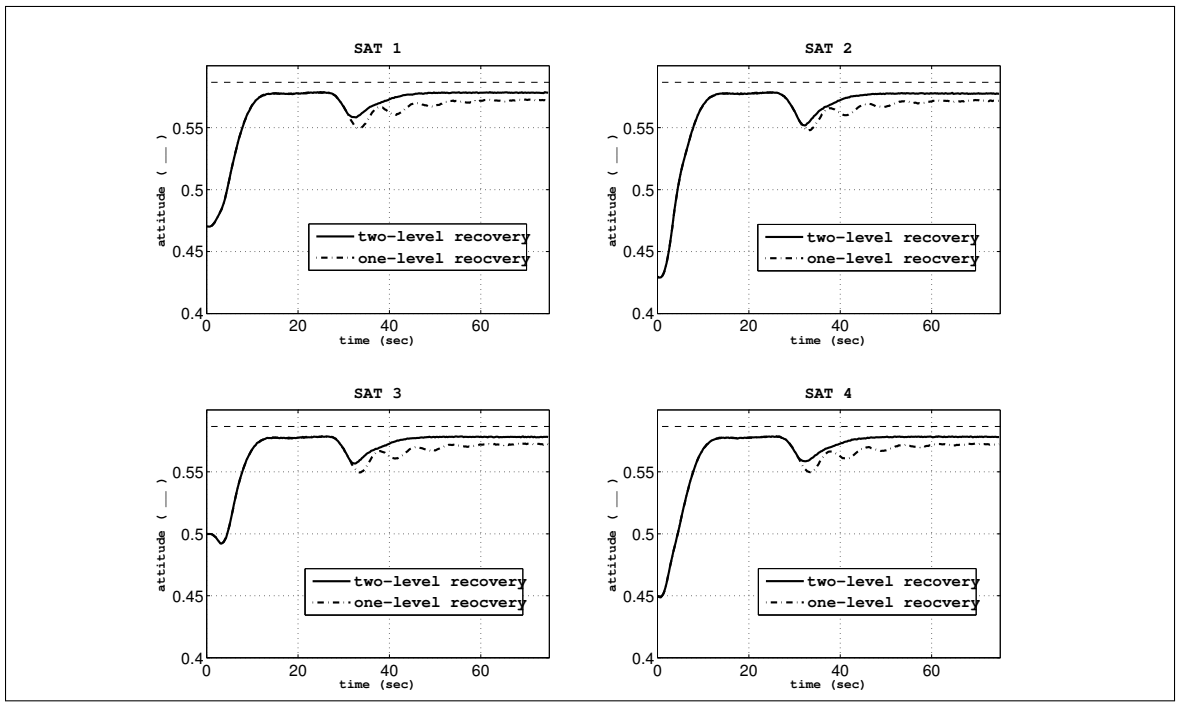

Figure 4.1: X-axis Attitude Quaternion After Control Recovery, 90% LOE Fault with 5% FDI Inaccuracy.

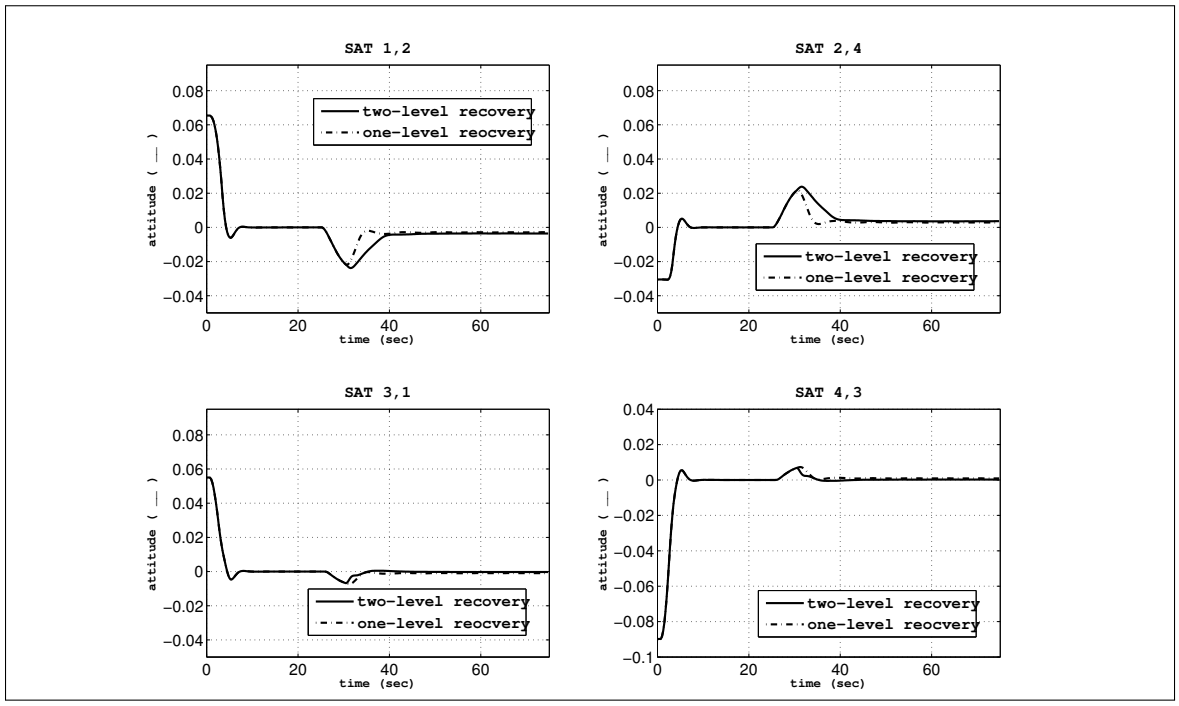

Figure 4.2: X-axis Relative Attitude Quaternion After Control Recovery, 90% LOE Fault with 5% FDI Inaccuracy.

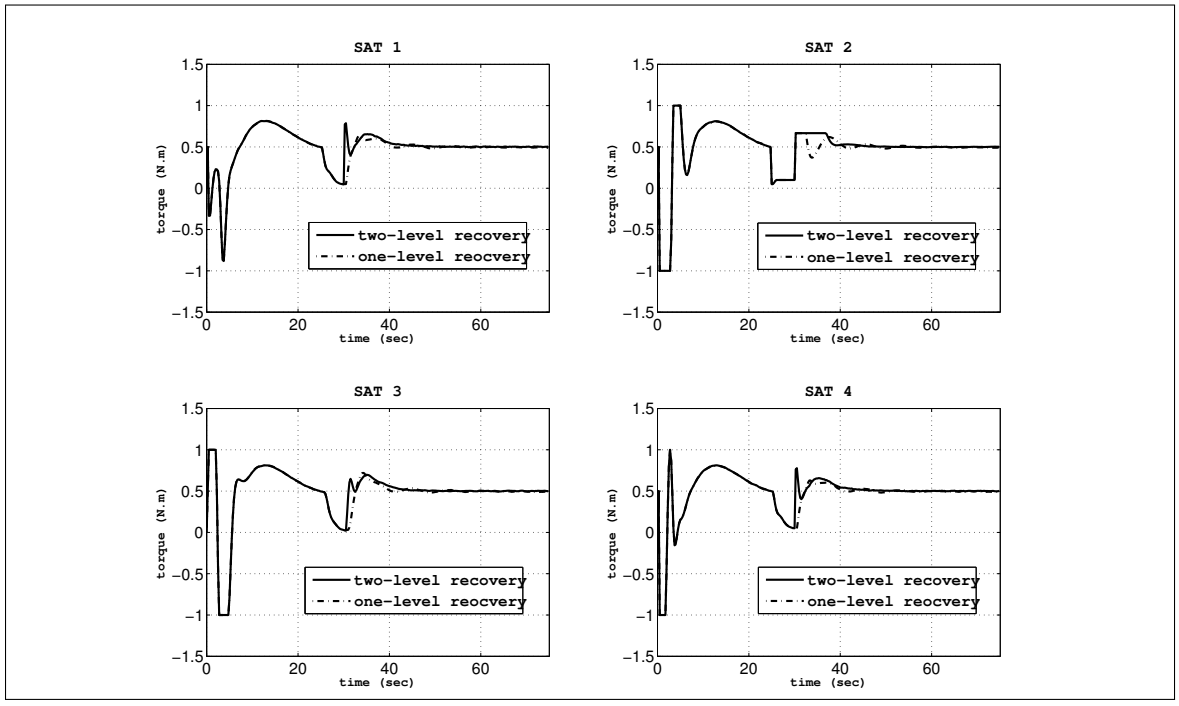

Figure 4.3: X-axis RW Torque After Control Recovery, 90% LOE Fault with 5% FDI Inaccuracy.

4.5.1.2 Friction Fault - Scenario b.1

The simulation results in Figures 4.4, 4.5, 4.6 and Table 4.2 show that reasonably similar results hold in the fault scenario b.1. A magnified view of the attitude recovery behavior is shown in Figure 4.4 to provide an indication of the two-level recovery performance, as due to lower levels of performance degradation in case of friction faults, the influence of the two-level recovery is modest.

Table 4.2: Goal Seeking/Formation Performance, Time Response for the x-axis, and Control Effort Costs, Computational Efforts after One-Level and Two-Level Semi-Decentralized Fault Recovery, 90% Friction Fault with 50% FDI Inaccuracy

	$\widetilde{J}_{tr}$	J_{ss}	$\widetilde{J}_{ss}$	J_u	$\widetilde{t}_s$	t_s	t_{solv}	$ITER$
Two-level recovery	0.158	4.9×10^{-5}	8.04×10^{-6}	766.49	38.79	58.55	0.37	24
One-level recovery	0.158	5.006×10^{-5}	8.1×10^{-6}	809.45	33.7	65.5	0.36	23

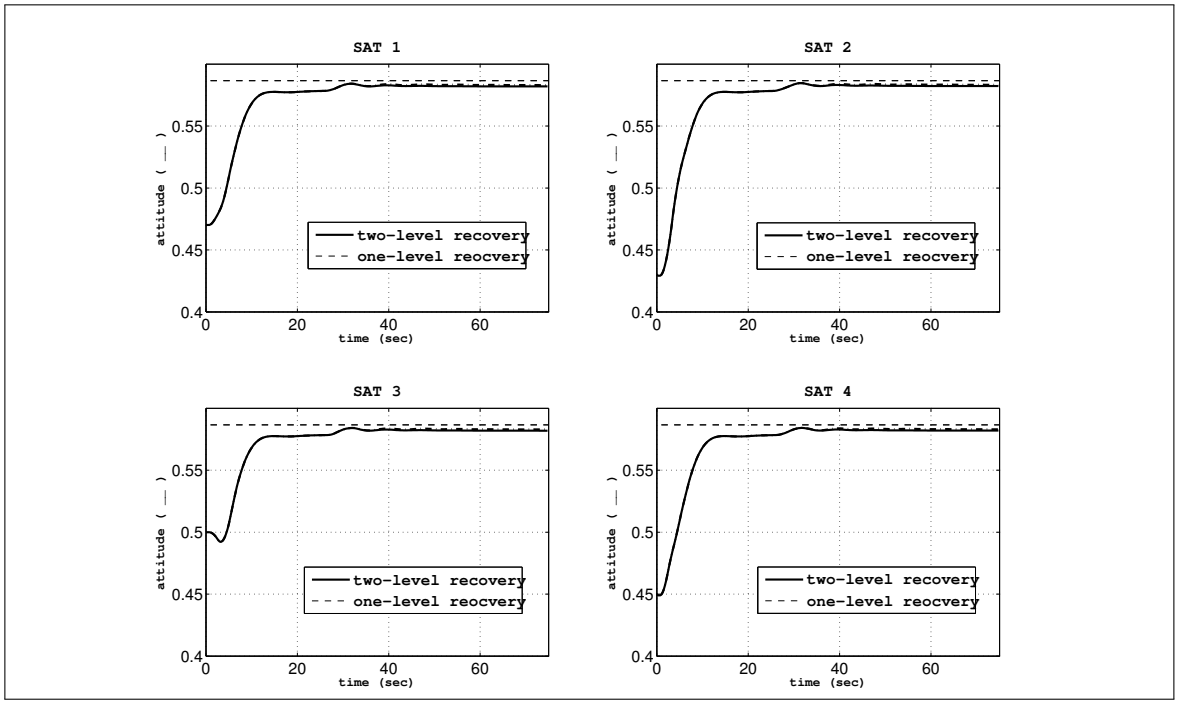

(a) Original View.

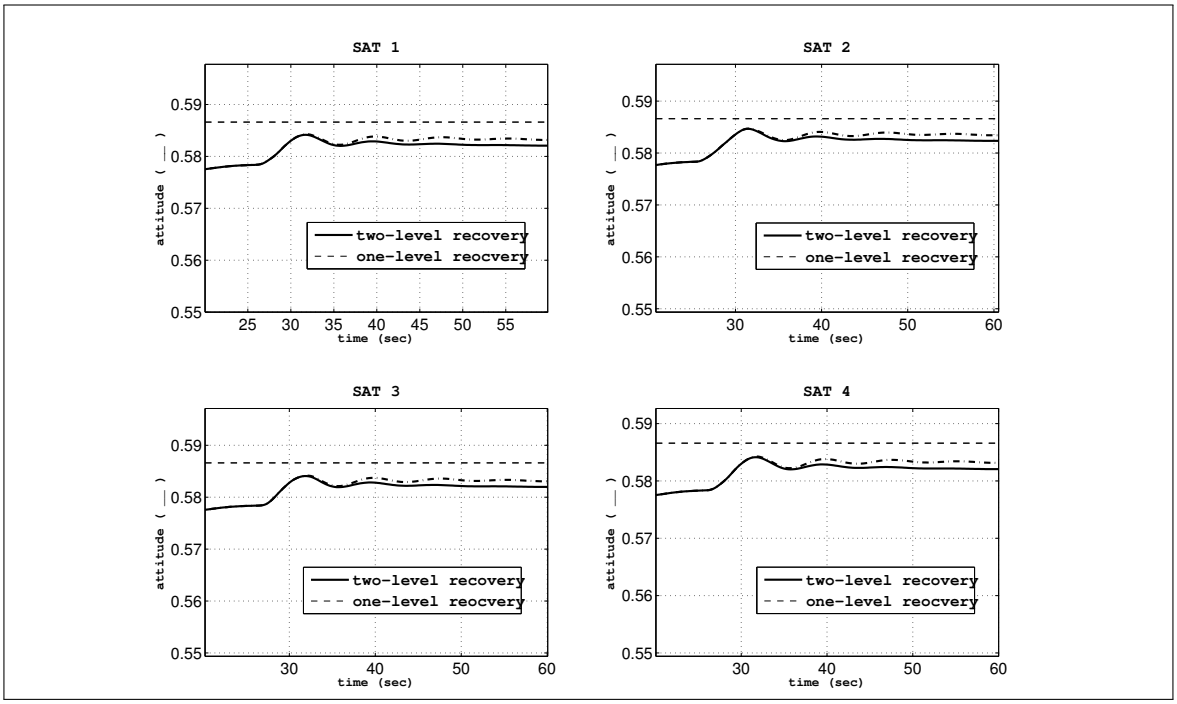

(b) Magnified View.

Figure 4.4: X-axis Attitude Quaternion After Control Recovery, 90% Friction Fault with 50% FDI Inaccuracy.

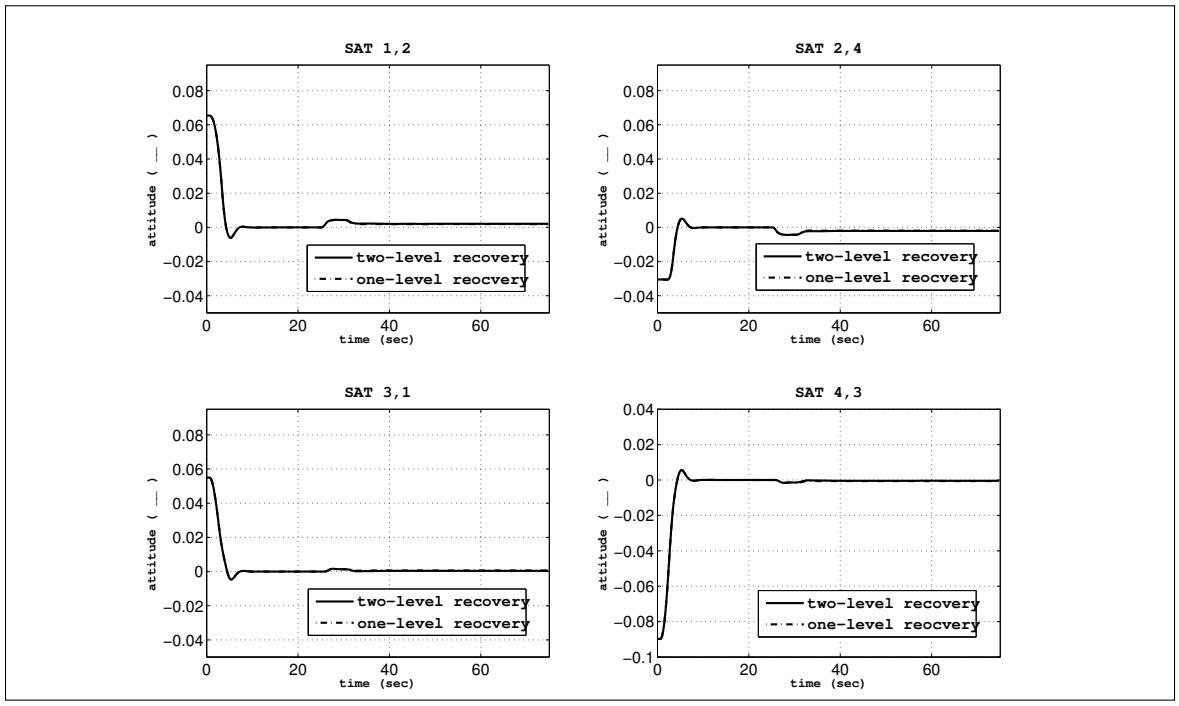

Figure 4.5: X-axis Relative Attitude Quaternion After Control Recovery, 90% Friction Fault with 50% FDI Inaccuracy.

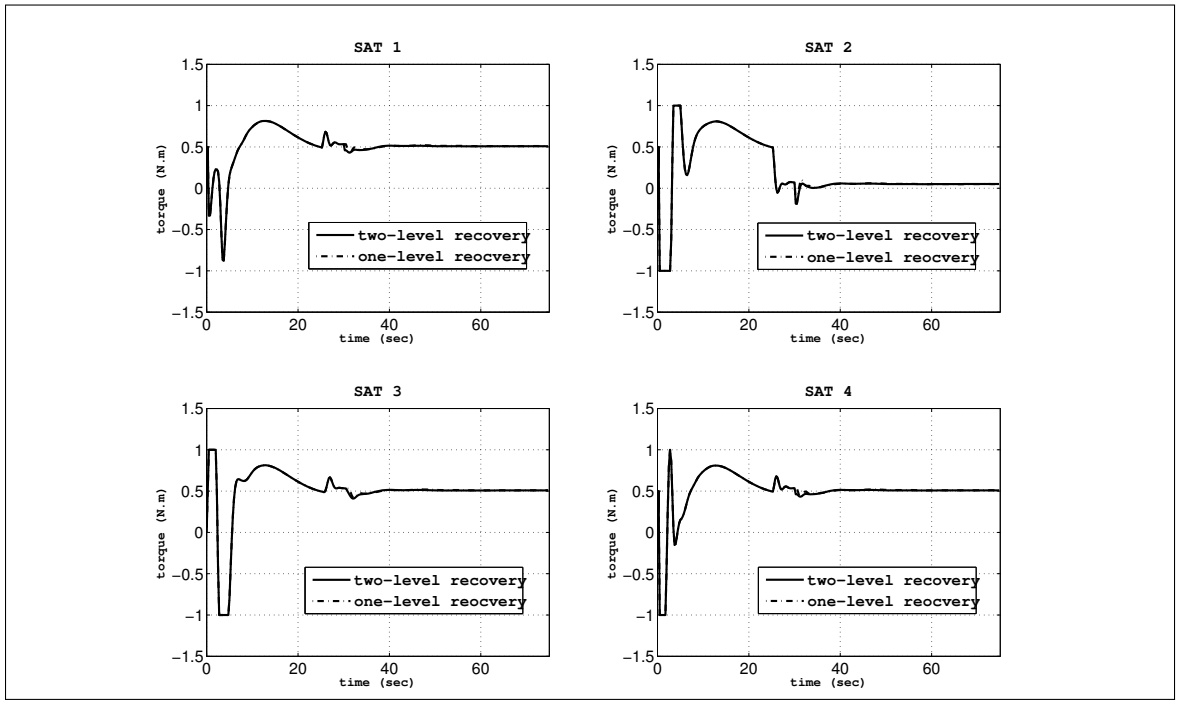

Figure 4.6: X-axis RW Torque After Control Recovery, 90% Friction Fault with 50% FDI Inaccuracy.

4.5.2 Semi-Decentralized vs. Centralized Fault Accommodation

In this subsection, the recovery performance of the centralized and semi-decentralized recovery schemes are evaluated and compared subject to LOE and friction faults and under different fault severity scenarios. The FDI fault detection time delays for all of the cases are assumed to be $t_d = 5\ sec$. In Section 4.5.4 we consider the effects of different time delays on the performance of the recovery system.

4.5.2.1 LOE Fault - Scenario a.1

In this part of simulations a high severity LOE fault (90%) is injected to the system and the recovery performance of the semi-decentralized and centralized recovery schemes are compared.

Figures 4.7, 4.8 and 4.9 show that in this fault scenario, if the FDI information inaccuracy is 20%, that is, larger than the maximum allowable values that we evaluated earlier, then it yields an unstable closed-loop behavior. Therefore, it necessitates employing a more accurate FDI module and recovery scheme in this case.

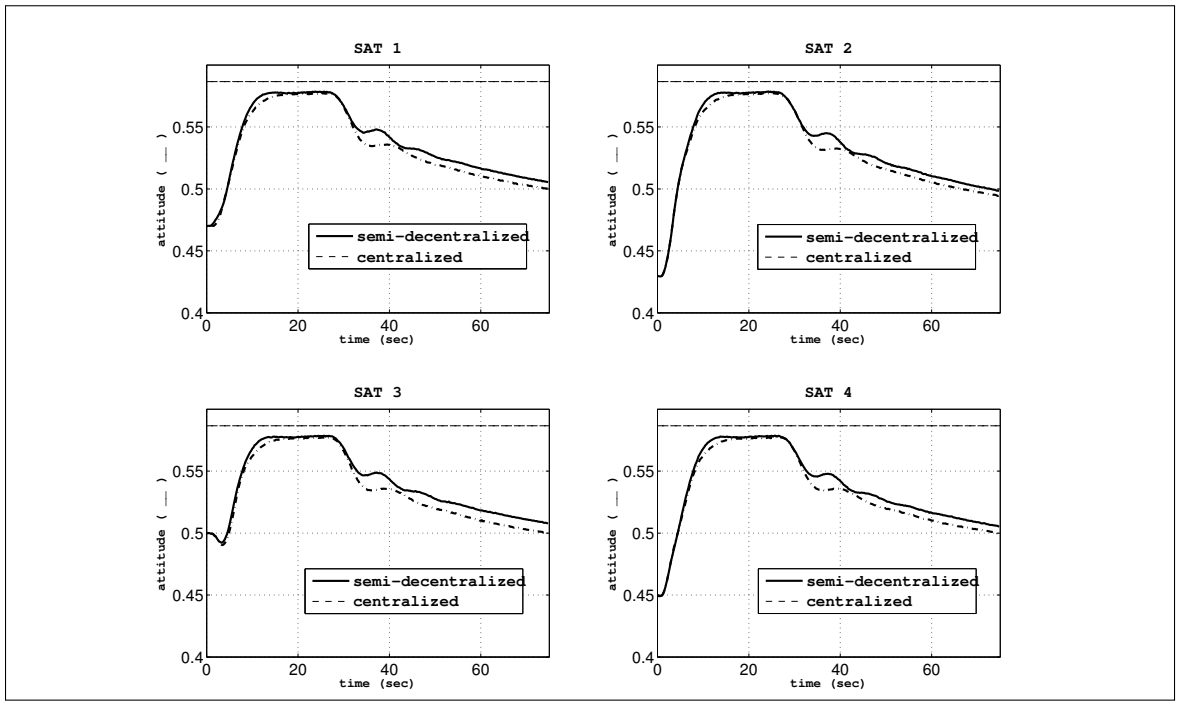

Figure 4.7: X-axis Attitude Quaternion After Control Recovery, 90% LOE Fault with 20% FDI Inaccuracy.

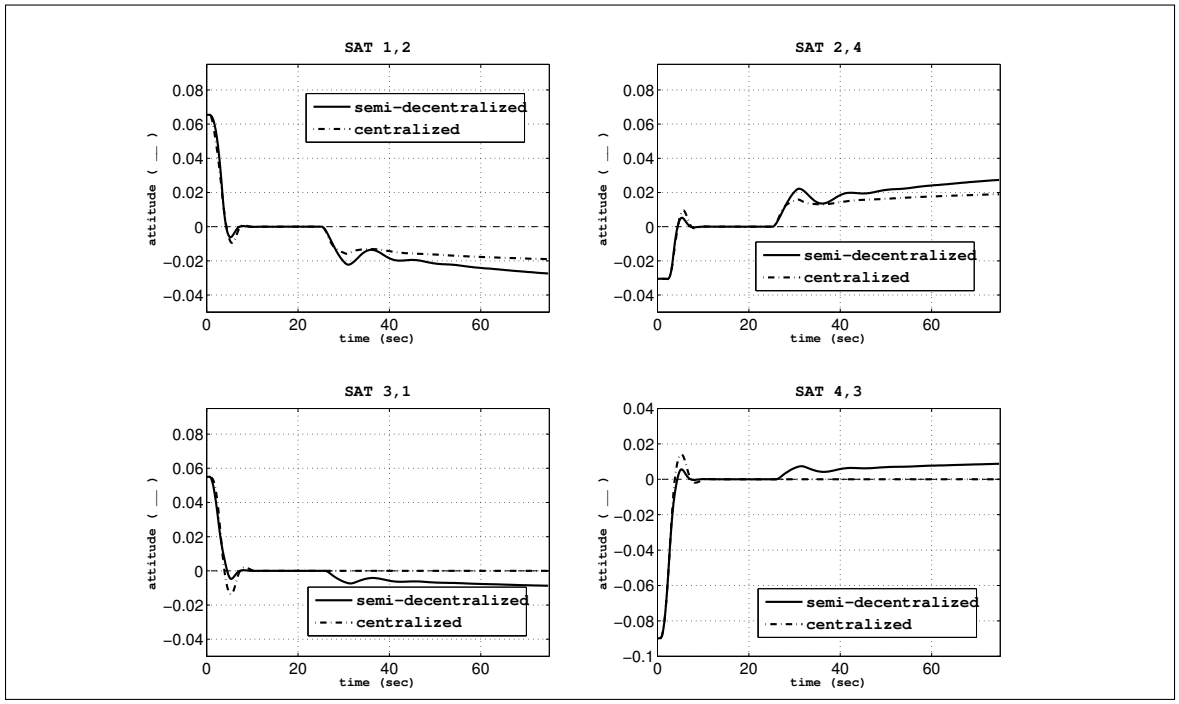

Figure 4.8: X-axis Relative Attitude Quaternion After Control Recovery, 90% LOE Fault with 20% FDI Inaccuracy.

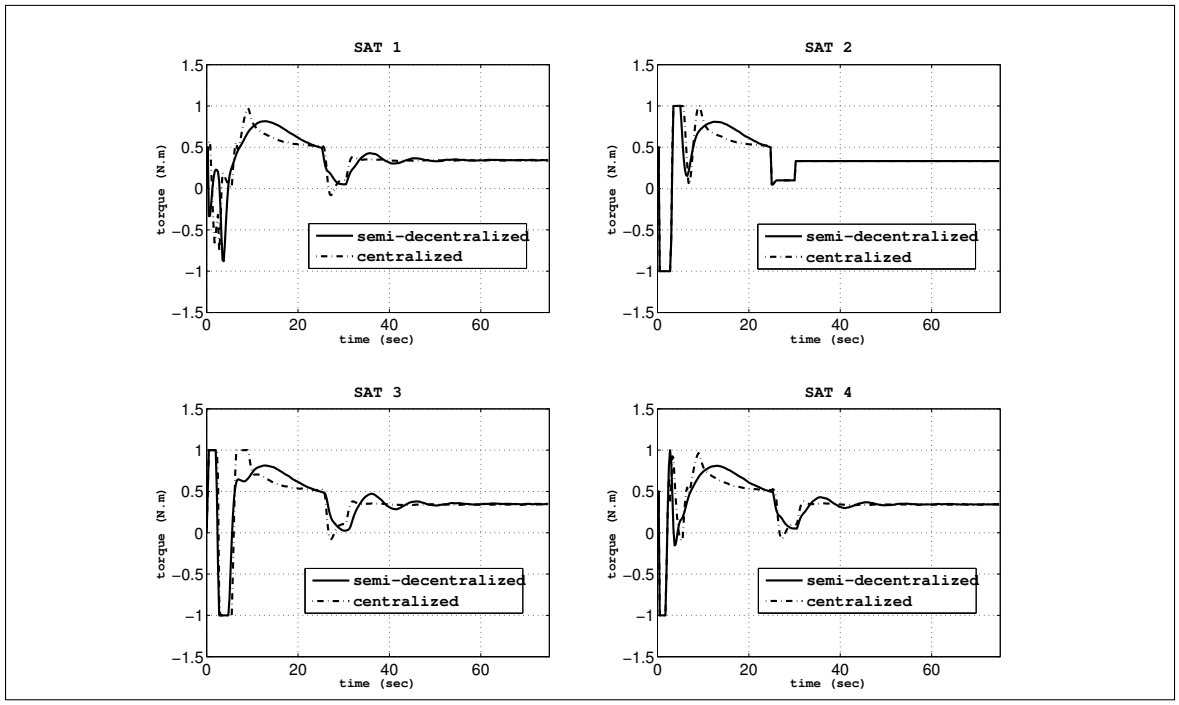

Figure 4.9: X-axis RW Torque After Control Recovery, 90% LOE Fault with 20% FDI Inaccuracy.

The maximum FDI information inaccuracy that provides an acceptable degraded performance after fault recovery is evaluated to be 5% as stated previously. Figures 4.10, 4.11 and 4.12 show the x-axis absolute attitude quaternion of all the satellites, the relative attitude quaternion and the corresponding control torques for the semi-decentralized and centralized recovery schemes under the fault scenario a.1.

Figures 4.10, 4.11 and also the PIs J_{ss} and $\widetilde{J}_{ss}$ for this scenario verify that the desirable set-point tracking and formation specifications after fault recovery are met by using the semi-decentralized fault accommodation but without imposing significant computational complexity associated with solving one problem of higher dimensions, as shown by comparing t_{solv} and $ITER$ in Table 4.3, and without imposing significant communication requirements in terms of states information and fault information associated with the centralized scheme. Furthermore, Figure 4.11 shows that the formation performance between the healthy agents is not influenced by the fault occurrence in the centralized recovery approach and the agents keep their formation while their absolute attitudes are being recovered. As can be observed in Figure 4.12, the RW constraints are satisfied in these control design schemes and the RW torque never exceeded the specified threshold. The cumulative control effort costs (J_u) for the two schemes show that the semi-decentralized recovery scheme yields lower fault compensation control effort costs.

Table 4.3: Goal Seeking/Formation Performance, Time Response for the x-axis, and Control Effort Costs, Computational Efforts after Semi-Decentralized and Centralized Fault Recovery, 90% LOE Fault with 5% FDI Inaccuracy

	$\widetilde{J}_{tr}$	J_{ss}	$\widetilde{J}_{ss}$	J_u	$\widetilde{t}_s$	t_s	t_{solv}	$ITER$
Semi-Dec. Recovery	0.158	2.94×10^{-4}	2.5×10^{-5}	817.2	45.6	70.8	0.30	20
Centralized Recovery	0.082	5.5×10^{-4}	2.5×10^{-5}	1148.2	59.6	51.2	3.78	89.04

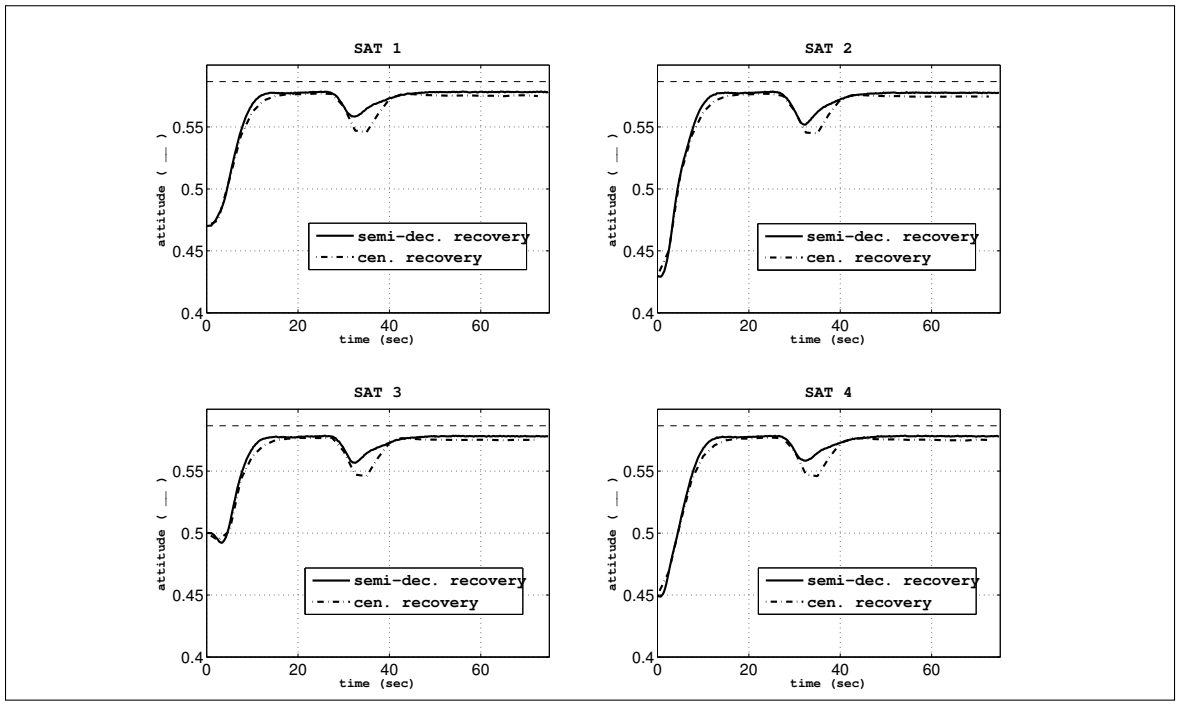

Figure 4.10: X-axis Attitude Quaternion After Control Recovery, 90% LOE Fault with 5% FDI Inaccuracy.

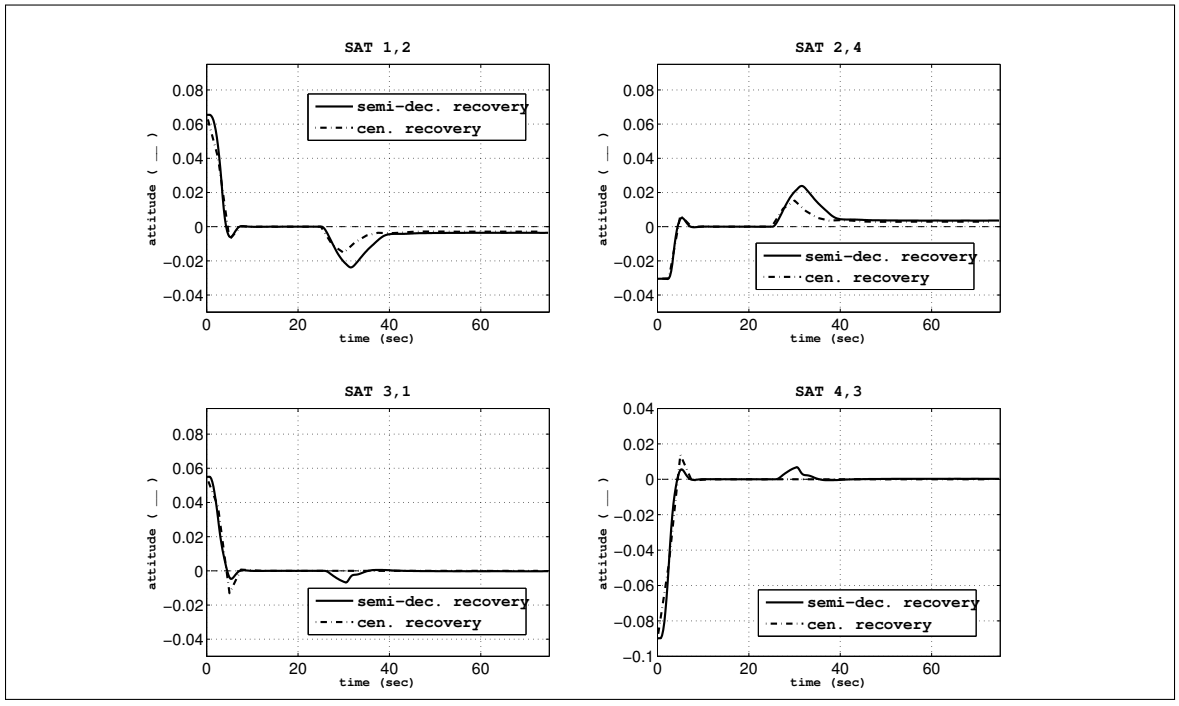

Figure 4.11: X-axis Relative Attitude Quaternion After Control Recovery, 90% LOE Fault with 5% FDI Inaccuracy.

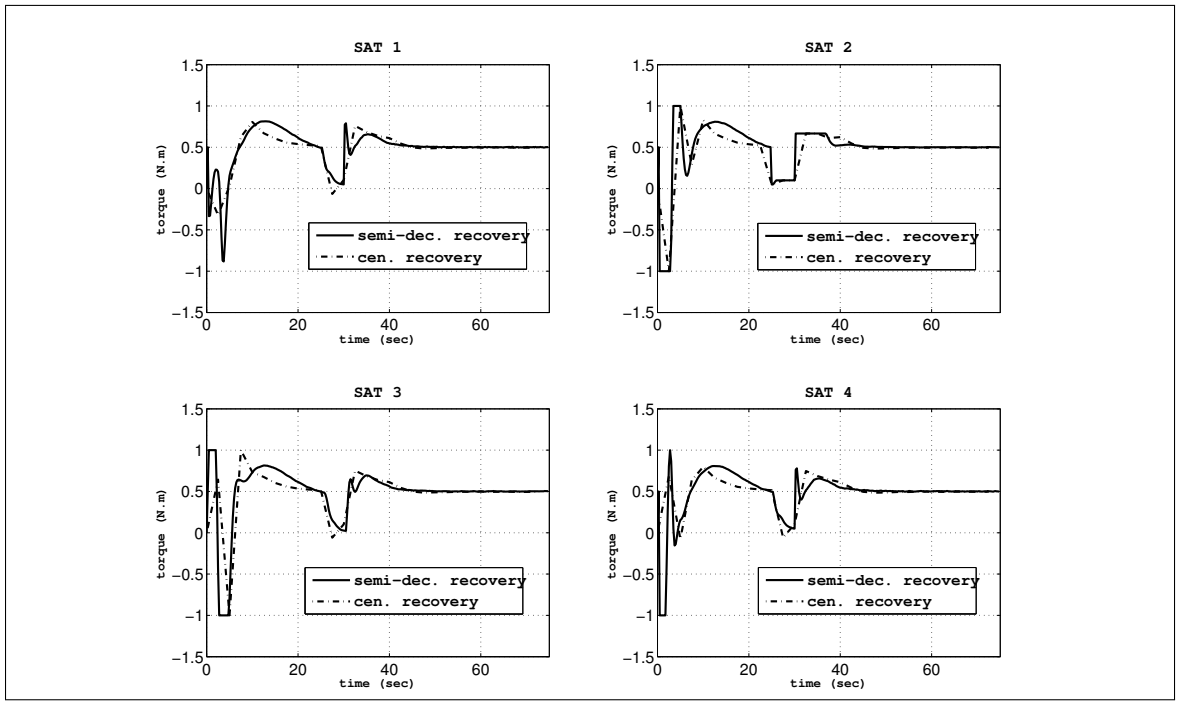

Figure 4.12: X-axis RW Torque After Control Recovery, 90% LOE Fault with 5% FDI Inaccuracy.

4.5.2.2 LOE Fault - Scenario a.2

In this part of simulations a moderate magnitude LOE fault (70%) is injected to the system and the recovery performance of the semi-decentralized and centralized recovery schemes are compared. The maximum FDI information accuracy that provides an acceptable degraded performance after fault recovery is evaluated to be 30% as stated previously.

Figures 4.13, 4.14 and 4.15 show the x-axis absolute attitude quaternion of all the satellites, the relative attitude quaternion and the corresponding control torques for the semi-decentralized and centralized recovery schemes under the fault scenario a.2.

Figures 4.13, 4.14 and also the PIs J_{ss} and $\widetilde{J}_{ss}$ for this scenario verify that similar to the high severity LOE fault scenario, the desirable set-point tracking and formation specifications after fault recovery are met by using the semi-decentralized fault accommodation as well as the centralized scheme. Furthermore, Figure 4.14 shows that, similar to the high severity LOE fault scenario, the formation performance between the healthy agents is not influenced by the fault occurrence in the centralized recovery approach and the agents keep their formation while their absolute attitudes are being recovered. Figure 4.15 also shows that the RW constraints are satisfied in these control design schemes and the RW torque never exceeded the specified threshold. The cumulative control effort costs (J_u) for the two schemes show that the semi-decentralized recovery scheme yields lower fault compensation control effort costs.

Compared with the previous high severity fault condition, a moderate magnitude fault condition is less sensitive to the FDI information inaccuracy. However, the larger FDI inaccuracy that is considered in this case yields more oscillatory behavior and longer settling times under this fault scenario.

Table 4.4: Goal Seeking/Formation Performance, Time Response for the x-axis, and Control Effort Costs, Computational Efforts after Semi-Decentralized and Centralized Fault Recovery, 70% LOE Fault with 30% FDI Inaccuracy

	$\widetilde{J}_{tr}$	J_{ss}	$\widetilde{J}_{ss}$	J_u	$\widetilde{t}_s$	t_s	t_{solv}	$ITER$
Semi-Dec. recovery	0.158	6.9×10^{-4}	2.2×10^{-5}	969.71	45.03	74.71	0.32	21
Centralized recovery	0.082	4.7×10^{-4}	4×10^{-5}	1161.3	59.59	73.5	3.45	83

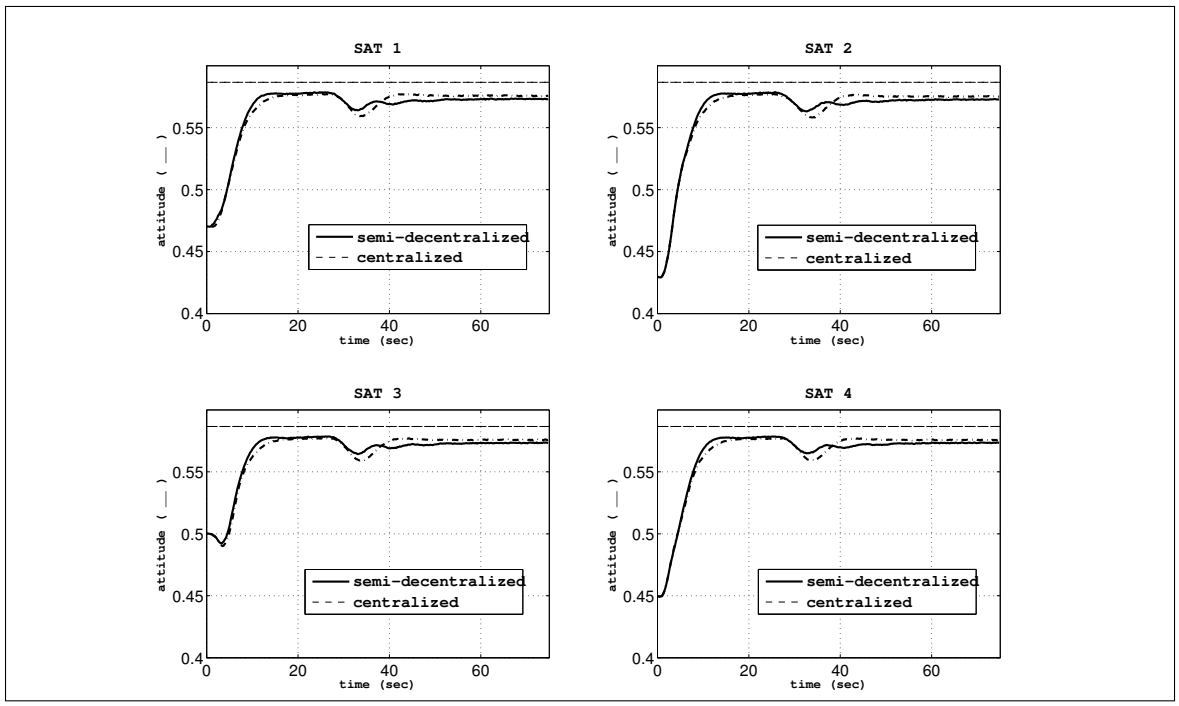

Figure 4.13: X-axis Attitude Quaternion After Control Recovery, 70% LOE Fault with 30% FDI Inaccuracy.

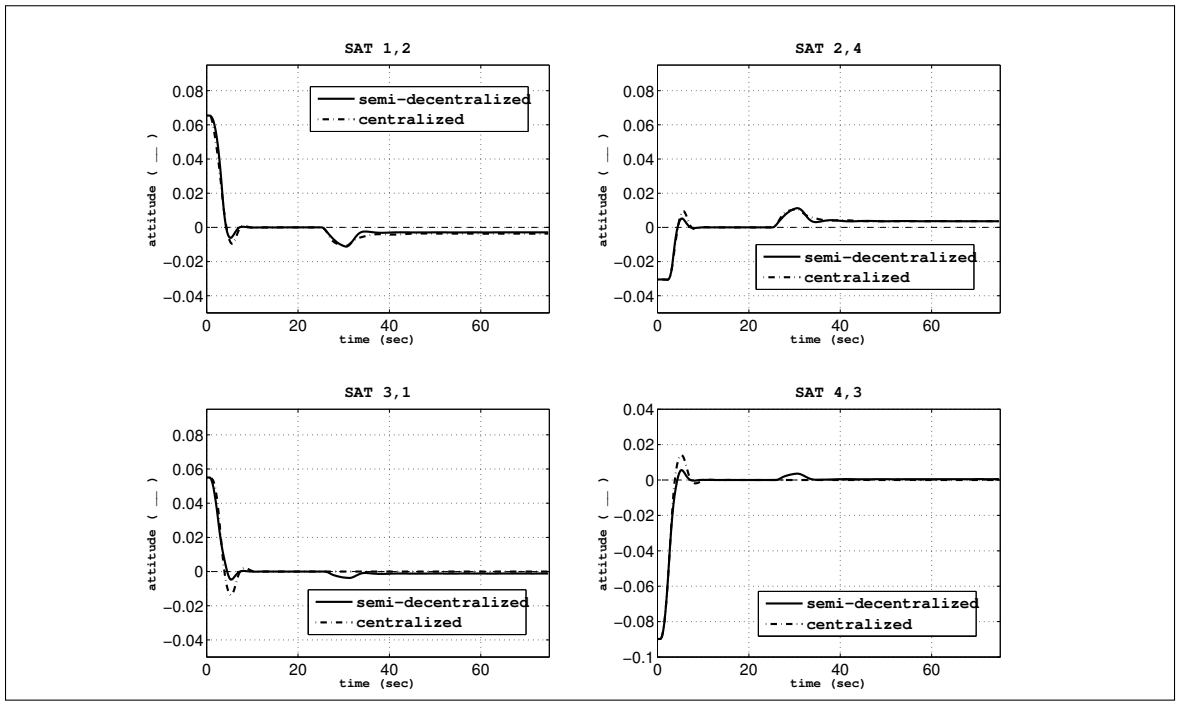

Figure 4.14: X-axis Relative Attitude Quaternion After Control Recovery, 70% LOE Fault with 30% FDI Inaccuracy.

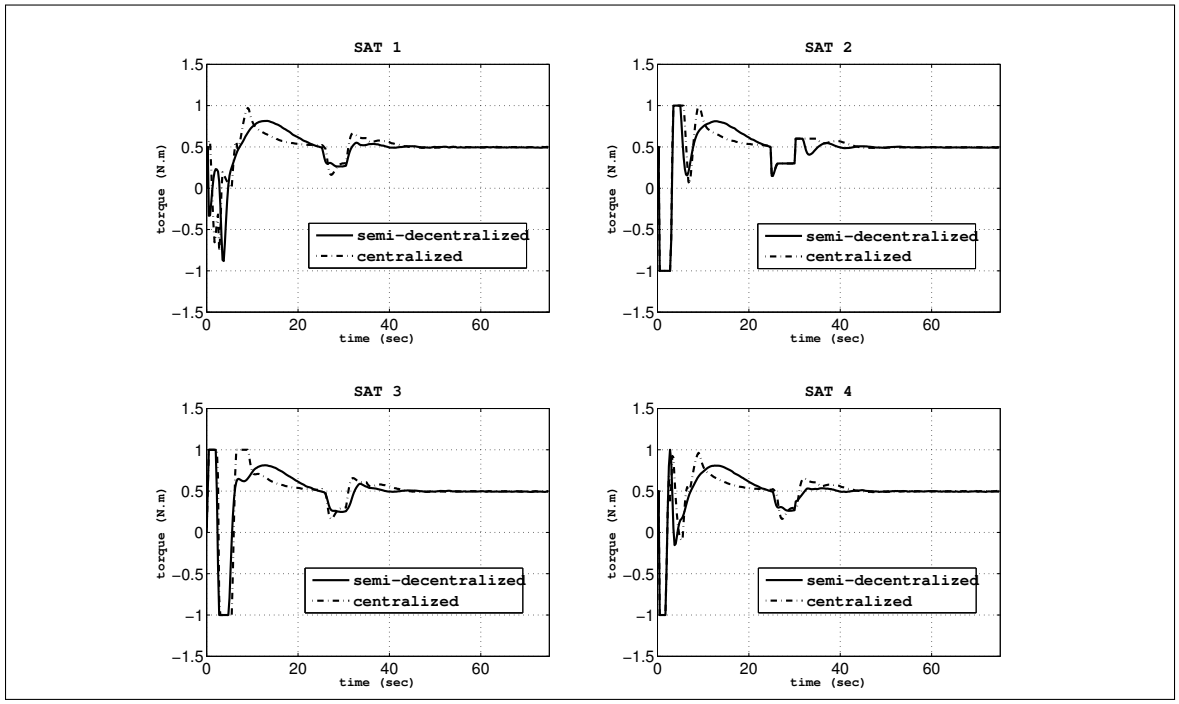

Figure 4.15: X-axis RW Torque After Control Recovery, 70% LOE Fault with 30% FDI Inaccuracy.

4.5.2.3 LOE Fault - Scenario a.3

In this part of simulations a low-severity LOE fault (15%) is injected to the system. The simulation results show that the nominal control schemes can handle this fault and recover the system without any system recovery schemes. The recovery performance of the semi-decentralized and centralized control schemes are compared.

Figures 4.16, 4.17 and 4.18 show the x-axis absolute attitude quaternion of all the satellites, the relative attitude quaternion and the corresponding control torques for the semi-decentralized and centralized control schemes under the fault scenario a.3.

Figures 4.16, 4.17 and also the PIs J_{ss} and $\widetilde{J}_{ss}$ for this scenario verify that the desirable set-point tracking and formation specifications are met by using the semi-decentralized and centralized control scheme without any system recovery. In the semi-decentralized scheme, the significant computational complexity associated with solving one problem of higher dimensions and communication requirements associated with centralized scheme is not imposed on the system. Figure 4.17 shows that neither the individual performance of healthy agents, nor the formation performance between the healthy agents, are influenced by fault occurrence in the centralized control approach and they keep their goal seeking formation. It can be observed from Figure 4.18 that the RW constraints are satisfied in these control design schemes and the RW torque never exceeded the specified threshold. The cumulative control effort costs (J_u) for the two schemes show that the centralized control scheme yields lower control effort costs.

Table 4.5: Goal Seeking/Formation Performance, Time Response for the x-axis, and Control Effort Costs, Computational Efforts for Semi-Decentralized and Centralized Control Schemes, 15% LOE Fault with no FDI and Reocvery

	$\widetilde{J}_{tr}$	J_{ss}	$\widetilde{J}_{ss}$	J_u	$\widetilde{t}_s$	t_s	t_{solv}	$ITER$
Semi-Dec. Control	0.158	3.6×10^{-4}	1.4×10^{-6}	1121.7	73.56	74.88	0.37	24
Centralized Control	0.0827	3.7×10^{-4}	2.7×10^{-6}	1743.2	73.81	74.98	4.89	112

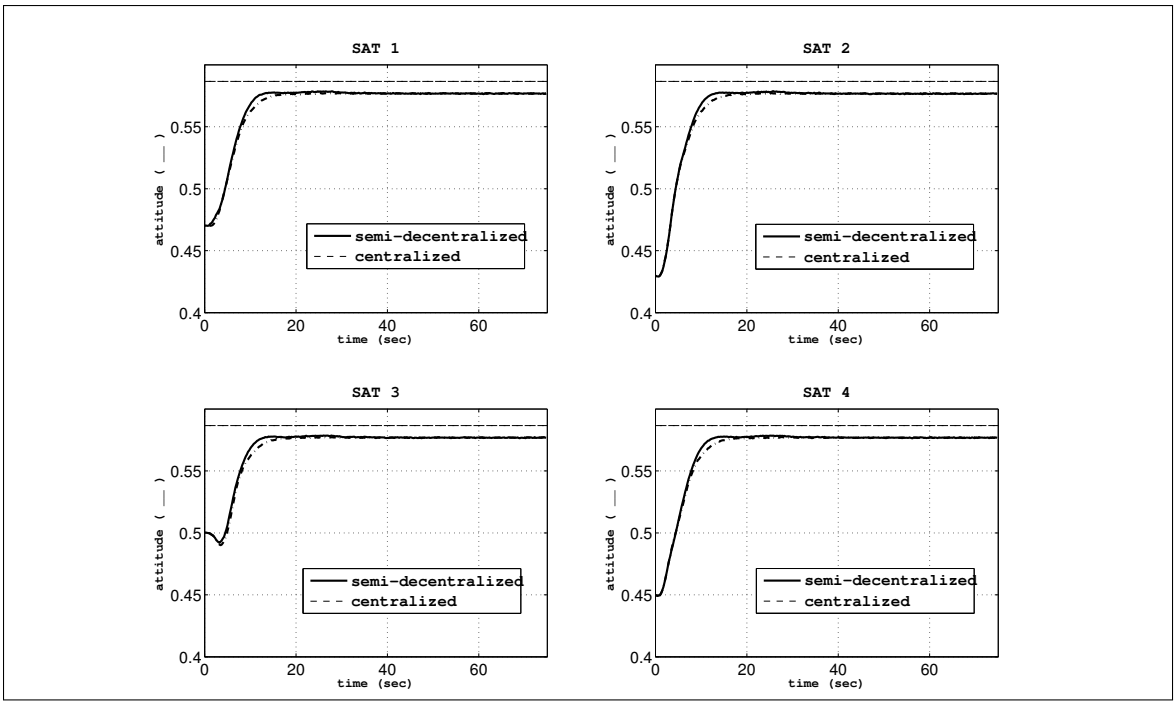

Figure 4.16: X-axis Attitude Quaternion, 15% LOE Fault with No FDI and Recovery.

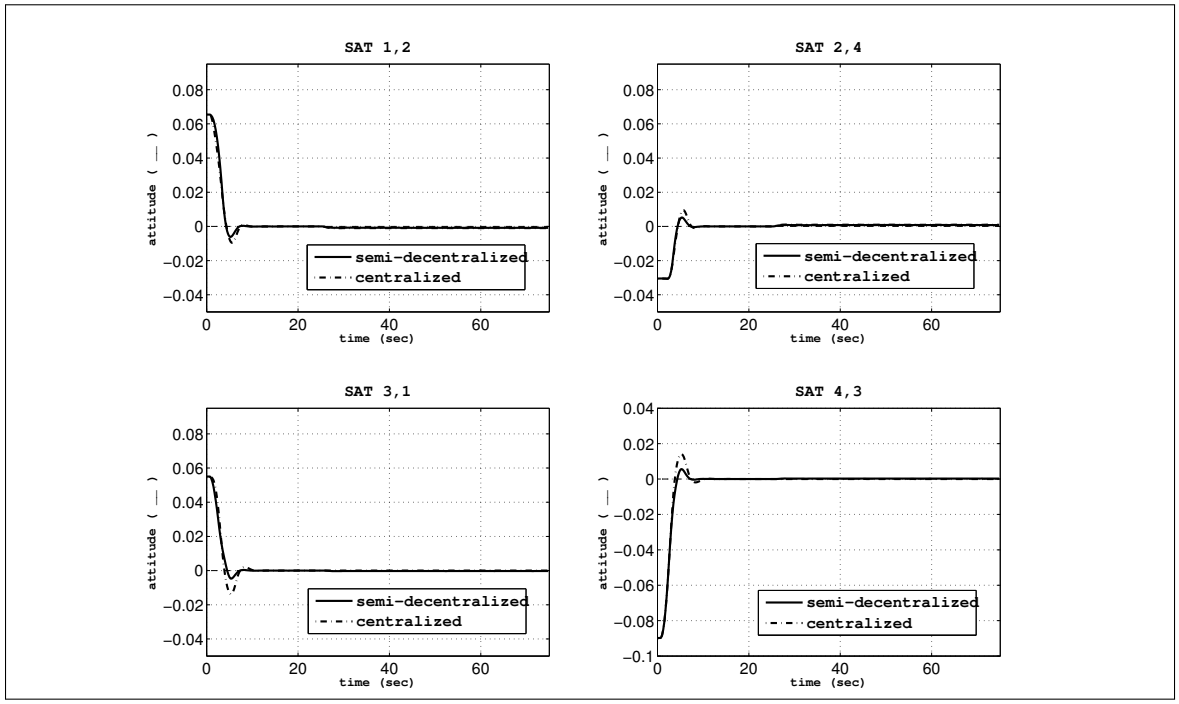

Figure 4.17: X-axis Relative Attitude Quaternion, 15% LOE Fault with No FDI and Recovery.

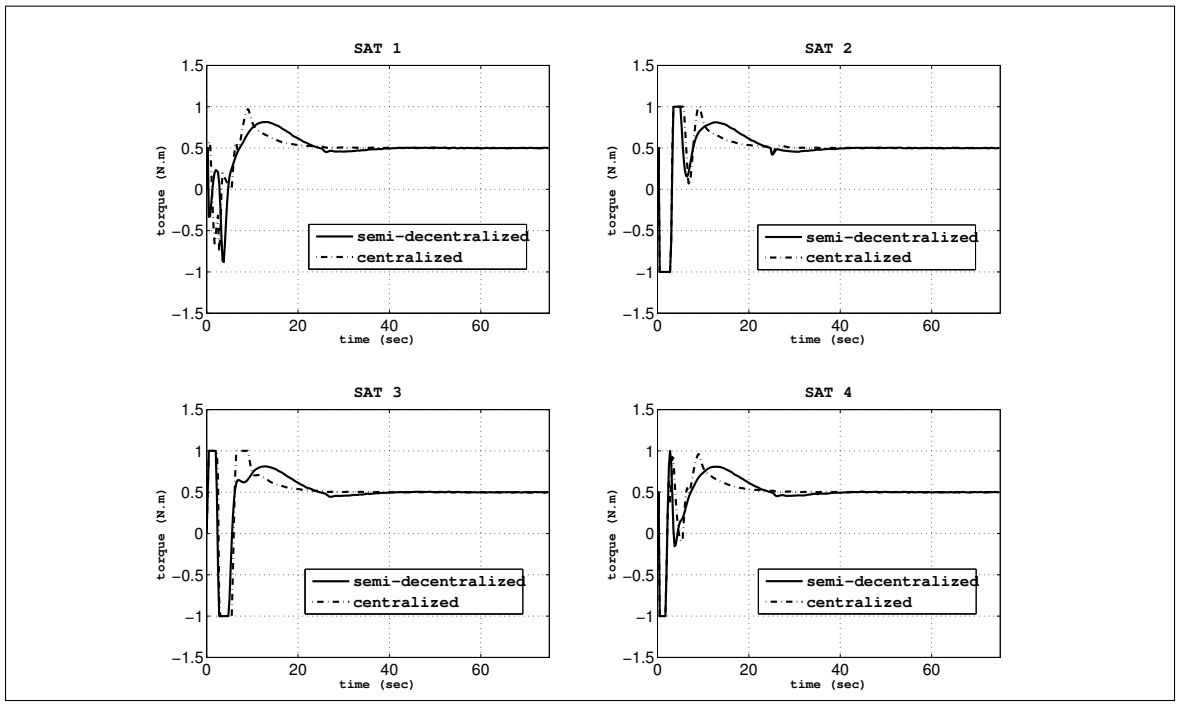

Figure 4.18: X-axis RW Torque, 15% LOE Fault with No FDI and Recovery.

4.5.2.4 Friction Fault - Scenario b.1

In this part of simulations a high severity friction fault (90%) is injected to the system and the recovery performance of the semi-decentralized and centralized recovery schemes are compared. The maximum FDI information accuracy that provides an acceptable degraded performance after fault recovery is evaluated to be 50% as stated previously. As discussed in Section 4.1.1, inaccurate estimations of this fault by the FDI does not violate the closed-loop system stability and it only violates the steady-state error offset.

Figures 4.19, 4.20 and 4.21 show the x-axis absolute attitude quaternion of all the satellites, the relative attitude quaternion and the corresponding control torques for the semi-decentralized and centralized recovery schemes for the fault scenario b.1.

Figures 4.19, 4.20 and also the PIs J_{ss} and $\widetilde{J}_{ss}$ for this scenario verify that the desirable set-point tracking and formation specifications after fault recovery are met by using the semi-decentralized fault accommodation as well as the centralized scheme. Figure 4.21 also shows that healthy agents input signals are subject to considerably larger overshoots in the semi-decentralized recovery approach. Furthermore, Figure 4.20 shows that the formation performance between the healthy agents is influenced by the fault occurrence in the centralized as well as the semi-decentralized recovery approach. It can be observed from Figure 4.21 that the RW constraints are satisfied in these control design schemes and the RW torque never exceeded the specified threshold.

Table 4.6: Goal Seeking/Formation Performance, Time Response for the x-axis, and Control Effort Costs, Computational Efforts after Semi-Decentralized and Centralized Fault Recovery, 90% Friction Fault with 50% FDI Inaccuracy

	$\widetilde{J}_{tr}$	J_{ss}	$\widetilde{J}_{ss}$	J_u	$\widetilde{t}_s$	t_s	t_{solv}	$ITER$
Semi-Dec. recovery	0.158	4.8×10^{-5}	1.07×10^{-5}	998.05	55.37	74.86	0.34	22
Centralized recovery	0.082	2.7×10^{-4}	1.8×10^{-5}	1469.2	54.6	74.96	3.4	70

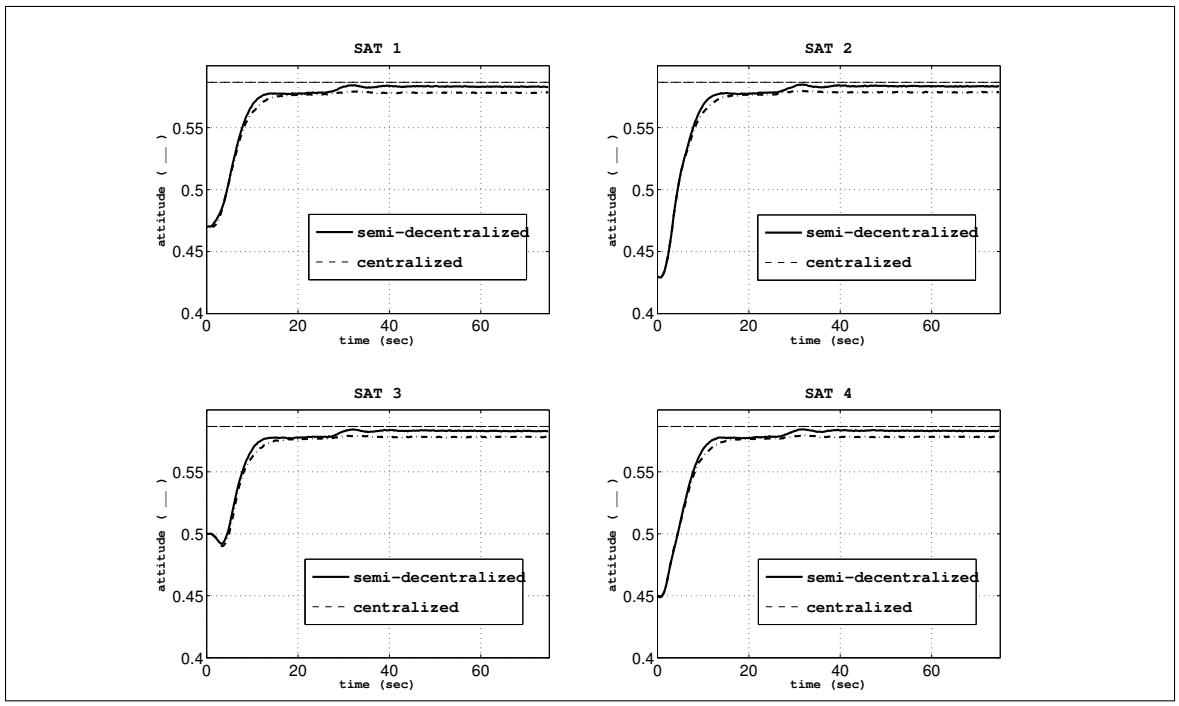

Figure 4.19: X-axis Attitude Quaternion After Control Recovery, 90% Friction Fault with 50% FDI Inaccuracy.

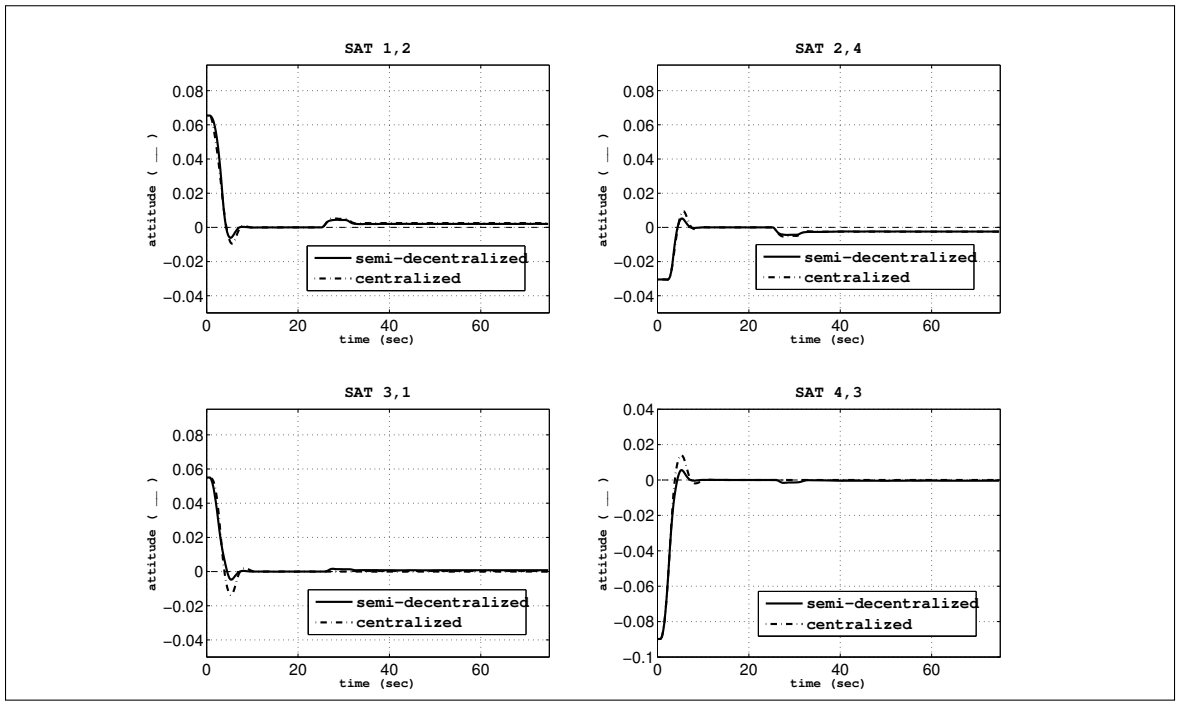

Figure 4.20: X-axis Relative Attitude Quaternion After Control Recovery, 90% Friction Fault with 50% FDI Inaccuracy.

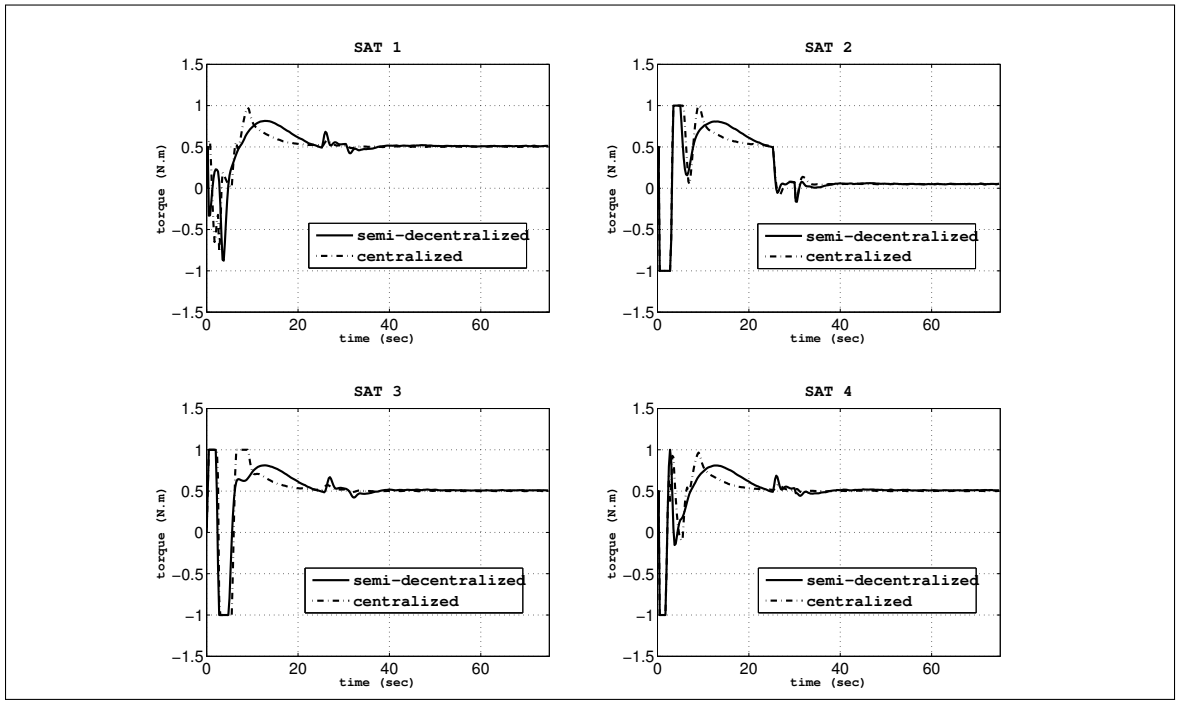

Figure 4.21: X-axis RW Torque with Control Recovery, 90% Friction Fault with 50% FDI Inaccuracy.

4.5.2.5 Friction Fault - Scenario b.2

In this part of simulations a moderate friction fault (50%) is injected to the system. The simulation results show that the nominal control schemes can handle this fault and recover the system without any system recovery scheme. The recovery performance of the semi-decentralized and centralized control schemes are compared.

Figures 4.22, 4.23 and 4.24 show the x-axis absolute attitude quaternion of all the satellites, the relative attitude quaternion and the corresponding control torques for the semi-decentralized and centralized recovery schemes for the fault scenario b.2.

Figures 4.22, 4.23 and also the PIs J_{ss} and $\widetilde{J}_{ss}$ for this scenario verify that the desirable set-point tracking and formation specifications are met by using the semi-decentralized and centralized control scheme without any system recovery. The observations corresponding to the previous case, the high severity fault case, are also observed in this case, that is, the healthy agents input signals are subject to considerably larger overshoots in the semi-decentralized control approach as it is shown in Figure 4.24. Furthermore, Figure 4.23 shows that the formation performance between the healthy agents are influenced by the fault occurrence in the centralized as well as the semi-decentralized control approach. Figure 4.24 shows that the RW constraints are satisfied in these control design schemes and the RW torque never exceeded the specified threshold. The cumulative control effort costs (J_u) for the two schemes show that the centralized control scheme yields lower control effort costs.

Compared with the previous severe faulty condition, a moderate magnitude faulty condition is less sensitive with respect to the FDI information inaccuracy.

Table 4.7: Goal Seeking/Formation Performance, Time Response for the x-axis, and Control Effort Costs, Computational Efforts for Semi-Decentralized and Centralized Control Schemes, 50% Friction Fault with No FDI and Recovery

	$\widetilde{J}_{tr}$	J_{ss}	$\widetilde{J}_{ss}$	J_u	$\widetilde{t}_s$	t_s	t_{solv}	$ITER$
Semi-Dec. control	0.158	2.3×10^{-5}	1.23×10^{-5}	1035.5	49.83	74.81	0.35	23
Centralized control	0.082	2.6×10^{-4}	2.2×10^{-5}	1636.8	51.91	74.96	2.97	69

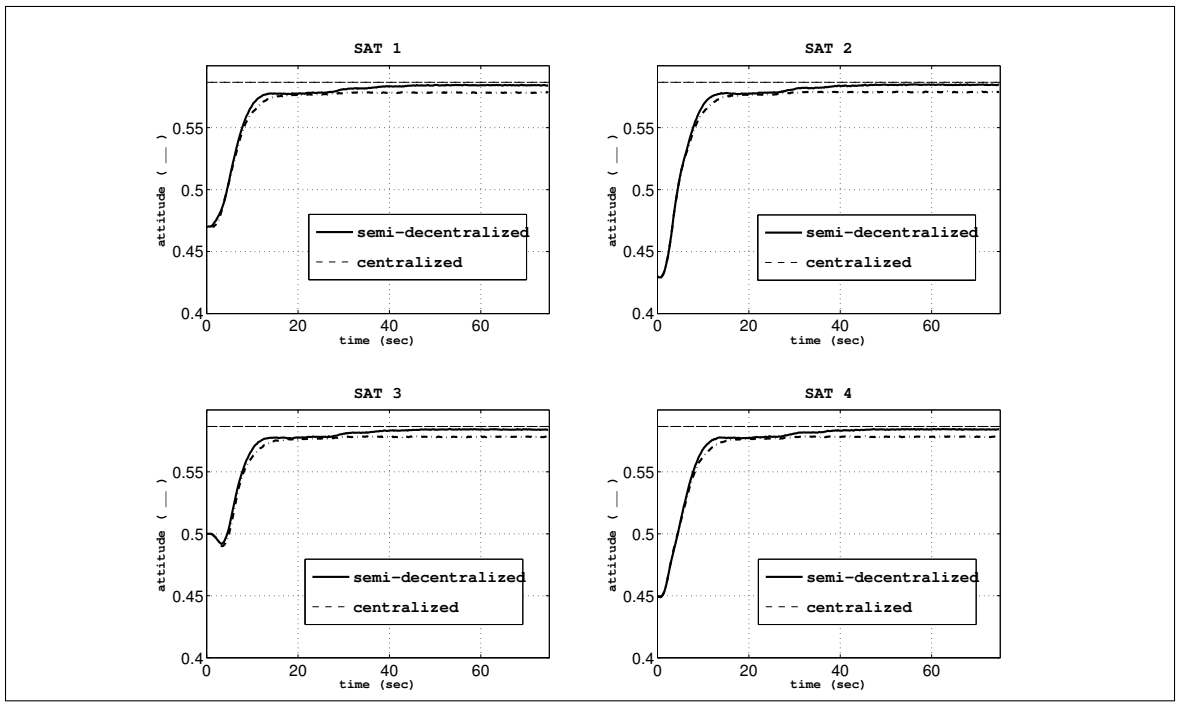

Figure 4.22: X-axis Attitude Quaternion, 50% Friction Fault with No FDI and Recovery.

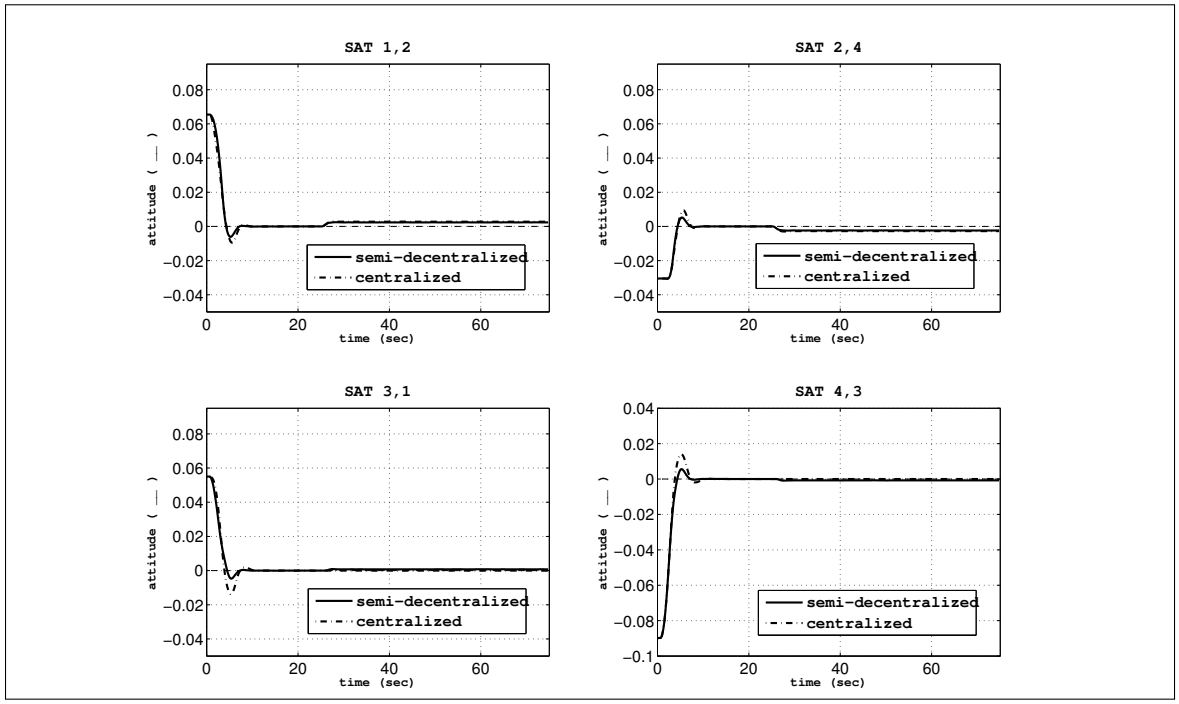

Figure 4.23: X-axis Relative Attitude Quaternion, 50% Friction Fault with No FDI and Recovery.

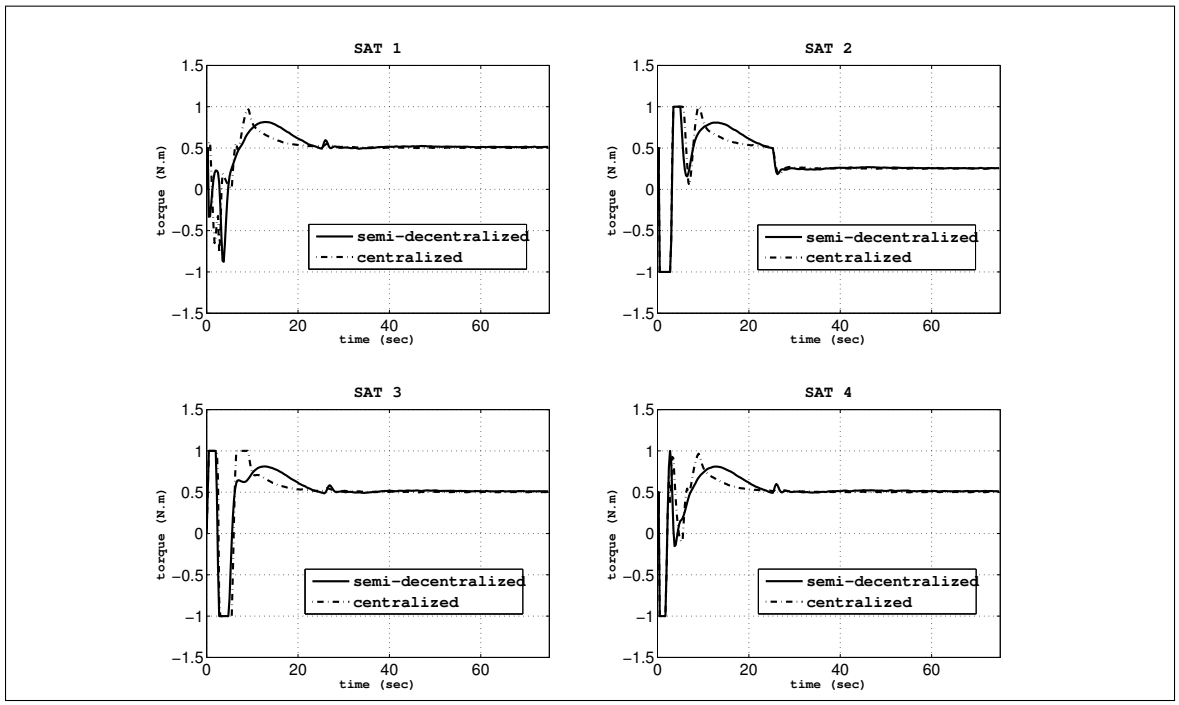

Figure 4.24: X-axis RW Torque, 50% Friction Fault with No FDI and Recovery.

4.5.3 Semi-Decentralized vs. Decentralized Fault Accommodation

In this subsection, the recovery performance of the decentralized and semi-decentralized recovery schemes are compared subject to a high severity LOE fault. The FDI fault detection time delay is assumed to be $t_d = 5\ sec$.

In this part of simulations a high severity LOE fault (90%) is injected to the system and the recovery performance of the semi-decentralized and decentralized recovery schemes are compared. The FDI information inaccuracy is considered to be 5% in the following simulations in order to keep consistency with the previous simulations performed in Section 4.5.2.

Figures 4.25, 4.26 and 4.27 show the x-axis absolute attitude quaternion of all the satellites, the relative attitude quaternion and the corresponding control torques for the semi-decentralized and decentralized recovery schemes under the fault scenario a.1.

Figures 4.25, 4.26 and also the PI $\widetilde{J}_{ss}$ for this scenario verify that the desirable formation specifications after fault recovery is not satisfied by using the decentralized fault accommodation. As can be observed in Figure 4.27, the RW constraints are satisfied in these control design schemes and the RW torque never exceeded the specified threshold. The cumulative control effort costs (J_u) for the two schemes show that the decentralized recovery scheme yields lower fault compensation control effort costs.

Table 4.8: Goal Seeking/Formation Performance, Time Response for the x-axis, and Control Effort Costs, Computational Efforts after Semi-Decentralized and Decentralized Fault Recovery, 90% LOE Fault with 5% FDI Inaccuracy

	$\widetilde{J}_{tr}$	J_{ss}	$\widetilde{J}_{ss}$	J_u	$\widetilde{t}_s$	t_s	t_{solv}	$ITER$
Semi-Dec. Recovery	0.158	4.02×10^{-4}	2.6×10^{-5}	869.38	50.16	70.2	0.30	20
Decentralized Recovery	0.38	3.5×10^{-4}	1.1×10^{-3}	1176.7	63.39	74.63	0.23	19

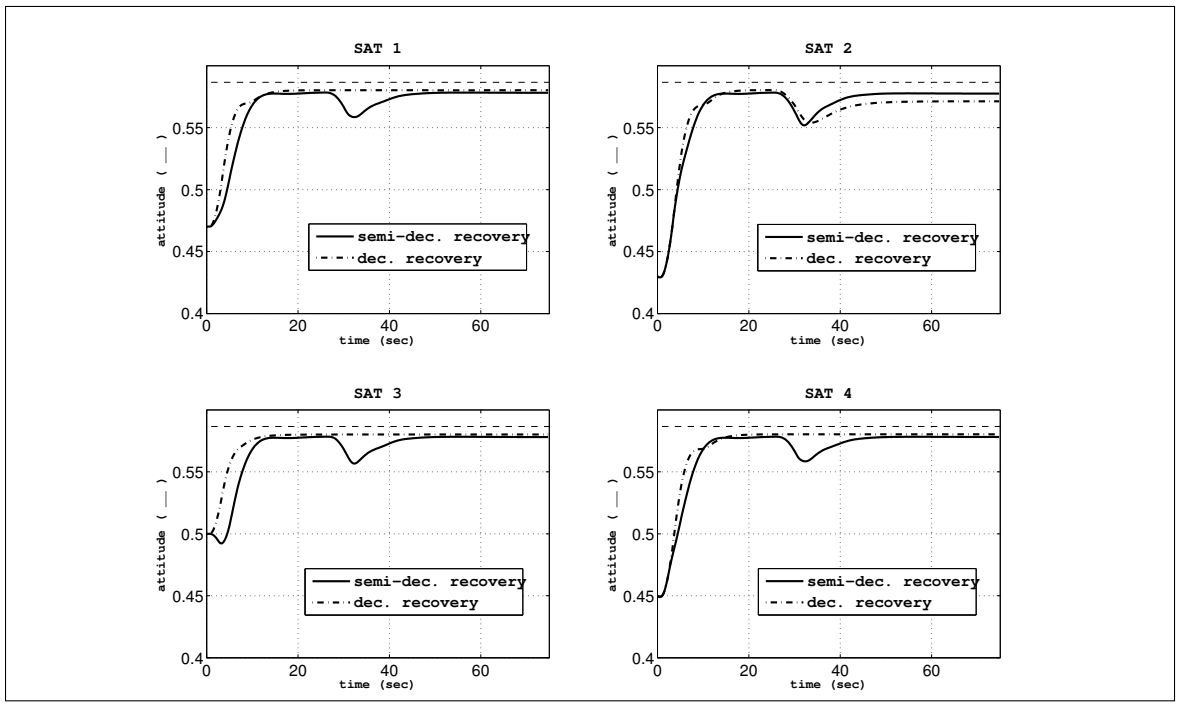

Figure 4.25: X-axis Attitude Quaternion After Control Recovery, 90% LOE Fault with 5% FDI Inaccuracy.

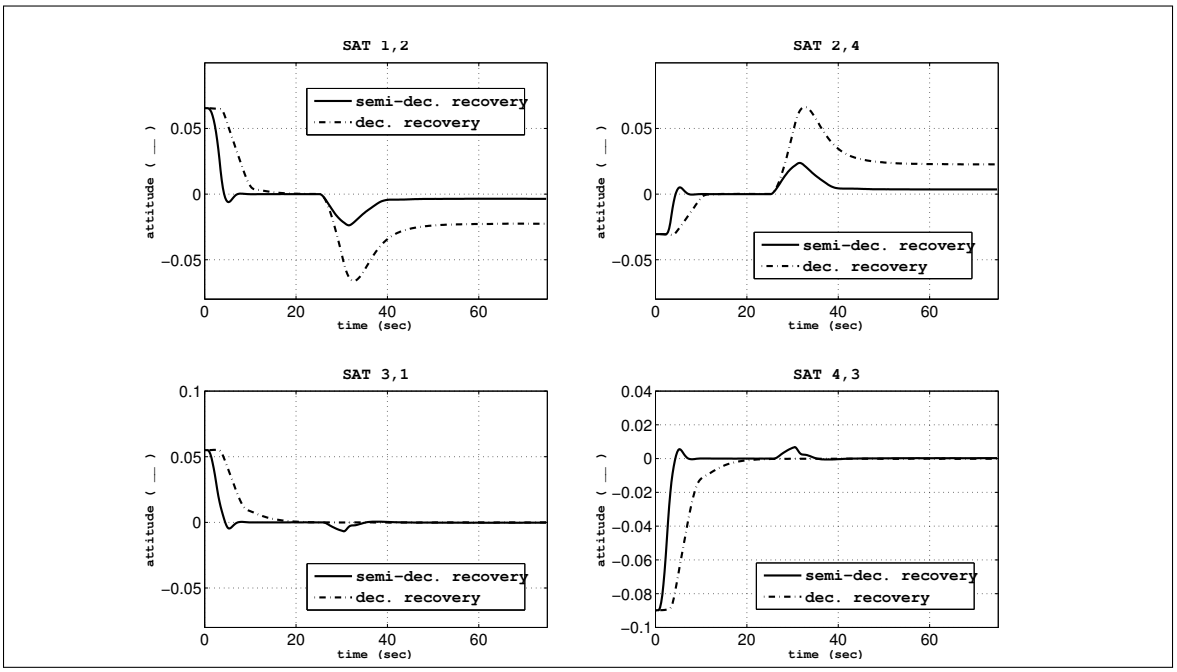

Figure 4.26: X-axis Relative Attitude Quaternion After Control Recovery, 90% LOE Fault with 5% FDI Inaccuracy.

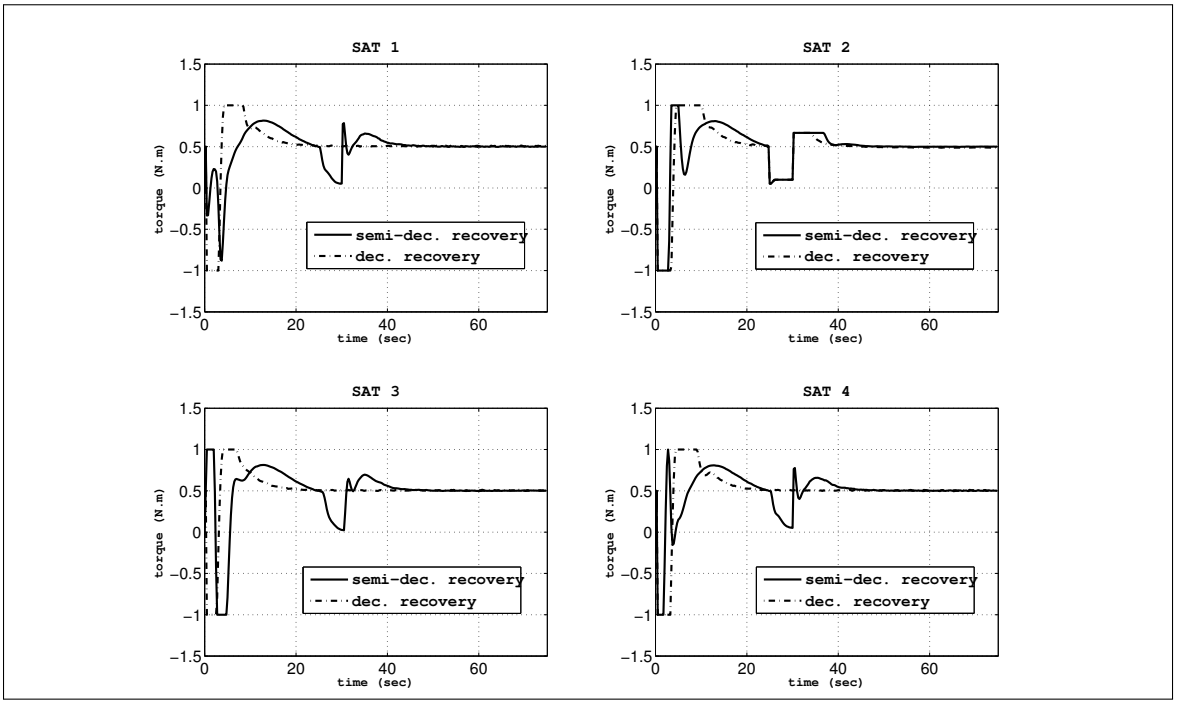

Figure 4.27: X-axis RW Torque After Control Recovery, 90% LOE Fault with 5% FDI Inaccuracy.

4.5.4 Influence of the Fault Detection Time Delay

In this subsection, the influence of fault detection time delay on the recovery performance of the semi-decentralized recovery scheme is investigated. A moderate magnitude LOE fault (70%) is injected to the system where the FDI information inaccuracy is considered as the value evaluated before (30% FDI inaccuracy). The recovery performances of the formation system when the fault detection time delays are considered as $t_{d_1} = 3\,sec$, $t_{d_2} = 5\,sec$, $t_{d_3} = 7\,sec$ are investigated. Table 4.9 shows that a longer fault detection time delay imposes larger fault compensation control effort costs as expected.

Table 4.9: Goal Seeking/Formation Performance, Time Response for the x-axis, and Control Effort Costs after Semi-Decentralized Fault Recovery, 70% LOE Fault with 30% FDI Inaccuracy

	$\widetilde{J}_{tr}$	J_{ss}	$\widetilde{J}_{ss}$	J_u	$\widetilde{t}_{ss}$	t_{ss}
$t_{d_1} = 3\,sec$	0.158	4.05×10^{-4}	2.6×10^{-5}	883.39	48.8	66.64
$t_{d_2} = 5\,sec$	0.158	7.1×10^{-4}	2.3×10^{-5}	959.6	46.7	74.79
$t_{d_3} = 7\,sec$	0.158	7.02×10^{-4}	2.3×10^{-5}	1032.7	48.45	74.37

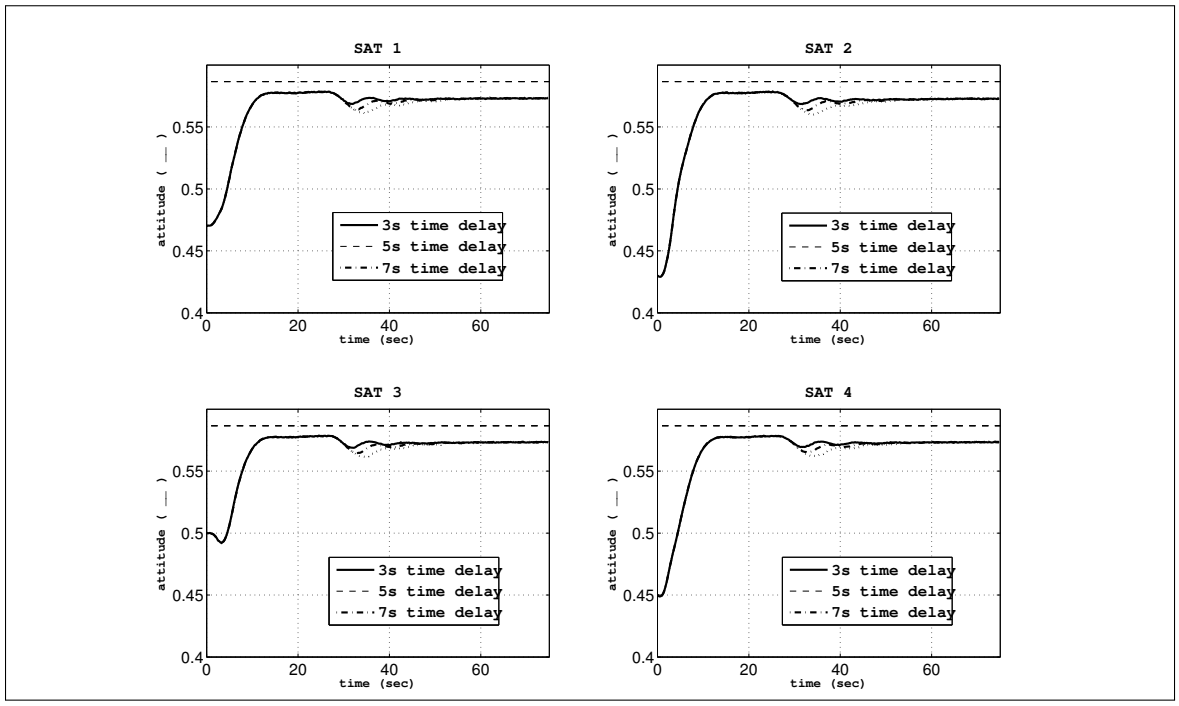

Figure 4.28: X-axis Attitude Quaternion After Control Recovery, 70% LOE Fault with 30% FDI Inaccuracy.

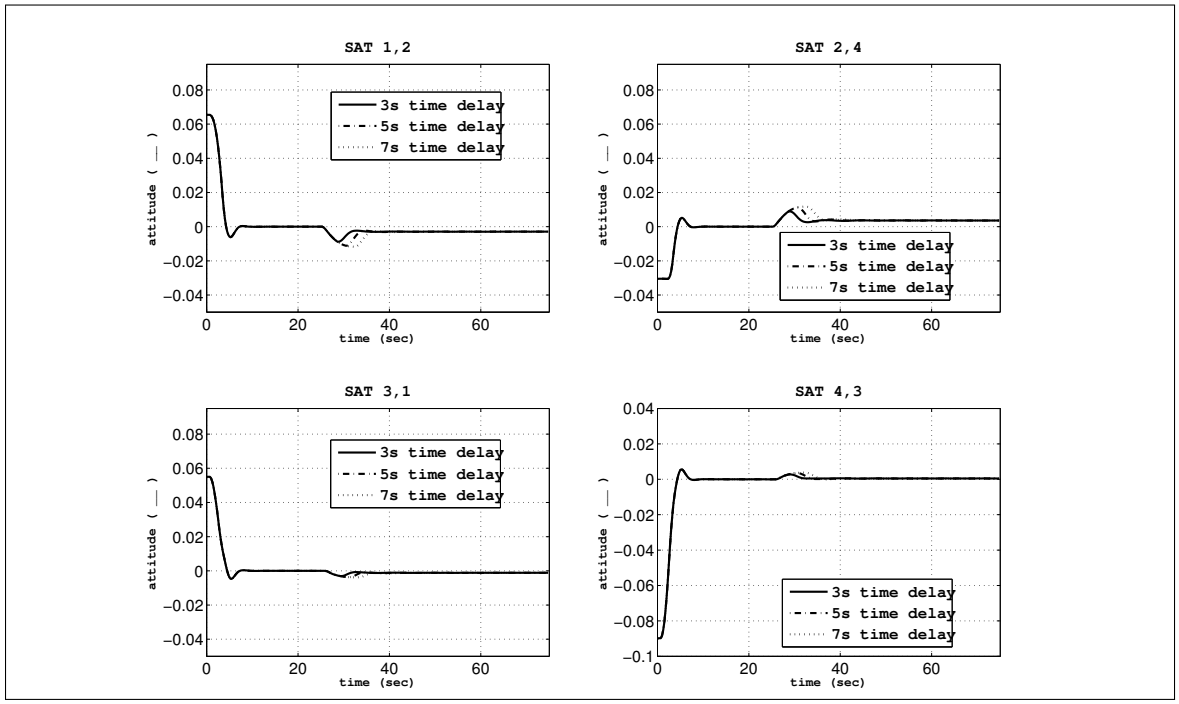

Figure 4.29: X-axis Relative Attitude Quaternion After Control Recovery, 70% LOE Fault with 30% FDI Inaccuracy.

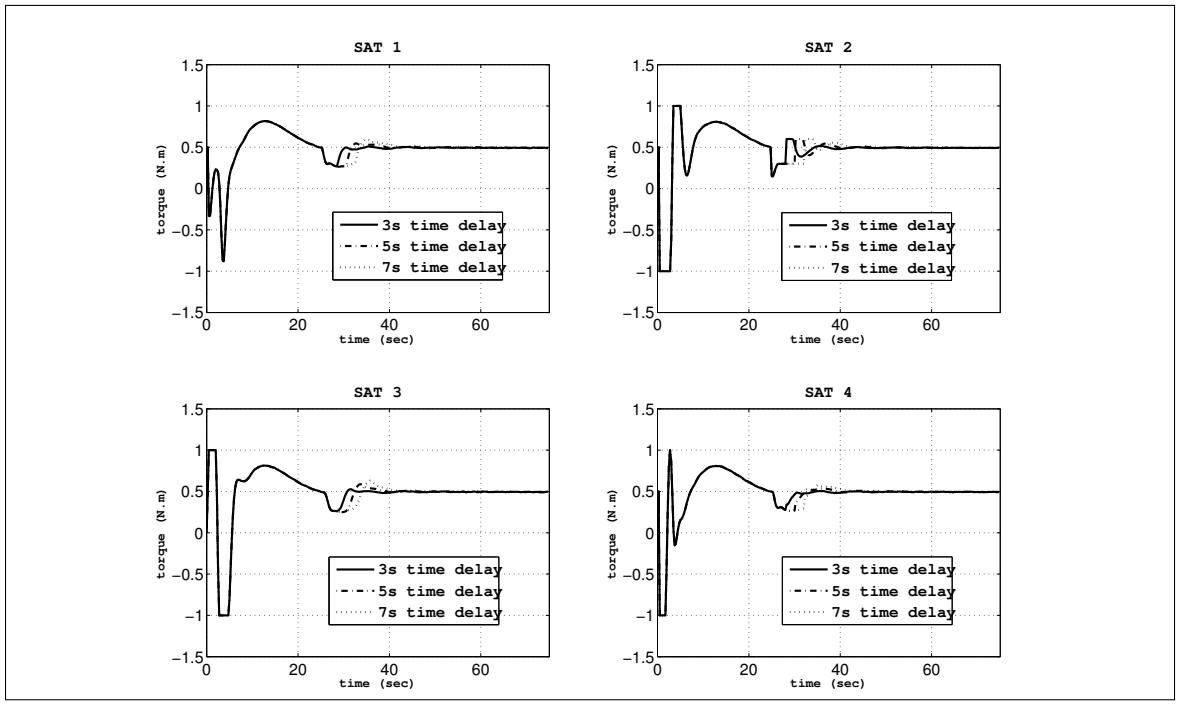

Figure 4.30: X-axis RW Torque After Control Recovery, 70% LOE Fault with 30% FDI Inaccuracy.

4.6 Conclusions

In this chapter, the fault accommodation of an actuator fault in formation flying satellites is addressed. The MPC-based recovery strategies for two types of actuator faults of loss of effectiveness (LOE) and reduced friction fault are provided and the implementation procedure for the overall multi-agent system, namely centralized, semi-decentralized and decentralized recovery schemes are proposed.

The proposed semi-decentralized recovery strategy is performed at two levels. At the local level, the faulty agent controller is reconfigured according to the local fault information. Due to the conservative control recovery by the exclusive recovery of the faulty agent, executing this recovery results in an oscillatory performance. At the formation level recovery, the control laws of the faulty agent's neighbors are reconfigured to account for the fault and therefore the conservatism is reduced by increasing the neighboring agents role in the system recovery and consequently a graceful recovery performance without the previous oscillations is achieved.

It has been validated through multiple fault severity scenarios that the performance of the semi-decentralized scheme after fault recovery satisfies the design specifications (based on the performance indices $\widetilde{J}_{ss}$ and J_{ss}) without imposing significant computational efforts (based on the performance indices t_{solv} and $ITER$) and stringent communication requirements of the centralized approach. Moreover, the semi-decentralized recovery scheme imposes less cumulative fault compensation control effort costs (based on the performance index J_u). On the other hand, the simulation results reveal that a non-cooperative decentralized fault accommodation scheme fails to provide an acceptable recovery performance under fault conditions.

Studying different fault scenarios also leads to the following observations:

1. Robustness of the Control Approaches

The simulation results show that both semi-decentralized and centralized control

approaches have the capability to accommodate low severity faults (up to 15% LOE and 50% reduced friction fault) without any recovery action. This property arises because in the MPC method the feedback gain is determined in every control update.

2. Influence of the FDI Information Accuracy and Fault Detection Time Delay

   The simulation results reveal that the FDI information inaccuracy influences the high severity faults more than moderate or low severity faults. Moreover, LOE faults are more sensitive than friction faults to this information inaccuracy. The last part of simulations analyzed the influence of different fault detection time delays on the recovery performances. A longer fault detection time imposed larger fault compensation control effort costs as expected.

Chapter 5

Conclusions and Future Work

In this thesis we have explored the problem of attitude control of formation flying satellites. The purpose of the work is to improve the formation precision, incorporate actuator constraints, take into account the stringent communication requirements, and provide an automated system recovery scheme subject to common actuator faults.

A more accurate relative state modeling for the attitude dynamics is developed which takes into account the actuator dynamics and also provides a generic relative dynamical modeling which is valid for any operating condition of the formation flying satellite system. The relative state measurements and the coupled dynamics model are used for achieving the desirable formation behavior. In other words, we propose to incorporate the interactions among the agents in the control design by using coupled dynamics model. The coupled dynamics model contributes to achieving a precise formation by (i) providing a precise knowledge through a relative attitude determination system, and (ii) development of a novel behavior-based control formulation based on coupled dynamic modeling.

A centralized approach to solving the formation problem is presented and a semi-decentralized MPC-based scheme is proposed that divides the centralized formation problem into sub problems of lower dimension which leads to lower computational

complexity and communication requirements and does not inherit the problem of a single point of failure, and therefore, provides the formation control method with significant advantages over the centralized scheme. The simulation results show that the control objectives are satisfied by using the proposed semi-decentralized control scheme. More specifically, the formation and the individual tracking performances are fairly comparable with a centralized control approach.

Towards obtaining an automated system recovery subject to common actuator faults, a semi-decentralized system recovery scheme is proposed that incorporates the fault information into the previously developed semi-decentralized MPC-based control to compensate for the identified characteristics losses. The recovery strategy is performed at two levels where the first level accommodates the fault locally and the second level enhances the recovery performance through the formation control. Simulation studies show that the recovered system meets the design specifications without imposing stringent communication requirements of a centralized recovery approach. Moreover, the proposed semi-decentralized recovery scheme imposes less cumulative fault compensation control effort costs.

In this thesis, a high precision formation control scheme is proposed where the control law design incorporates the process constraints and communication requirement limitations. Furthermore, a fault accommodation approach corresponding to the proposed formation control scheme subject to common actuator faults is developed. To evaluate the performance of the proposed semi-decentralized control and fault recovery schemes, the results on comparing their performance with centralized and decentralized control and recovery schemes and by using another control law method, namely, the LQR method are presented and the behavior under different fault severity conditions is examined. We now suggest some of the areas of possible future research related to this work.

- The proposed formation control formulation which is based on coupled dynamical

modeling was employed for developing a behavior-based formation method. However, the formulation has the potential to be modified to address a leader-follower formation method as well. Once the approach is adapted to address the leader-follower formation method, two cases of centralized control and semi-decentralized control schemes can be investigated.

- The developed methodology can be adapted and applied to any other attitude formation control of multi-agents including robotics, unmanned aerial vehicles (UAVs) and autonomous underwater vehicles (AUVs).

- Our system recovery approach accommodates the faults of loss of effectiveness (LOE) and reduced friction. It can be adapted to address other types of structural faults as well as actuator faults and sensor faults.

- Due to the nature of the MPC scheme and its control law being updated in each step, a progressive method of FDI in which the information accuracy increases over time is also capable of being incorporated into an MPC control scheme. The approach might save costs because of taking faster actions compared with our proposed scheme in which the fault information is available after the fault detection time delay.

- The development of nonlinear MPC-based control and fault recovery approaches for formation flying satellites can be considered as another extension of this study. Due to the highly nonlinear dynamics of the attitude motion of formation flying satellites, nonlinear MPC might improve the formation precision due to not involving the approximation errors that are introduced by the linearization process in the linear MPC approach.

References

[1] T. Kyle, R. Srinivas, G. Pini, P. Jonathan, and S. Louis, *Spacecraft Formation Flying Dyanamics, Control and Navigation*. Elsevier, 2010.

[2] R. S. Smith and F. Y. Hadaegh, "Control topologies for deep space formaiton flying spacecraft," in *Proceedings of the American Conference*, (Anchorage), 2002.

[3] E. Kazerooni and K. Khorasani, "Semi-decentralized optimal control of a cooperative team of agents," in *IEEE International Conference on System of Systems Engineering*, pp. 1–7, 2007.

[4] R. Scottolini, "Arcitectures for distributed and hierachical model predictive control- a review," *Journal of Process Control*, no. 19, pp. 723–731, 2009.

[5] A. Bondhus, K. Pettersen, and J. Gravdahl, "Leader/follower synchronization of satellite attitude without angular velocity measurements," in *44th IEEE Conference on Decision and Control, and 2005 European Control Conference*, pp. 7270–7277, 2005.

[6] R. Kristiansen, A. Loría, A. Chaillet, and P. Nicklasson, "Output feedback control of relative translation in a leader-follower spacecraft formation," in *Group Coordination and Cooperative Control* (K. Pettersen, J. Gravdahl, and

H. Nijmeijer, eds.), vol. 336 of *Lecture Notes in Control and Information Science*, pp. 131–151, Springer Berlin Heidelberg, 2006.

[7] J. Shao, G. Xie, J. Yu, and L. Wang, "Leader-following formation control of multiple mobile robots," in *Proceedings of the 2005 IEEE International Symposium on, Mediterrean Conference on Control and Automation*, pp. 808–813, 2005.

[8] X. Chen, A. Serrani, and H. Ozbay, "Control of leader-follower formations of terrestrial UAVs," in *42nd IEEE Conference on Decision and Control*, vol. 1, pp. 498–503 Vol.1, 2003.

[9] K.-H. Tan and M. Lewis, "Virtual structures for high-precision cooperative mobile robotic control," in *Proceedings of the 1996 IEEE/RSJ International Conference on Intelligent Robots and Systems*, vol. 1, pp. 132–139 vol.1, 1996.

[10] W. Ren and R. W. Beard, "A decentralized scheme for spacecraft formation flying via the virtual structure approach," *AIAA Journal of Guidance, Control, and Dynamics*, vol. 27, pp. 73–82, 2004.

[11] J. R. T. Lawton and R. W. Beard, "Elementary attitude formation maneuver via leader-following and behavior-based control," in *in Proceedings of the AIAA Guidance, Navigation and Control Conference*, pp. 2000–4442, 2000.

[12] M. Egerstedt and X. Hu, "Formation constrained multi-agent control," *IEEE Transactions on Robotics and Automation*, vol. 17, no. 6, pp. 947–951, 2001.

[13] I. Chang, S. Y. Park, and K. H. Choi, "Decentralized coordinated attitude control for satellite formation flying via the state- dependent ricatty eqation technique," *Internationl Journal of Non-Linear Mechanics*, pp. 891– 904, 2009.

[14] J. R. Lawton, B. J. Young, and R. W. Beard, "A decentralized approach to elementary formation maneuvers," in *Proceedings of the 2000 IEEE International Conference on Robotics and Automation*, 2000.

[15] S. H. Wang and E. Davison, "On the stabilization of decentralized control systems," *IEEE Transactions on Automatic Control*, vol. 18, no. 5, pp. 473–478, 1973.

[16] B. L. Wu, D. L. He, and X. bin Cao, "Multi-objective output-feedback control for satellite formation keeping: An LMI approach," in *International Conference on Machine Learning and Cybernetics*, pp. 528–533, 2006.

[17] C. E. Garcia, D. M. Prett, and M. Morari, "Model predictive control: Theory and practice-a survey," *Automatica*, vol. 25, no. 3, pp. 335 – 348, 1989.

[18] M. Morari and J. H. Lee, "Model predictive control: past, present and future," *Computers & Chemical Engineering*, vol. 23, no. 4-5, pp. 667 – 682, 1999.

[19] J. Maciejowki, *Predictive Control with Constraints*. Prentice Hall, 2000.

[20] L. Wang, *Model Predicitve Control System Design and Implementaiton Using MATLAB*. Springer, 2009.

[21] F. Borrelli, J. Pekar, M. Baotic, and G. Stewart, "On the computation of linear model predictive control laws," in *Proceedings of the 48th IEEE Conference on Decision and Control, 2009 held jointly with the 2009 28th Chinese Control Conference.*, pp. 7375–7380, 2009.

[22] A. Bemporad, M. Morari, V. Dua, and E. N. Pistikopoulos, "The explicit linear quadratic regulator for constrained systems," *Automatica*, vol. 38, no. 1, pp. 3 – 20, 2002.

[23] A. Bemporad, F. Borrelli, and M. Morari, "Model predictive control based on linear programming-the explicit solution," *IEEE Transactions on Automatic Control*, vol. 47, no. 12, pp. 1974–1985, 2002.

[24] M. Seron, J. De Dona, and G. Goodwin, "Global analytical model predictive control with input constraints," in *Proceedings of the 39th IEEE Conference on Decision and Control*, vol. 1, pp. 154–159 vol.1, 2000.

[25] W. Dunbar and R. Murray, "Receding horizon control of multi-vehicle formations: a distributed implementation," in *43rd IEEE Conference on Decision and Control*, vol. 2, pp. 1995–2002 Vol.2, 2004.

[26] V. Manikonda, P. Arambel, M. Gopinathan, R. Mehra, and F. Hadaegh, "A model predictive control-based approach for spacecraft formation keeping and attitude control," in *Proceedings of the 1999 American Control Conference*, vol. 6, pp. 4258–4262 vol.6, 1999.

[27] S. Longhi, A. Monteriù, and M. Vaccarini, "Cooperative control of underwater glider fleets by fault tolerant decentralized MPC," in *Proceedings of the 17th IFAC World Congress*, pp. 16021–16026, 2008.

[28] A. Richards and J. How, "Decentralized model predictive control of cooperating UAVs," in *IEEE Conference on Decision and Control*, 2004.

[29] E. Camponogara, D. Jia, B. Krogh, and S. Talukdar, "Distributed model predictive control," *Control Systems, IEEE*, vol. 22, no. 1, pp. 44–52, 2002.

[30] Z. Wang, Y. He, and J. Han, "Distributed receding horizon formation control for multi-vehicle systems with relative model," in *18th IFAC World Congress*, 2011.

[31] T. Keviczky, F. Borrelli, and G. Balas, "A study on decentralized receding horizon control for decoupled systems," in *Proceedings of the 2004 American Control Conference*, vol. 6, pp. 4921–4926 vol.6, 2004.

[32] T. Keviczky, F. Borrelli, and G. J. Balas, "Decentralized receding horizon control for large scale dynamically decoupled systems," *Automatica*, vol. 42, no. 12, pp. 2105 – 2115, 2006.

[33] T. Keviczky, F. Borrelli, K. Fregene, D. Godbole, and G. Balas, "Decentralized receding horizon control and coordination of autonomous vehicle formations," *IEEE Transactions on Control Systems Technology,*, vol. 16, no. 1, pp. 19–33, 2008.

[34] P. Ioannou and J. Sun, *Robust Adaptive Control*. Pearson Education, Inc., 1995.

[35] J. Bošković and R. Mehra, "Multiple model-based adaptive reconfigurable formation flight control design," in *Conference on Decision and Control*, 2002.

[36] N. E. Wu, Y. Zhang, and K. Zhou, "Detection, estimation, and accommodation of loss of control effectiveness," *Internaitonal Journal of Adaptive Control and Signal Processing*, vol. 14, pp. 775–795, 2000.

[37] E. Semsar and K. Khorasani, "Adaptive formation control of UAVs in the presence of unknown vertex forces and leader commands," in *American Control Conference, Minneapolis*, 2006.

[38] B. Jiang, M. Staroswiecki, and V. Cocquempot, "Fault accommodation for nonlinear dynamic systems," *IEEE Transactions on Automatic Control*, vol. 51, no. 9, pp. 1578–1583, 2006.

[39] S. Azizi and K. Khorasani, "A decentralized cooperative actuator fault accomodation of formation flying satellites in deep space," in *3rd Annual IEEE International Systems Conference*, 2009.

[40] Y.-W. Liang, S.-D. Xu, and C.-L. Tsai, "Study of VSC reliable designs with application to spacecraft attitude stabilization," *IEEE Transactions on Control Systems Technology,*, vol. 15, no. 2, pp. 332–338, 2007.

[41] I. Hwang, S. Kim, Y. Kim, and C. E. Seah, "A survey of fault detection, isolation, and reconfiguration methods," *IEEE Transactions on Control Systems Technology*, vol. 18, no. 3, pp. 636–653, 2010.

[42] V. Venkatasubramanian, R. Rengaswamy, K. Yin, and S. N. Kavuri, "A review of process fault detection and diagnosis part 1: Quantitative model-based methods," *Computer and Chemical Engineering*, pp. 293–311, 2003.

[43] N. Tudoroiu and K. Khorasani, "Satellite fault diagnosis using a bank of interacting kalman filters," *IEEE Transactions on Aerospace and Electronic Systems*, vol. 43, pp. 1334–1350, 2007.

[44] N. Meskin, K. Khorasani, and C. A. Rabbath, "A hybrid fault detection and isolation strategy for a network of unmanned vehicles in presence of large environmental disturbances," *IEEE Transactions on Control Systems Technology,*, vol. 18, no. 6, pp. 1422–1429, 2010.

[45] T. Jiang and K. Khorasani, "Autonomous precision formation flying: a proposed fault tolerant attitude control strategy," in *Proceedings of the SPIE* (6555, ed.), 2007.

[46] J. F. Magni and P. Mouyon, "On residual generation by observer and parity space approaches," *IEEE Transactions on Automatic Control*, vol. 39, no. 2, pp. 441–447, 1994.

[47] R. Isermann, "Process fault detection based on modeling and estimation methods-a survey," *Automatica*, vol. 20, no. 4, pp. 387–404, 1984.

[48] J. Gertler, "Analytical redundancy methods in fault detection and isolation, survey and synthesis," in *IFAC Conference on Fault Detection, Supervision and Safety*, (Germany), pp. 9–22, 1991.

[49] P. Frank and X. Ding, "Survey of robust residual generation and evaluation methods in observer-based fault detection systems," *Journal of Process*, vol. 7, no. 6, pp. 403–424, 1997.

[50] R. Patton and J. Chen, "Observer-based fault detection and isolation : Robustness and applications," *Control*, vol. 5, no. 5, pp. 671–682, 1997.

[51] J. Gertler, "Fault detection and isolation using parity relations," *Control Engineering Practice*, vol. 5, no. 5, pp. 653–661, 1997.

[52] H. Talebi and R. Patel, "An intelligent fault detection and recovery scheme for reaction wheel actuator of satellite attitude control systems," in *IEEE International Conference on Control Applications, 2006 IEEE International Symposium on Intelligent Control*, pp. 3282–3287, 2006.

[53] A. Srinivasan and C. Batur, "Hopfield/ART-1 neural network-based fault detection and isolation," *IEEE Transactions on Neural Networks*, vol. 5, no. 6, pp. 890–899, 1994.

[54] H. Talebi, K. Khorasani, and S. Tafazoli, "A recurrent neural-network-based sensor and actuator fault detection and isolation for nonlinear systems with application to the satellite's attitude control subsystem," *IEEE Transactions on Neural Networks*, vol. 20, no. 1, pp. 45–60, 2009.

[55] Y. Maki and K. Loparo, "A neural-network approach to fault detection and diagnosis in industrial processes," *IEEE Transactions on Control Systems Technology*, vol. 5, no. 6, pp. 529–541, 1997.

[56] I.-D. Al-Zyoud and K. Khorasani, "Detection of actuator faults using a dynamic neural network for the attitude control subsystem of a satellite," in *IEEE International Joint Conference on Neural Networks*, vol. 3, pp. 1746–1751 vol. 3, 2005.

[57] R. J. Patton, "Fault-tolerant control systems: The 1997 situation, in IFAC symposium on fault detection supervision and safety for technical processes," in *IFAC SAFEPROCESS'1997*, pp. 1033–1054, 1997.

[58] Y. Zhang and J. Jiang, "Bibliographical review on reconfigurable fault-tolerant control systems," *Annual Reviews in Control*, vol. 32, no. 2, pp. 229 – 252, 2008.

[59] M. J. Sidi, *Spacecraft Dynamics and Control: A Practical Engineering Approach*. Cambridge University Press, 1997.

[60] R. Kristiansen and D. Hagen, "Modelling of actuator dyanamics for spacecraft attitude control," *American Institude of Aeronautics and Astronautics*, pp. 1022–1025, 2009.

[61] H. Schaub and J. L. Junkins, *Analytical Mechanics od Space Systems*. American Institue of Aeronautics and Astronautics, 2009.

[62] V. L. Pisacane, *Fundamentals of Space Systems*. OXFORD UNIVERSITY PRESS, 2005.

[63] J. R. C. Cook, "Dawn engineers assess reaction wheel," tech. rep., Jet Propulsion Laboratory, 2012.

[64] G. Webster, "Test of spare wheel puts orbiter on path to recovery," tech. rep., Jet Propulsion Laboratory, 2012.

[65] A. Bemporad and M. Morari, "Robust model predictive control: A survey," in *Robustness in identification and control* (A. Garulli and A. Tesi, eds.), vol. 245 of *Lecture Notes in Control and Information Sciences*, pp. 207–226, Springer London, 1999.

[66] M. V. Kothare, V. Balakrishnan, and M. Morari, "Robust constrained model predictive control using linear matrix inequalities," *Automatica*, vol. 32, no. 10, pp. 1361 – 1379, 1996.

[67] P. J. Campo and M. Morari, "Robust model predictive control," in *American Control Conference*, pp. 1021–1026, 1987.

[68] D. Mayne, M. Seron, and S. Rakovic, "Robust model predictive control of constrained linear systems with bounded disturbances," *Automatica*, vol. 41, no. 2, pp. 219 – 224, 2005.

[69] J. M. Maciejowsky and C. N. Jones, "MPC fault-tolerant fligh control case study: Flight 1862," in *Proceedings of the 5th IFAC symposium on fault detection, supervision and safety for technical processes*, 2003.

[70] H. K. Khalil, *Nonlinear Systems*. Prentice Hall, 1996.

[71] U. Maeder, F. Borrelli, and M. Morari, "Linear offest-free model predicitve control," *Automatica*, vol. 45, pp. 2214–2222, 2009.

[72] J. Prakash, S. Narasimhan, and S. C.Patwardhan, "Integrating model based fault diagnosis with model predictive control," *Industrial and Engineering Chemistry Research*, vol. 44, no. 12, pp. 4344–4360, 2005.

[73] E. Kerrigan and J. Maciejowski, "Fault tolerant control of a ship propulsion system using model predictive control," in *European Control Conference*, 1999.

[74] T. Miksch, A. Gambier, and E. Badreddin, "Real-time implementation of fault-tolenat control using model predictive control," in *International Federation of Automatic Control*, (Seoul), 2008.

[75] C. O. Martínez and V. Puig, "Fault-tolerant model predictive control within the hybrid systems framework: application to sewer networks," *International journal of Adaptive Control and Signal Processing*, vol. 23, no. 8, pp. 757–787, 2009.

[76] M. Benosman and K. Y. Lum, "Online references reshaping and control reallocation for nonlinear fault tolerant control," *IEEE Transactions on Control Systems Technology*, vol. 17, no. 2, pp. 366–379, 2009.

[77] M. Kale and A. Chipperfield, "Stabilized MPC formulations for robust reconfigurable flight control," *Control Engineering Practice*, vol. 13, no. 6, pp. 771 – 788, 2005.

[78] S. Q. Sun, L. Dong, L. Li, and S. S. Gu, "Fault-tolerant control for constrained linear systems based on MPC and FDI," *International Journal of Information and Systems Sciences*, vol. 4, no. 4, pp. 512–523, 2008.

[79] H. A. Izadi, B. W. Gordon, and Y. Zhang, "Decentralized model predictive control for cooperative multiple vehicles subject to communication loss," *International Journal of Aerospace Engineering*, 2011.

[80] D. Joosten, T. van den Boom, and T. Lombaerts, "Fault-tolerant control using dynamic inversion and model-predictive control applied to an aerospace benchmark," in *Proceedings of the 17th World Congress The International Federation of Automatic Control*, 2008.

[81] J. Dong, M. Verhaegen, and E. Holweg, "Closed-loop subspace predictive control for fault tolerant MPC design," in *The Internationl Federation of Automatic Control*, 2008.

[82] M. Abdel-Geliel, E. Badreddin, and A. Gambier, "Applicaiton of model predictive control for fault tolerant system using dynamic safety margin," in *Proceedings of the 2006 American Control Conference*, 2006.

[83] C. Ocampo-Martinez, P. Guerra, V. Puig, and J. Quevedo, "Actuator fault-tolerance evaluation of linear constrained model predictive control using zonotope-based set computations," *Journal of Systems and Control Engineering*, vol. 221, pp. 915–926, 2007.

[84] S. G. Kim, J. L. Crassidis, Y. Cheng, A. M. Fosbury, and J. L. Junkins, "Kalman filtering for relative spacecraft attitude and position estimation," *Journal of Guidance Control and Dynamics*, vol. 30, no. 1, 2007.

[85] J. R.Wertz, *Spacecraft Attitude Determination and Control*. Kluwer Academic Publishers, 1978.

[86] J. Diebel, "Representing attitude: Euler angles, unit quaternions, and rotation vectors," *Matrix*, 2006.

[87] Y. Yang, "Spacecraft attitude determination and control : Quaternion based method," *Annual Reviews in Control*, vol. 36, pp. 198–219, 2012.

[88] W. J. Larson and J. R. Wertz, "Space mission analysis and design," tech. rep., Torrance, CA (United States); Microcosm, Inc., 1992.

[89] B. Bialke, "High fidelity mathematical mopdeling of reaction wheel performance," in *21st Annual American Austronautical Society Guidance and Control Conference*, 1998.

[90] C. Godsil and G. Royle, *Algebraic Graph Theory*. Springer, 2001.

[91] Y. Liu and K. M.Passino, "Cohesive behaviors of multiagent systems with information flow constraints," *IEEE Transactions on Automatic Control*, vol. 51, pp. 1734–1748, 2006.

[92] H. Tanner, A. Jadbabaie, and G. Pappas, "Stable flocking of mobile agents, part i: fixed topology," in *Proceedings. 42nd IEEE Conference on Decision and Control*, vol. 2, pp. 2010–2015 Vol.2, 2003.

[93] J. A. Fax and R. M.Murray, "Information flow and cooperative control of vehicle formations," *IEEE Transaction on Automatic Control*, vol. 49, pp. 1465–1476, 2004.

[94] R. Isermann, *Fault-diagnosis systems: an introduction from fault detection to fault tolerance*. Springer-Verlag, 2005.

[95] O. Moseler and R. Isermann, "Application of model-based fault detection to a brushless DC motor," *IEEE Transaction on Industrial Electronics*, vol. 47, pp. 1015–1020, 2000.

[96] M. Cannon, "C21-model predictive control- lecture notes," 2012.

[97] D. Gay, "A trust-region approach to linearly constrained optimization," in *Numerical Analysis* (D. Griffiths, ed.), vol. 1066 of *Lecture Notes in Mathematics*, pp. 72–105, Springer Berlin Heidelberg, 1984.

[98] D. P.Bertsekas, *Dynamic Programming And Optimal Control*. Athena Scientific, 1995.

[99] D. Q. Mayne, J. B. Rawlings, C. V. Rao, and P. O. M. Scokaert, "Constrained model predictive control : Stability and optmiality," *Automatica*, no. 36, pp. 789–814, 2000.

[100] S. S. Keerthi and E. G. Gilbert, "Optimal infinite-horizon feedback laws for a general class of constrained discrete-time system: Stability and moving - hozrizon approximations," *Journal of Optimzation Theory and Applications*, vol. 57, no. 2, pp. 265–293, 1988.

[101] D. Q. Mayne and H. H. Michalska, "Receding horizon control of nonlinear systems," *IEEE Transactions on Automatic Control*, vol. 35, no. 7, pp. 814–824, 1990.

[102] K. R. Muske and J. B. Rawlings, "Linear model predictive control of unstable processes," *Journal of Process Control*, vol. 3, no. 2, pp. 85 – 96, 1993.

[103] karl Johan Astrom and R. M. Murray, *Feedback Systems*. Princeton University Press, 2010.

[104] H. Rosenbrock, *State-space and Multivariable Theory*. Thomas Nelson and Sons, 1970.

[105] Ø. Hegrenæs, J. T. Gravdahl, and P. Tøndel, "Spacecraft attitude control using explicit model predictive control," *Automatica*, vol. 41, no. 12, pp. 2107 – 2114, 2005.

[106] R. Wisniewski and P. Kulczycki, "Slew maneuver control for spacecraft equipped with star camera and reaction wheels," *Control Engineering Practice*, vol. 13, no. 3, pp. 349 – 356, 2005.

[107] J. R. Carpenter, "Decentralized control of satellite formations," *International Journal of Robust and Nonlinear Control*, vol. 12, pp. 141–161, 2002.

[108] H. Noura, D. Sauter, F. Hamelin, and D. Theilliol, "Fault-tolerant control in dynamic systems: application to a winding machine," *IEEE Control Systems*, vol. 20, no. 1, pp. 33–49, 2000.